OBSERVATIONS OF THE DYNAMICS AND STABILITY OF Z PINCHES

James Michael Bayley

Submitted in partial fulfilment of the requirements
for the degree of Doctor of Philosophy of the
University of London
and for the
Diploma of Membership of Imperial College

Plasma Physics Group
Blackett Laboratory
Imperial College
London SW7 2BZ

January 1991

ABSTRACT

This thesis presents studies of the compressional Z pinch and the occurrence of hotspots in an argon doped plasma focus. The design and testing of a new compressional pinch driven by a 3 Ω water filled transmission line is described.

The compressional pinch is formed in a quartz tube filled with either hydrogen or argon at pressures of about 1 $mbar$. The circuit current rose to a maximum of 150 kA in 70 ns and remained constant for 100 ns before it began to fall but it was found that the pinch current fell at a lower rate. The hydrogen plasma produced had the following parameters $I = 150\ kA$, line density $N_e = 2.0 \times 10^{19}\ m^{-1}$, Lunquist number $S = 1.6 \times 10^3$, $\omega_i \tau_{ii} = 7$ and $a_{Larmor}/a_{pinch} = 0.18$. The observations we report here are the first detailed set of measurements of a collisionless compressional pinch where finite Larmor radius (FLR) effects may be present. The pinch dynamics were measured using optical framing and streak photography. To measure the electron density and investigate stability a new side-on holographic interferometric technique was developed. This detected an $m = 0$ (sausage) instability which formed during the flat top of the current pulse. However its growth rate was less than the ideal mhd value and it saturated at approximately 30%. The instability did not cause the immediate disruption of the pinch.

The SPEED2 plasma focus Z-pinch was shown to be capable of generating argon plasmas with very high temperatures and densities (1.5 keV, $10^{28}\ m^{-3}$). Argon hotspots were created by injecting a stream of argon gas in front of the collapsing deuterium sheath. The hotspots were measured using many diagnostics including an X-ray streak camera and an X-ray crystal spectrometer. These provided the first spectral resolution of hotspots on a 100 ps timescale. The hotspots were shown to be formed during the expansion of the pinch and have a duration of only 1 ns. The helium-like emission from highly ionised atoms was present for only 250 ps. These measurements showed that the formation mechanisms of hotspots are much faster than had been previously reported. Each pinch generated about 7 hotspots which were about 250 μm diameter and very close to the axis. The pinch formed a point-like source of 700 μm diameter and emitted 1 J of soft X-rays ($\lambda \leq 2.0\ nm$) into 4π over 30 ns. Such a high power point source may prove exploitable for X-ray lithography and flash X-ray microscopy.

ACKNOWLEDGEMENTS

It gives me pleasure to acknowledge the help and advice of those without whom this work would not have been possible. Mr A. E. Dangor my supervisor for his excellent criticism of the first draft, Michael Coppins for his explanations of Theory and my fellow students for their assistance and encouragement. I would particularly like to thank Peter Baldock for his help in my first year and Jack Beckwith for converting my drawings into a brass reality. My work in Düsseldorf was as part of the SPEED2 team and I thank Professor Decker for the invitation and Michael Mälzig for agreeing to work with me. Finally, thank you Elaine for all your support (and spelling corrections!).

CONTENTS

Chapter 1: Introduction

1.0 Why study Z-pinch plasmas? 8

1.1 The pinch effect 8

1.2 The compressional pinch: A review 8

1.2.1 The collapse

1.2.2 The pinch

1.2.3 Stability of Z-pinches

1.3 The plasma focus - A review 9

1.3.1 The focus experiment

1.3.2 Hotspots

1.4 Aims and results 23

Chapter 2: The compressional pinch apparatus

2.0 Introduction 24

2.1 The current generator 24

2.2 Modelling the line with BERTHA 27

2.3 Improvement of the line-marx interface 29

2.4 Results - modifications to the marx-line interface 29

2.4.1 Surface treatment

2.4.2 Electrodes and shielding

2.4.3 Moving the marx

2.4.4 Distributed resistor

2.4.5 Dump gap

2.5 Discussion of transmission line modifications 34

2.6 The new compressional pinch 37

2.7 Results - the new pinch assembly 38

2.8 Summary 41

Chapter 3: The compressional pinch diagnostics

3.0 An overview 42

3.1 Diagnostics 42

3.1.1 The gated image intensifier

3.1.2 The optical streak camera

3.1.3 Holographic interferometry

3.2 Analysis 48

3.2.1 Models of the collapse

3.2.2 The analysis of interferograms

3.2.3 The computer program FRINGE

Chapter 4: Compressional pinch results

4.0 An overview 54
4.1 The collapse 54
4.2 The wall plasma 54
4.3 The pinch 61

Chapter 5: Interpretation of the compressional pinch results

5.1 The collapse 67
5.2 The wall plasma 69
5.3 The pinch 69
5.4 Pinch stability 72
5.5 Summary 74

Chapter 6: The Düsseldorf SPEED2 plasma focus

6.0 Introduction 77
6.1 SPEED 2 - a new design philosophy for the plasma focus 77
6.2 The argon valve 77
6.3 Diagnostics 80
- 6.3.1 Kentech X-ray streak camera
- 6.3.2 The X-ray crystal spectrometer.
- 6.3.3 Neutron Counters
- 6.3.4 Pinhole camera
- 6.3.5 X-ray diodes
- 6.3.6 Electrical signals
- 6.3.7 P.I.N. diodes

6.4 Results and discussion 83
- 6.4.1 Effect of argon on neutron output
- 6.4.2 Electron beam activity - XRD and PIN diode signals
- 6.4.3 The pinch

6.5 Summary 93

Chapter 7: Conclusions

7.0 Introduction 96
7.1 Summary of compressional pinch results 96
7.2 Compressional Z-pinch Conclusion 97
7.3 Summary of plasma focus pinch results 100
7.4 Plasma focus - discussion 100
7.5 Suggestions for further work 102

References 103

FIGURES

Chapter 1: Introduction

1.1 Fluid and particle models of the pinch effect 10

1.2 The compressional pinch is formed in a quartz tube which is initially filled with gas at low pressure 11

1.3 A streak photograph, 1 torr Argon, 1 μs full screen 13

1.4 $B_1 > B_2$, a) The $m = 0$ (sausage) instability, b) The $m = 1$ (kink) instability 17

1.5 The Haines Coppins diagram of stability regimes of the hydrogen Z- pinch

1.6 The plasma focus a) The accelerating plasma sheath, b) The pinch 20

1.7 An X-ray pinhole photograph of a deuterium plasma focus pinch 21

Chapter 2: The compressional pinch apparatus

2.1 The current generator 25

2.2 The transmission line model used in BERTHA 28

2.3 Streamers on the marx-line interface 30

2.4 The dump gap at the marx-line interface 31

2.5 The distributed resistor at the line-marx interface 33

2.6 The current trace (100 ns, 30 kV/div) and the interface **without** the dump gap 33

2.7 The current trace (100 ns, 30 kV/div) and the interface **with** the dump gap 35

2.8 The pinch chamber 36

2.9 The preionisation current and main current pulse 100 ns, 30 kA/div 39

Chapter 3: Diagnostics of the compressional pinch

3.1 The timing sequence 43

3.2 The arrangement for holographic interferometry with a diffuse scene beam. Inset: The quartz tube containing the pinch has one side diffusing. 46

3.3 The coordinate system for analysing interferograms 49

3.4 A background fringe pattern and the fringe shift caused by an axially uniform plasma 50

Chapter 4: Compressional pinch results

4.1 The current trace and a streak photograph 55

4.2 A streak photograph and side on frames at 4 times. 1 $torr$ Argon,100 kA 56

4.3 An interferogram of a collapsing pinch 57

4.4 A side-on framing photograph taken at peak current, 1 $torr$ Hydrogen, 100 kA, $t = 80$ ns 58

4.5 A sequence of interferograms of the 2 *torr*, 150 kA compressional pinch
4.6 Radius v time for the 1 and 2 *torr* hydrogen pinches 63
4.7 Electron density profiles of the 2 *torr*, 150 kA hydrogen pinch obtained by Abel inversion 64
4.8 Line density versus time from the interferograms at 150 kA 65

Chapter 5: Interpretation of compressional pinch results

5.1 The slug model 68
5.2 A computer generated model of an interferogram of the wall plasma 70
5.3 An interferogram showing the wall plasma, 1 *torr* hydrogen pinch, 150 kA, $t = 300$ ns 71
5.4 2 torr hydrogen, 150 kA, $t = 180$ ns. An interferogram and its computer model showing and $m = 0$ instability 73

Chapter 6: The Düsseldorf SPEED2 plasma focus

6.1 Plasma focus with gas inlet valve 79
6.2 Focus and diagnostics 81
6.3 The geometry used to streak the x-ray spectra 82
6.4 An x-ray diode (XRD) 84
6.5 X-ray diode and pin diode sensitivities 85
6.6 Typical signals from a pair of filtered X-ray diodes. Upper trace (green): 0.16 μm Al on 12 μm mylar, 50 mV, 50 ns/div. Lower trace (black): 10 μm Cu, 20 mV, 50 ns/div 87
6.7 Pinhole camera images of shot 4028 taken through different filters 88
6.8 Pinhole camera picture 30 μm pinhole, 10 μm Be filter 89
6.9 (shot 4192) The image on the left is a time integrated pinhole camera picture (300 μm pinhole, 510 μm Be filter). The image on the right is an X- ray streak photograph of the same pinch (300 μm pinhole, 10 μm Be)
6.10 A microdensitometer trace of the argon spectrum near the helium-like lines 92
6.11 Line ratios predicted by RATION and SPECTRA 94
6.12 A streak photograph of the argon lines (10 ns full screen) 95

Chapter 7: Conclusions

7.1 The Haines Coppins diagram of stability regimes of the H Z-pinch 98
7.2 The crowbarred pinch 101

TABLES

Chapter 2: The compressional pinch apparatus

2.1 Current generator parameters 26

Chapter 3: The compressional pinch diagnostics

3.1 Details of the holographic setup 47

Chapter 4: Compressional pinch results

4.1 Comparison of pinch parameters to the slug model predictions 59

4.2 Wall plasma parameters 60

4.3 Pinch data from the interferograms at the time the pinches disappear 66

Chapter 6: The Düsseldorf SPEED2 plasma focus

6.1 SPEED2 parameters 78

Chapter 7: Conclusion

7.1 Values of important parameters of the Imperial College compressional pinch 99

CHAPTER 1: INTRODUCTION

1.0 Why study Z-pinch plasmas?

Ever since Prometheus brought fire from the heavens to mankind we have sought new energy sources. In 1929 Atkinson and Houtermans again looked heavenward and suggested that thermonuclear fusion of hydrogen was the power source of the sun. At the time it was considered unlikely that we would ever be able to obtain the extremely high temperatures ($\approx 10^8 K$) required for nuclear fusion on Earth (Gamow 1949). However the second world war and superpower rivalry spurred on fusion research and 23 years later in 1952 the first hydrogen bomb was exploded and man-made thermonuclear fusion was achieved. Since then the major goal of civilian plasma physicists has been to attain the controlled release of energy from thermonuclear reactions.

The problems of heating and confining a plasma for long enough for sufficient thermonuclear reactions to take place has been approached in two principal ways. Currents and their associated magnetic fields can be used to confine a low density plasma for a long time in a stable configuration (magnetically confined fusion MCF). The most studied machine of this type is the tokamak. An alternative approach is to heat the plasma so rapidly (eg. with a laser pulse) that fusion reactions occur while it is confined by its own inertia (inertially confined fusion ICF). This method produces very high density plasmas which are confined for a short time. In this chapter we will introduce the Z-pinch which can produce magnetically confined plasmas with density and confinement times which are a median of the MCF and ICF approaches and has been suggested as a possible fusion reactor (Haines 1982). Z pinch plasmas are prone to instabilities which limit the confinement time and the investigation of their stability forms part of this thesis.

Recent research has concentrated on Z pinches as radiation sources and several different schemes for using the pinch effect to form a plasma have been developed. Devices such as the plasma focus (x-rays, neutrons), fibre pinch (x-rays, neutrons) and gas puff (x-rays) can produce very high power radiation pulses (see a review by Pereira and Davis 1988). These very intense radiation pulses are used for materials testing and may offer a route to successful xuv and x-ray laser schemes. These and other uses of Z pinches are reviewed by Dangor (1986). Much of the radiation from these pinches comes from small bright regions called hotspots and this thesis reports investigations of these interesting phenomena in the plasma focus.

1.1 The pinch effect

A plasma column carrying a large current will contract under the influence

of its own magnetic field if the magnetic force is greater than the kinetic pressure. The pinch effect can be represented by a particle or fluid particle model as is shown in figure 1.1. In the particle model a current carrying particle, charge q, is subject to a force $q\vec{v} \times \vec{B}$ towards the axis. When these are summed over the plasma we get the magnetohydrodynamic (mhd) model, the plasma fluid element is subject to a $\vec{j} \times \vec{B}$ force inward.

For a pinch in equilibrium the magnetic force is exactly balanced by the thermal pressure of the plasma. If we assume that the pinch ~~is isothermal and has constant current density~~ has zero pressure at the edge we can derive the Bennett (1934) equation.

$$8(Z+1)N_i k_B T = \mu_0 I^2 \tag{1.1}$$

$Z = mean\ ionisation$

$N_i = \int_0^a n_i(r) 2\pi r dr \ = \ ion\ line\ density\ [m^{-1}]$

$a = pinch\ radius$

$k_B = Boltzmann\ constant$

$\mu_0 = permittivity\ of\ free\ space$

$I = current$

$T = pinch\ temperature$

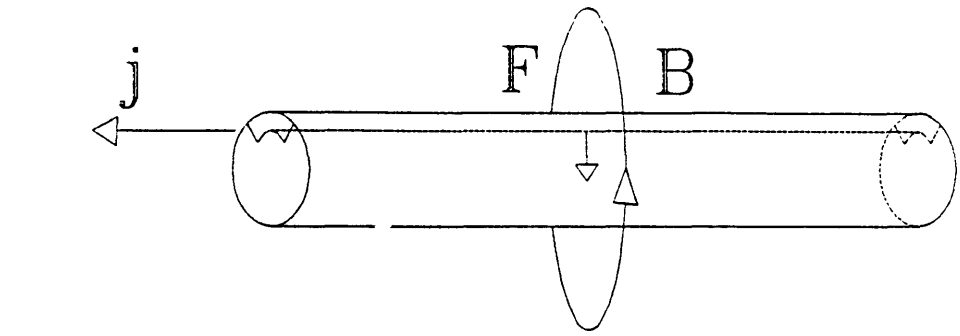
Z pinches were quickly disregarded as a path to fusion primarily because of the mhd instabilities which were observed (Carruthers et al 1957 and Rumport. and Anderson et al 1958). Renewed interest in Z pinches came with the availability of high current generators. The development in the 1970s of physically small high voltage capacitors with large capacities and of pulse shaping technology, allowed new Z pinch regimes to be explored by researchers and as was explained above they are now primarily studied as radiation sources.

Studies of the stability of the compressional pinch and the occurrence of strongly radiating hotspots in the plasma focus are presented in this thesis and these devices are discussed in the following sections.

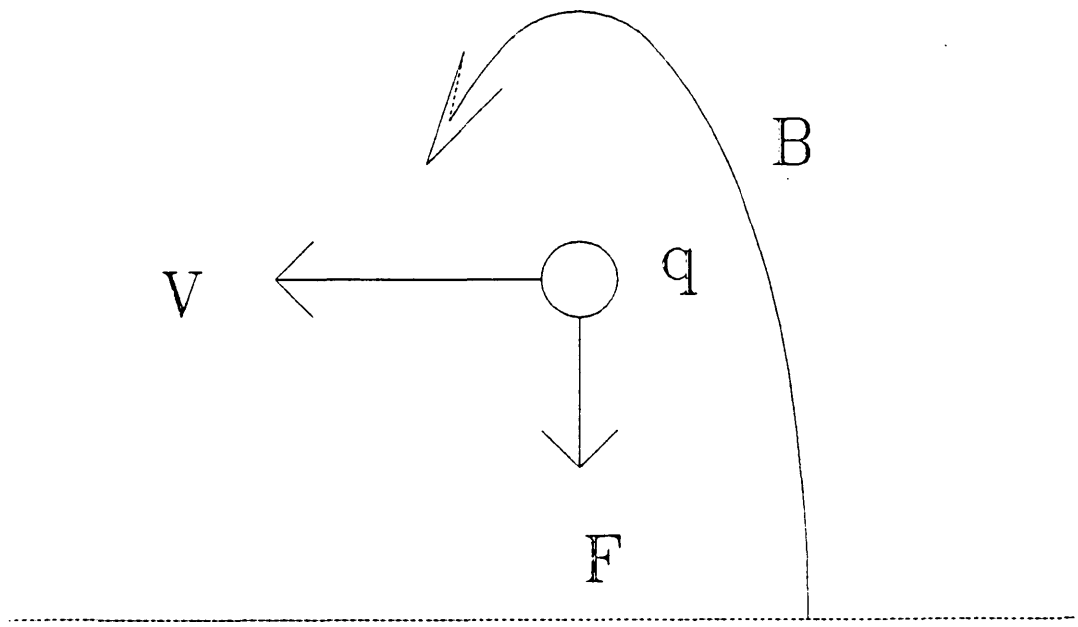
1.2 The compressional pinch: A review

The compressional pinch is simple in concept and implementation (figure 1.2). A large voltage is applied across an insulating tube containing gas at low pressure. Breakdown occurs first on the wall and if the rate of rise of current is sufficiently large the sheath will implode accreting and ionising the gas ahead of it.

Any gas may be used but this thesis deals only with hydrogen and argon. Hydrogen is favoured because the more tractable atomic physics makes more interpretation possible. The plasmas produced in compressional pinches can have



a)



b)

Figure 1.1: Fluid and particle models of the pinch effect

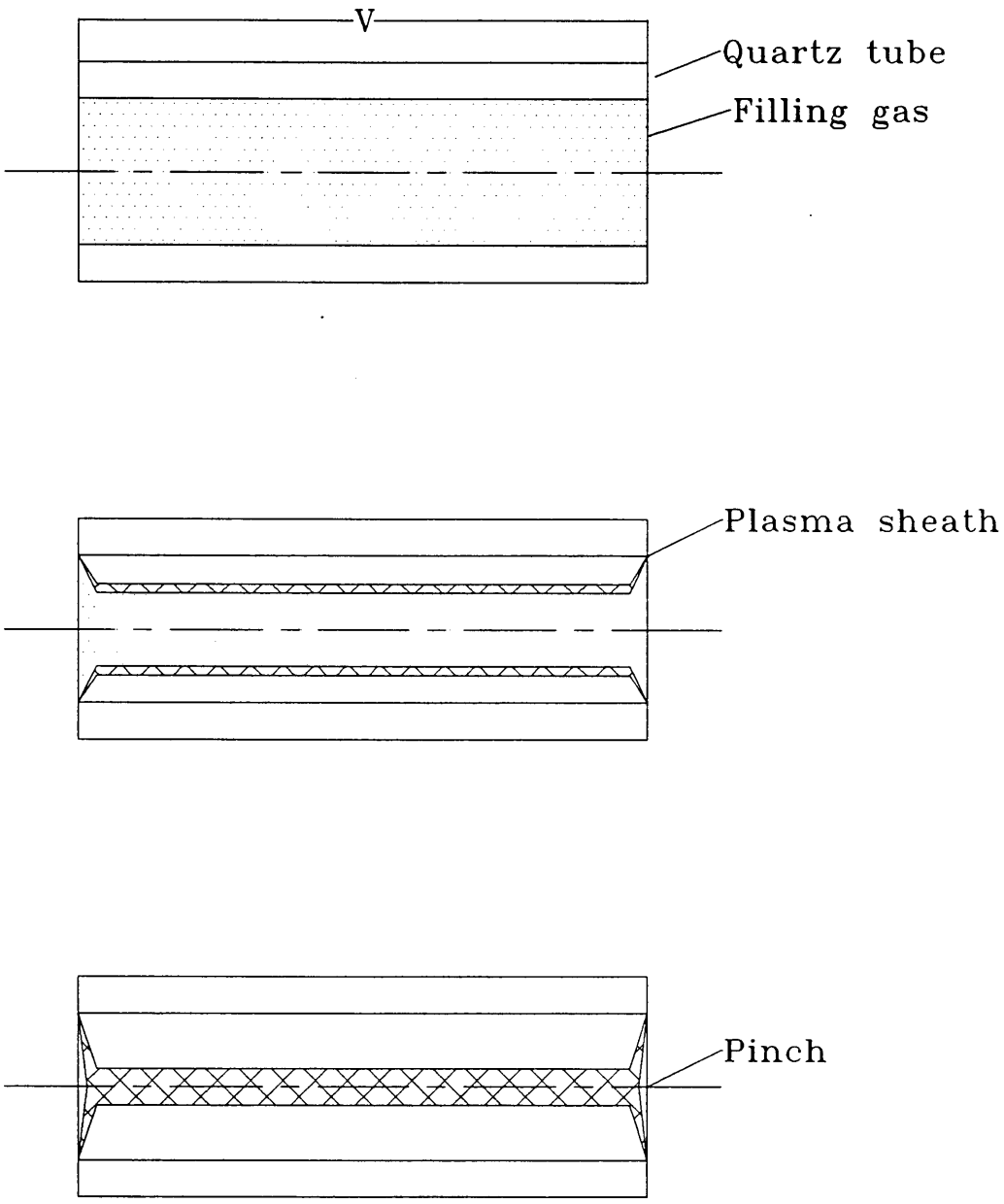


Figure 1.2: The compressional pinch is formed in a quartz tube which is initially filled with gas at low pressure

a large range of densities, temperatures and lifetimes. Low density, low current pinches are used by spectroscopists and others as ion sources but are of little relevance to the work in this thesis. The pinches we refer to here are produced by pulsed current sources supplying about $100kA$. These produce plasmas with densities of order $10^{23}m^{-3}$, temperatures about $100eV$and lifetimes of a few hundred nanoseconds. These are particularly interesting for stability studies relevant to possible fusion schemes.

Figure 1.3 shows an end-on streak photograph of such a pinch. The camera is looking though a slit at the end of the pinch tube. The position of the walls of the quartz tube are marked. The image is then streaked from left to right. Thus we can observe the radial motion of the plasma. The life of the pinch has three parts. First the plasma sheath forms on the walls and then it detaches and collapses in (run-down). When the run-down is complete there is a uniform pinched column on axis. This is the pinch phase. Finally the plasma expands until it fills the tube and is no longer confined.

1.2.1 The collapse

A plasma was first observed to detach from the walls of the vessel and implode in a toroidal device (Thonemann and Cowig (1951) and Cousins and Ware (1951)). In 1952 plasma physics was classified and when it was declassified in 1958 the pinch effect was well known in both linear and toroidal vessels. The collapse phase was first modelled by Rosenbluth (1954).

Rosenbuth's snowplough model assumes that all the mass is swept up and accreted onto a thin current carrying shell which implodes under the magnetic force of the current. The model neglects plasma pressure. This simple model is capable of analytic solution (Krall and Trivelpiece) and states that with a constantly rising current the shell will hit the axis at :

$$t_p = 1.5\left[\frac{2\pi\rho_0 a^3}{\mu_0 \dot{I}_0^2}\right]^{1/4} \tag{1.2}$$

$$\rho_0 = initial\ mass\ density$$

$$\dot{I} = initial\ rate\ of\ rise\ of\ current$$

$$a = initial\ radius$$

A major limitation of the snowplough model is that it does not give any spatial structure. Allen (1957) provided this using a $1d$ plane shock model. This was improved on by the slug model which was proposed by Potter (1978) and has a cylindrically imploding shock. The name 'slug' may come from the long plasma

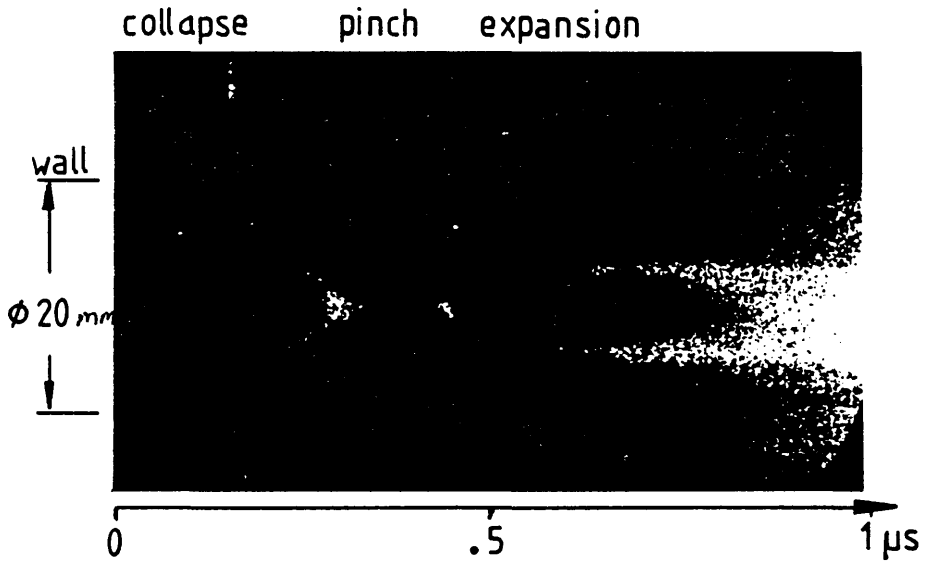


Figure 1.3: A streak photograph, 1 torr argon, 1 us full screen.

elements used in the numerical model. The model applies the Rankine-Hugoniot conditions to a strong shock which is driven by a current carrying plasma sheath known as the magnetic piston. Material is accreted on the surface of a magnetic piston as it collapses in and the shock ionises the gas ahead of it. The model assumes that the pressure between the shock and piston is constant in space but not time. This model predicts both the time to pinch and the final radius of the pinch; for a constant current hydrogen pinch:

$$t_p = 0.377\ (\rho_0/\mu_0)^{1/2}\,\frac{4\pi a^2}{I} \tag{1.3}$$

$$r_p = 0.309\ a \tag{1.4}$$

$\rho_0 = initial\ mass\ density$

$r_p = pinch\ radius\ when\ the\ shock\ hits\ the\ axis$

$I = current$

$a = initial\ radius$

The slug model stops when the shock hits the axis but the shock may reflect from the boundary causing an expansion of the pinch and subsequent oscillations. These were observed by Bodin et al (1960) who reported a $360kA$ compressional pinch. This was driven by a capacitor bank and this current was reached after $600ns$. It was found that after the first compression at $1.2\mu s$ the current flowed in a plasma on the wall of the vessel caused by irradiation from the plasma and not in the pinched column. They concluded that in low power pinches the compression took so long that the pinch was disrupted by instabilities before high temperatures were reached and that in higher power pinches the wall effects prevented the formation of a thermonuclear plasma.

With the development of pulse power new compressional pinch experiments were performed. Choi et al (1969) used a 3Ω pulse line supplying $60kA$ to produce hydrogen pinches. In these the magnetic piston and shock predicted by the slug model are clearly visible on streak photographs and no current loss or pinch bouncing was observed. Christie (1981) using a numerical simulation of this experiment showed that the presence of a conducting boundary at the wall due to the wall plasma prevented the expansion of the plasma by trapping the pinch flux.

1.2.2 The pinch

In the pinch phase there are two plasma characteristics of interest, the radial dynamics and the mhd stability. Experimentally this becomes 'does the plasma expand?' and 'do we see a $m = 0$ or $m = 1$ instability?'. The radial dynamics have been modelled first by Christie (above) and later by Culverwell et al (1989).

Both these investigators concluded that the conductivity of the wall plasma has a major effect on the expansion rate of the pinch, by trapping flux.

Z-pinch stability theory is applicable to all Z-pinches not just those produced by the compressional pinch and is discussed in detail in the next section. As was stated above compressional pinches were quickly seen to be unstable to $m = 0$ instabilities. With the arrival of pulsed power we can now make high density and temperature compressional pinches which are in a different stability regime. A $60kA$ pinch was reported by Choi et al (1969) and a $130kA$ pinch by Haines et al (1986).

Haines et al (1986) present end-on interferograms. These show that the line density of the pinch corresponds to the filling density and remains constant for 500 ns. These results are considered by Culverwell et al (1989). They use a $1d$ numerical simulation to show that if the pinch current falls the pinch should expand due to the inverse skin effect (Haines 1959)). Such an expansion is not observed so they predict that the pinch current and hence the plasma temperature remain high due to a current crowbar through the wall plasma. If this is correct then the pinch is anomalously stable.

The interferograms are end-on and made through hollow electrodes. It is likely that plasma flows out of the electrodes during the pinch and that the measured value of the line density is higher than the true value. In this thesis side-on interferograms are used to give accurate measurements of line density.

Baldock and Dangor (1988) report further work on the same 130 kA pinch. The soft xray emission from the end of the pinch is imaged through two filtered pinholes and streaked. Temporal and spatial profiles are deduced from the intensity ratios. The error in the derived profiles is large because of the small signal and the difficulty in spatially deconvolving the signal which comes from an extended source. The most important result is that the temperature of the pinch is 170 ± 20 eV for a 100 ns period during the pinch. This is the Bennett temperature corresponding to the initial filling pressure. These authors did not make direct observations of the stability of the pinches they produced. The diagnostics they used were end-on and would not necessarily detect an instability.

The final expansion of the pinch could be due several factors such as a cool wall plasma no longer trapping flux , a falling current or the growth of an instability.

This thesis will present side-on interferograms and framing photographs. Side-on interferograms have the advantage that they may detect plasma instabilities where this is not possible in the Z pinch with end-on diagnostics. The motivation for these experiments is described further in the next section.

1.2.3 Stability of Z-pinches

MHD theory is most easily applied to hydrogen or hydrogen-like plasmas because otherwise the presence of partially ionised elements provides sources and sinks of energy which must be accounted for. The following papers and results were all obtained for fully ionised plasmas usually of hydrogen.

Kruskal and Schwarzchild (1954) first predicted that the Z-pinch was an unstable plasma configuration and this was later observed to be true by Carruthers and Davenport (1957)($m = 1$ kink mode) and Curzon et al (1960)($m = 0$ sausage mode).

Many researchers considered mhd stability a prerequisite for a fusion plasma and for this reason the Z pinch was quickly discarded. Figure 1.4 shows how it is prone to sausage ($m = 0$) and kink ($m = 1$) instabilities. In 1.4a we see that if there is a dent in the plasma boundary $B_\theta(r)$ becomes stronger and the dent increases. This unstable situation results in the plasma necking off. In a linear theory applied to a long pinch the resulting plasma looks like a string of sausages. The kink instability arises in a similar manner. A gross displacement of the plasma is increased by the resultant field. This may result in a helical plasma. The letter $'m'$ is the azimuthal mode number. This appears in simple linear theory where one can write the perturbation of a plasma element as:

$$\vec{\xi}(\vec{r},t) = \vec{\xi}(r)\ Re\{e^{\gamma t + i(m\theta + kz)}\} \tag{1.5}$$

Haines et al (1989) show that for a pinch in Bennett equilibrium (eqn. 1.1) all important dimensionless parameters can be written in terms of $radius \times (current)^4$ and line density. Figure 1.5 is a stability diagram which shows regions of the aI^4, N plane defined by these three factors. A plasma is collisional if an ion cannot complete an orbit around a field line before it has a collision with another ion. The theory of collisional plasmas is easier than collisionless plasmas because collisions cause the distribution functions to be maxwellian and the pressure tends to be isotropic. However Z-pinches of current interest are usually collisionless.

If a plasma is cold or sufficiently dense then it may be resistive. The resistivity of the plasma allows magnetic field to diffuse through it. The ratio of the timescales for convection and diffusion of magnetic field lines through the plasma is called the Lunquist number S. At sufficiently low $S(< 100)$ the plasma may be stabilised (Culverwell et al (1989)). The compressional pinch investigated in this thesis has $S = 1600$ and is not resistive.

To apply a fluid model to a magnetised plasma requires that the particle motions occur on a scalelength much smaller than that of the bulk plasma. This is a strong restriction which is seldom, if ever, satisfied. Even if it holds for the

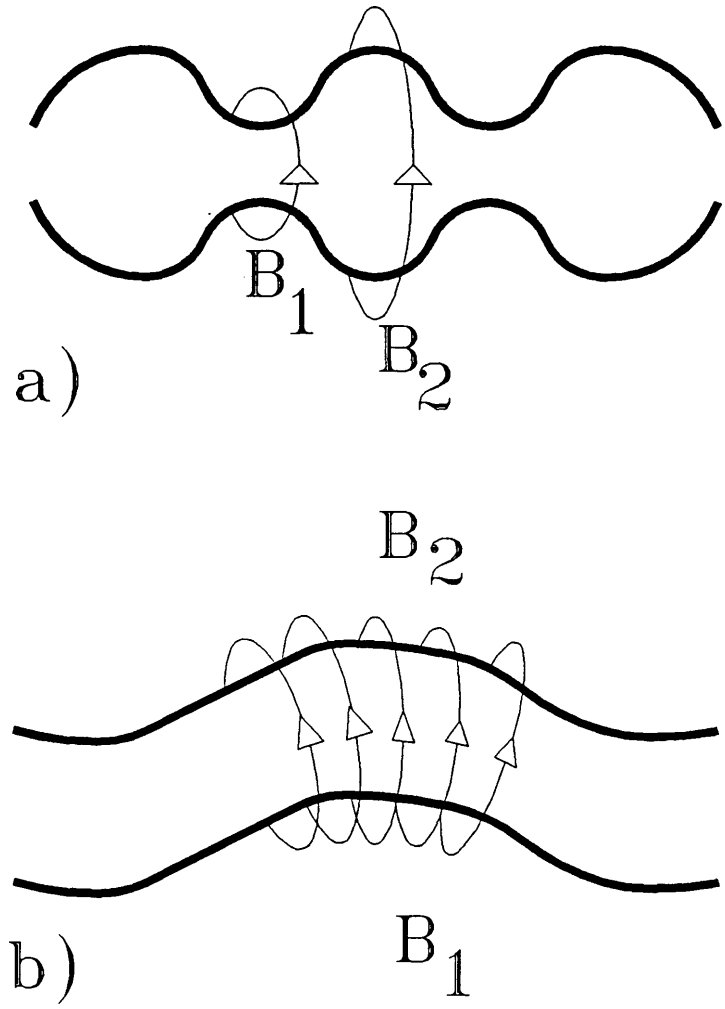


Figure 1.4: B1 > B2
a) The m = 0 (sausage) instability
b) The m = 1 (kink) instability

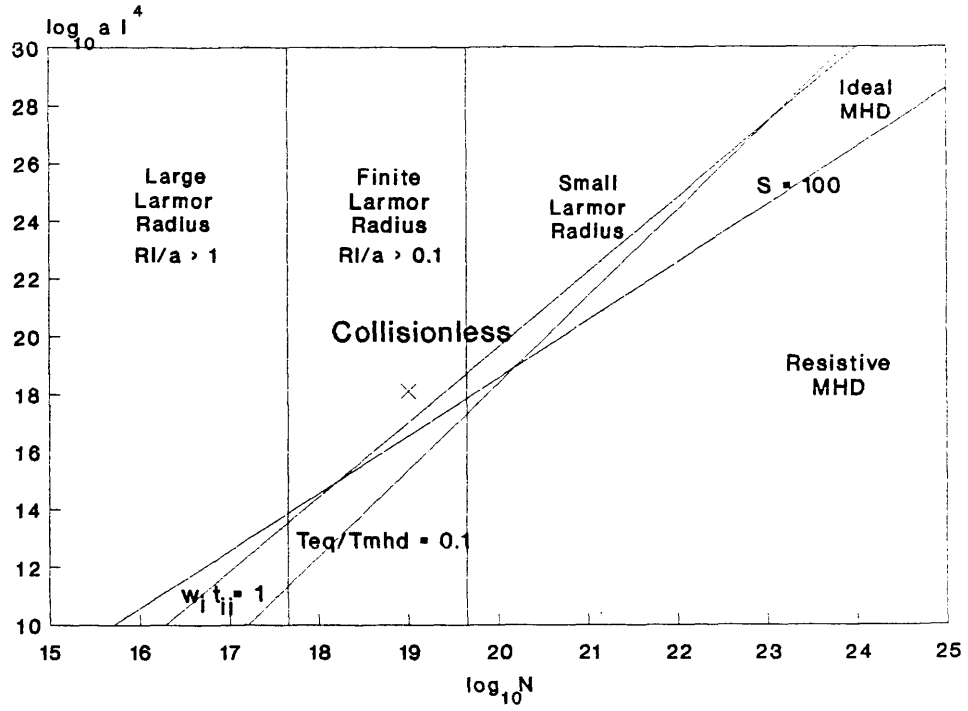


Figure 1.5: The Haines Coppins diagram of stability regimes of the hydrogen Z-pinch.

majority of the particles in the plasma there may be some particle with betatron ~~resonant~~ or singular orbits (Haines 1978) for which it is not true.

In the collisionless Z pinch an important particle scalelength is the ion Larmor radius. If the ratio of ion Larmor radius to pinch radius $a_i/a = 0$ then the pinch may be described by the model of Chew, Goldberger, and Low (1956) (the CGL model). If $a_i/a \neq 0$ then the regime is called finite Larmor radius (FLR). In some toroidal devices FLR effects have been observed to stabilise the plasma and as was mentioned above, Culverwell et al (1989) claim to observed enhanced stability in a 130 kA compressional pinch. FLR stabilisation is very important for new fusion schemes and it is investigated in this thesis. In the 'large Larmor radius' regime, where the ion radius is greater than the pinch radius little is understood.

1.3 The plasma focus - A review

1.3.1 The focus experiment

The plasma focus is a Z pinch which resembles the compressional pinch in several respects. The focus geometry is shown in figure 1.6. As in the compressional pinch a large voltage is applied across an insulator. This results in a breakdown through the filling gas on the insulator surface. The plasma sheath is detached and accelerated up the inner electrode by the $\vec{j} \times \vec{B}$ force. This long run-down is an important feature of the plasma focus as it enables a large amount of energy to be taken from a slow capacitor bank. A difference between the compressional pinch and the plasma focus is that the focus sheath is mhd stable during this run down. In a large machine with a high temperature sheath ($30eV$) and a long run down time ($1\mu s$) this may be necessary. However at high powers other, possibly thermal, instabilities cause the sheath to break up. At the end of the run down the large plasma sheath runs across the flat surface of the anode to form a small pinch. It is this which gives it its name of the plasma focus. Potter who developed the slug model of the compressional pinch also developed a numerical simulation of the working of a plasma focus (Potter 1971). An X-ray pinhole camera picture of a typical deuterium pinch is shown in figure 1.7.

The focus was originally developed independently by Filippov et al (1962) and Mather (1965)) and for many years has been studied as a possible nuclear fusion reactor. However recent experiments such as the SPEED 2 machine in Düsseldorf and POSEIDON at Stuttgart have indicated that the scaling of neutron yield is not favourable at high powers (Kies 1987). These machines produce about 10^{11} neutrons per shot, 90% of them are due to beam target interaction of accelerated deuterons with thermal ones (Herold and Jager 1987). Indeed in the SPEED focus it is fast ions that dominate its behaviour. The pinch is unusually stable, in some shots a pinch has been observed for over 100 ns when the peak current was over

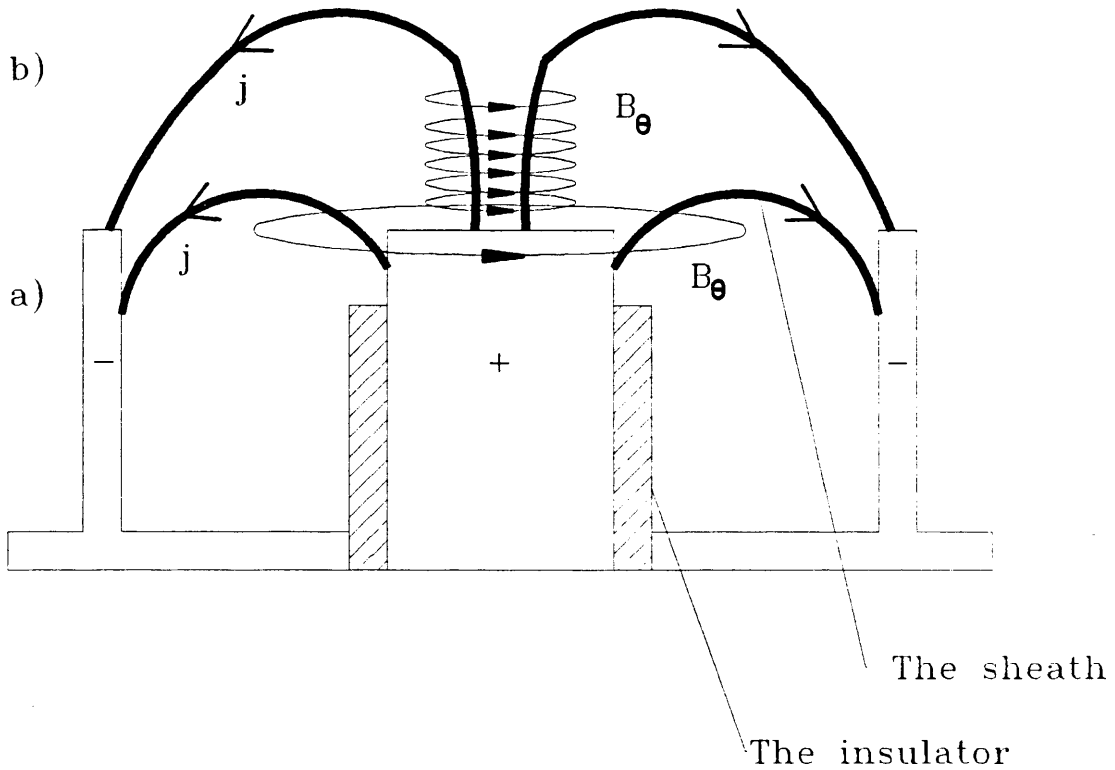


Figure 1.6: The plasma focus
a) The accelerating plasma sheath
b) The pinch

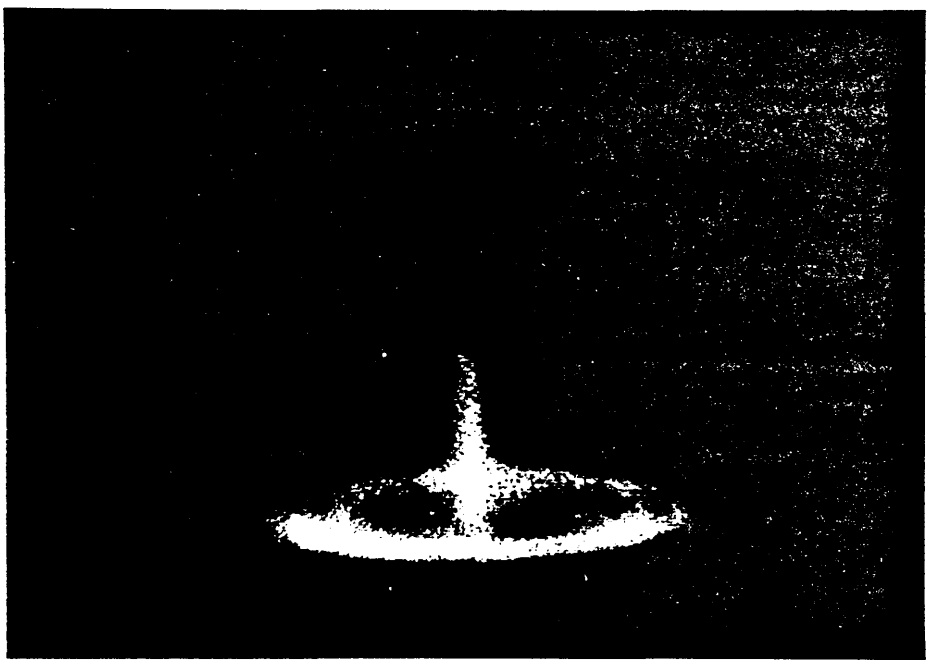


Figure 1.7: A x-ray pinhole photograph of a deuterium plasma focus pinch.

$1MA$. These machines are now used to study hotspots which are a phenomenon of contemporary interest and are investigated in this thesis. Existing studies of these hotspots are reviewed in the next section.

1.3.2 Hotspots

Small transient X-ray sources of great power have been seen in many dense Z-pinch experiments such as plasma foci, gas puffs, vacuum sparks and most recently deuterium fibre pinches. These have been called hotspots or plasma points. Previous results and papers were reviewed by Deeney (1988). These hotspots are small dense regions in the bulk plasma. Measurements have shown that they may have densities and temperatures ten times that of the background plasma values. Densities of $10^{27} - 10^{29} m^{-3}$ and temperatures of $1 - 10keV$ have been reported (Deeney 1988). These hotspots have been proposed as a source of neutrons in the focus (Vikhrev 1986).

Various mechanisms have been suggested for the formation of hotspots, these include radiative collapse, electron beam energy deposition, and $m = 0$ instabilities. These processes will be briefly reviewed. It is possible that in any particular Z-pinch experiment a combination of these processes take place. The appearance of hotspots in pure deuterium fibre experiments is particularly interesting because line radiation can play no part.

Pease (1957) and Braginksii (1958) developed theories of the radiative collapse of a Z pinch. The idea is simple, above the Pease-Braginskii current when the radiative power of a pinch exceeds the ohmic heating, the thermal pressure will be exceeded by the magnetic pressure and the pinch will contract. This contraction will increase the density and consequently the radiation losses. Shearer (1976) considers a collapse whose velocity is less than the ion sound speed (ie the pinch will remain in pressure balance) and shows that the collapse is isothermal for a constant current. Vikhrev (1986) uses a $1d$ code which includes a varying current, electron degeneracy and blackbody radiation. This shows an increase in density and a drop in temperature. A similar result is obtained by Chittenden (1989) who shows that in a one dimensional simulation the collapse will be terminated by free-free opacity or electron degeneracy. A real radiative collapse may be two dimensional in which case we would have to consider the effect of particle outflow.

Some Z pinches are unstable to mhd instabilities. As stated above the $m = 0$ instability makes the column "neck off". If the plasma collapses under pressure balance (Bennett relation holds) with a constant current then the temperature will rise due to the decreasing line density if material is ejected from the constriction. Although the line density decreases, the particle density may increase resulting in a hot, dense region. Such hot constricted regions have been proposed as hotspots.

(Vikhrev 1977, Sethian et al 1987).

It should be pointed out that both the radiative collapse and $m = 0$ models neglect the details of current flow to a greater or lesser extent. If such a constriction or collapse took place within a bulk plasma it is possible that the current would flow around the high inductance of the hot spot removing the magnetic pressure and terminating the collapse.

A fundamentally different mechanism of hotspot formation has been proposed by Lee (1975) and others. It is suggested that intense electron beams which have been observed in many Z-pinch devices may be focussed by a plasma constriction to form hotspots by direct heating. This theory is strongly supported by Deeney (1988) who finds a correlation between electron beam activity and hotspots in the gas puff and focus.

Hot spots are not observed in pure deuterium focii but have been reported when trace quantities of argon are added to the filling gas (Deeney 1988). Attempts to add argon into the filling gas of the SPEED 2 plasma focus in Düsseldorf were unsuccessful because this prevented the formation of a good sheath (Kies 1989).

1.4 Aims and results

The primary aim of the author has been to study the occurrence of instabilities in pinch plasmas. To investigate the stability of a pinch in the finite Larmor radius (FLR) regime a compressional pinch apparatus was developed. This required substantial modification of an existing current generator. These modifications and the design of the pinch assembly are presented in Chapter 2. Chapter 3 describes the diagnostics used to study of pure hydrogen and argon pinches and includes the development and application of a new holographic interferometric system. The results are presented in Chapter 4 and our interpretation in Chapter 5.

Chapter 6 contains details of the study of hotspot instabilities of argon-deuterium plasmas in the SPEED2 plasma focus in Düsseldorf. We present the design of a system to stream argon through the anode in front of the collapsing sheath and our observations of the resulting pinches. The diagnostics used included, time integrated and time resolved x-ray spectroscopy, PIN diodes, X-ray diode, pinhole cameras, and X- ray streak photography.

The last Chapter (7) discusses the results obtained and makes suggestions for future work.

CHAPTER 2: THE COMPRESSIONAL PINCH APPARATUS

2.0 Introduction

To do the experiments described in the later chapters it was necessary to design a new load chamber for a transmission line pulse generator. The generator itself had to be modified to produce higher currents more reliably.

This chapter is divided into two sections; the first part deals with the modifications to the generator and the second part the design and implementation of the load chamber.

2.1 The current generator

The current generator is shown in figure 2.1 and important values given in Table 2.1. Functionally it consists of four components, Marx, pulse forming line (PFL), transfer section and load chamber and the interfaces between them. The electrical energy is supplied from a Marx. When this erects it charges the pulse forming line (PFL) which is a section of 3Ω water filled transmission line before the gas switch. The gas switch is by-passed by a resistance of 400Ω so the transfer section is charged to a small fraction of the PFL voltage. This is sufficient to preionise the pinch gas. The gas switch is pressurised so that it is overvolted as the PFL reaches 80% of its maximum possible charge. The current then flows down the transfer section into the load. The water filled transmission line current generator has several advantages over a capacitor bank; the current is supplied from an high impedance and is not dependent on the dynamics of the plasma and the square output pulse has a faster rise time and higher power than could be obtained from the capacitor bank. These factors can outweigh the disadvantage of using a line, which is that the maximum current into a short circuit load is less than from a capacitor bank.

The marx generator has $8 \times 0.5\mu F$ BICC capacitors. These are charged in parallel though copper sulphate resistors. The column of gas switches is pressurised with nitrogen and is triggered by a $10kV$ pulse from an air cored transformer driven by a thyratron. The jitter between the pulse and the marx erecting is large ($2.3\mu s$) but this does not matter as trigger pulses for diagnostics are taken from later in the system. The marx is enclosed in a Faraday cage of wire mesh ($1\ cm^2\ holes$). This has two purposes: to reduce the electrical noise from the gas switches and to reduce the inhomogeneous field configurations which arise from the stray capacitance of a marx to its surroundings.

The marx is connected to the PFL by a steel hose which connects to an electrode in the centre of a perspex sheet $1.21\ m$ ($4\ foot$) square. The $7.9\ \mu H$ inductance of the marx is distributed between the inductance of the capacitors

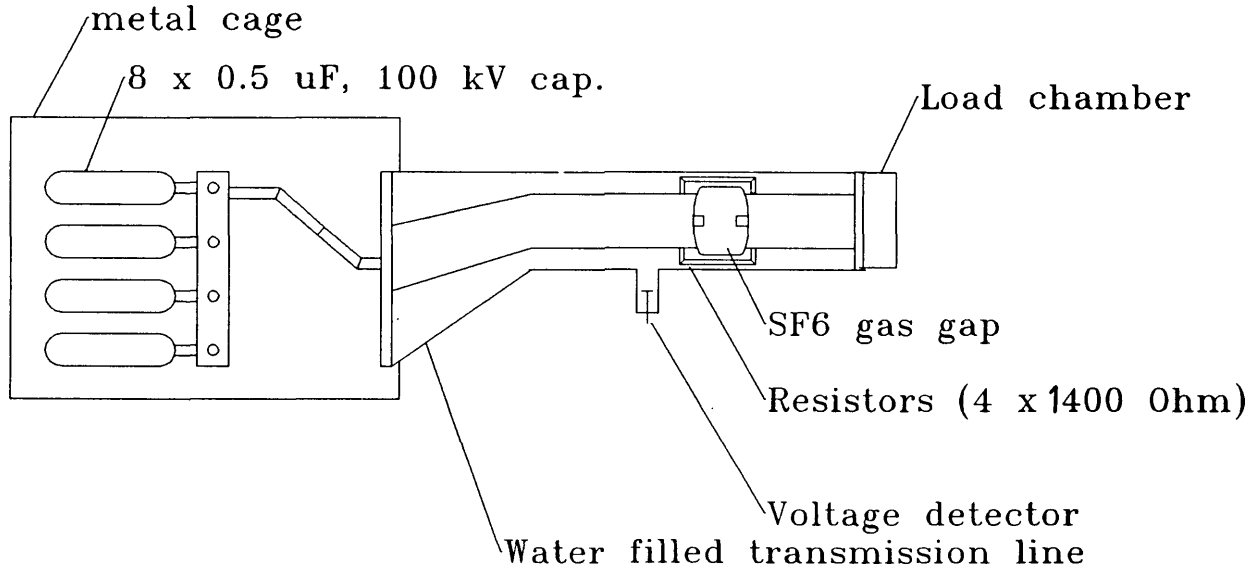


Figure 2.1: The current generator

Output parameter	
Peak current	150 kA
Risetime	70 ns
Flat top	100 ns
First I = 0	260 ns

Marx parameters	
Capacitors	8 x 0.5 μF BICC 100 kV
Maximum working voltage	70 kV
Trigger delay	2.3 μs

Line parameters	
Impedence	3.2 Ω
Dielectric	deionised water η > 1 MΩ cm
Max. working switch pressure	3.5 bar absolute
Outer diameter	15''

Chamber	
Diameter	0.25 m
Electrode inductance	43 nH

Table 2.1 : Current generator parameters

and switches and the inductance of the feed. Breakdown at this interface was a major problem and limited the maximum current which could be safely obtained from the line to about 100 kA. The modifications to this interface are discussed in the next section.

The PFL and the transfer line are separated by a gas switch the filling pressure of which is between 1 and 3.5 *bar absolute*. This determines the voltage at which the gap breaks down. The breakdown voltage is chosen to be 80% of the maximum voltage in the absence of a switch. By overvolting the switch in this way the jitter is reduced to only 10 ns.

Capacitive voltage dividers are used to monitor the performance of the line. There is one 3 ns from the pinch and another before the gas gap. The latter is the most important. The signal from this monitor is used to trigger a circuit which gives the trigger pulse for all the diagnostics.

The line is filled with deionised water. This is used because of its high dielectric constant (80) which gives a long pulse length ($c_{water} = 1/9\ c_{vacuum}$). The water is kept pure by constantly pumping it through barrels of deionising resin. A resistivity of 1 $M\Omega\ cm$ resulted in a 15% loss during the charging of the PFL.

2.2 Modelling the line with BERTHA

In the attempt to stop the breakdowns across the line-marx interface a system of resistors and switches were employed. Before these were installed their effect was modelled with a computer program called BERTHA. This allowed the optimum values to be chosen. This program is briefly described here.

BERTHA is a computer program written by Naval Research Laboratories (Washington). It allows the transmission line user to construct a model of his experiment by using standard line sections and junctions. The code lets the user put resistors between junctions and to ground. Variable impedance elements and switches are also catered for. The major restriction is that the lines cannot be lossy so the resistive loss in a section must be modelled by a junction resistance and this introduces a small error. The code is voltage following and calculates the reflections at each junction. The program stores large amounts of data and initially this limited us to a time step of 10 ns on the college mainframe. However we have rationalised data storage and output and a 1 ns time step is now possible. This is important because as can be seen from figure 2.2 the dummy sections are required for modelling switches. These are one time step long and if these are a significant fraction of the line transit time the model is disrupted. 1 ns is only 4% of the shortest relevant section, 10 ns is 40% and is not acceptable. The next section details the modifications to the line and where BERTHA was used to decide a value this is stated.

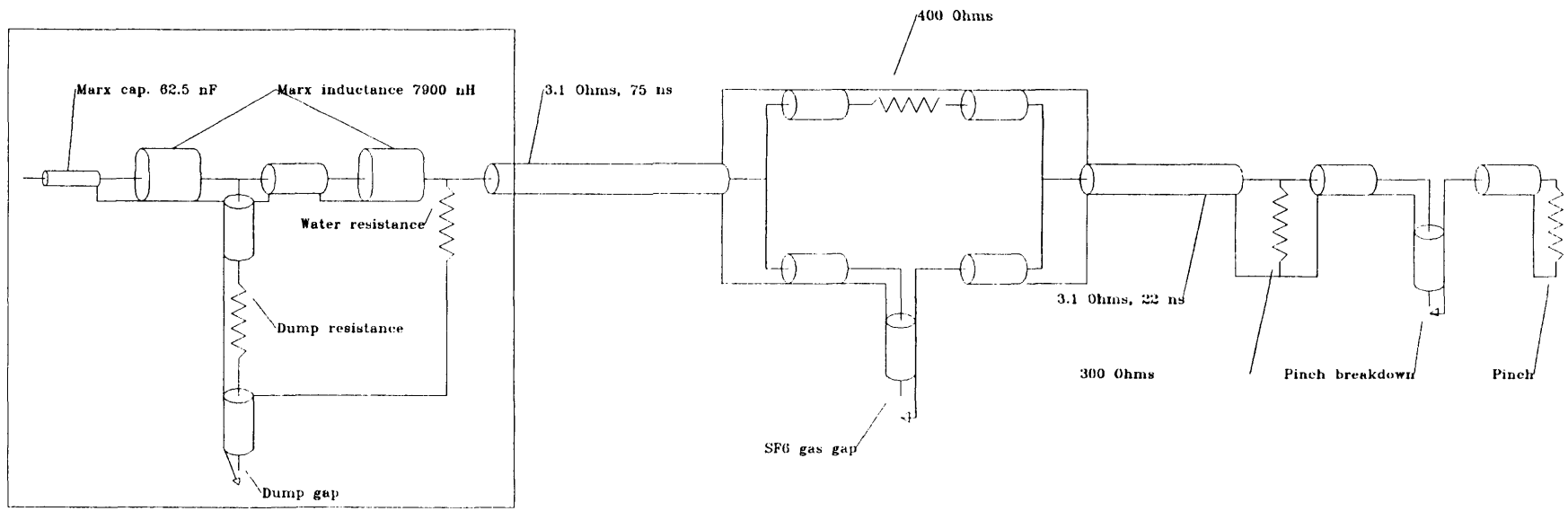


Figure 2.2: The transmission line model used in BERTHA

2.3 Improvement of the line-marx interface

To improve on previous experiments it was necessary to get shots with a peak current of $150kA$. Unfortunately at the higher voltages that this requires, streamers formed across the perspex interface between the marx and line. Figure 2.3. This did not affect the current obtained because the streamer connects after the pinch is over. However continued tracking across the surface may result in severe mechanical damage to the interface. If it should fail the water line would empty over the marx. To attempt to remove this problem the line was extensively modified. Initially we tried to improve the performance of the existing perspex sheet. A large diameter perspex pipe was fitted over the central conductor and cemented to the sheet. Unfortunately the streamers tracked over the tube and eventually the streamers passed though the joint between tube and sheet causing severe damage. Spraying the sheet with anti-corona spray and coating it with transformer oil were similarly unsuccessful and it was decided that a new surface was required.

The pinch experiment is over about 1300 ns after the initial voltage rise but the voltage stays on the line for many microseconds. This is because the capacitance of the line must discharge through the resistance of the water in the line. To remove this voltage we fitted a self-breaking water switch between the feed and earth. The switch is in series with a resistor and the separation of the electrodes is chosen so the gap closes at an appropriate time. This is shown in figure 2.4. To choose the best value of the dump resistance the line was modelled with the code BERTHA.

To increase the stand off voltage it was decided to replace the old perspex because this was badly damaged by tracking. We decided to place a new perspex sheet on top of it separated by a spacer. This volume was filled with conductive copper sulphate solution and acted as a distributed resistor across the interface (figure 2.5). For the dimensions of our resistor the resistance is 10.2 $\eta_{CuSO_4\ (aq)}\ \Omega$. This resistor should grade the field across the interface. Similarly, if a streamer forms on the surface the electric field at its tip is reduced by charge flow in the conducting fluid that is nearby. The effect of this damping resistor on the voltage history was modelled with BERTHA.

The third modification was to reduce the fields on the conductors. The bolts used to fix the perspex to the line were shielded by 40 mm diameter copper pipes and the central conductor had a hemisphere fitted to the interface. This reduced the radial field at the interface.

2.4 Results - modifications to the marx-line interface

Here we describe the effects of the several modifications and discuss the im-

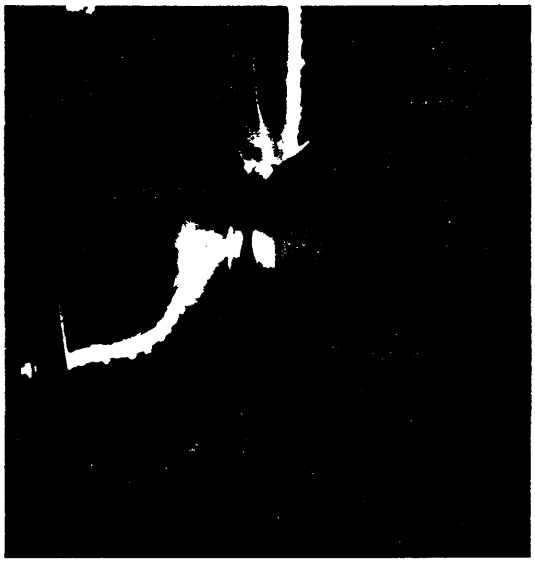


Figure 2.3: Streamers on the marx-line interface.

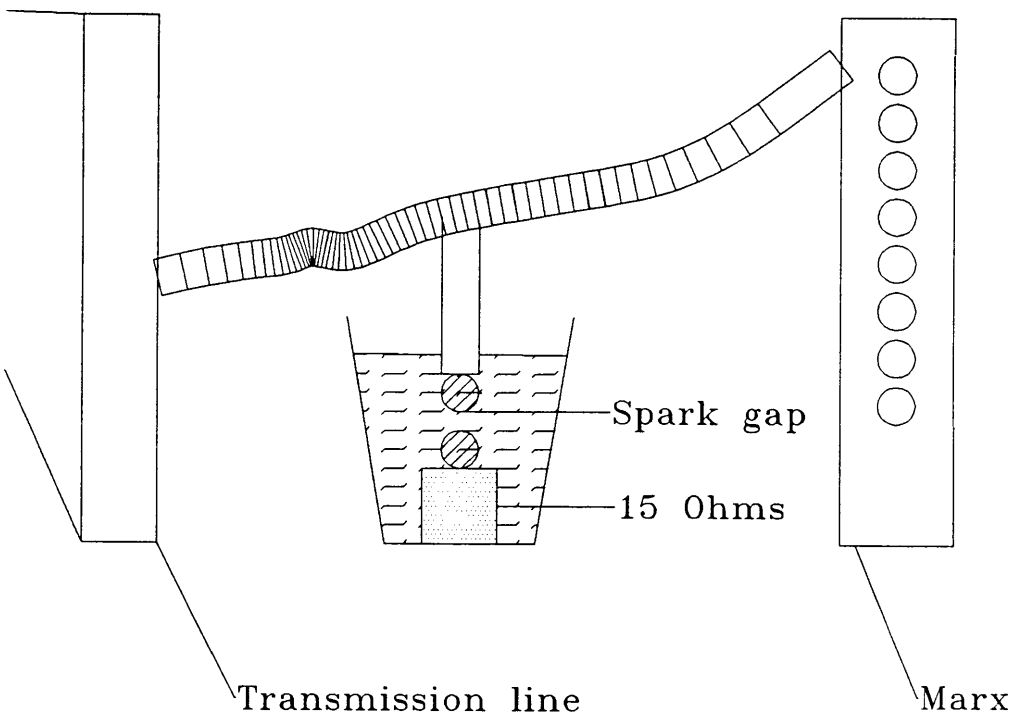


Figure 2.4: The dump gap at the marx-line interface

plications.

2.4.1 Surface treatment

It is frequently stated that the surface quality of an insulator is a very important factor in determining whether tracking will occur. It is known that microscopic surface impurities and dissolved gases can cause enhanced microfields and produce avalanche electrons. For this reason we took great care to remove burns from the interface with abrasives. However photographs showed that the tracking on successive shots was not in the same place and it did not matter whether burns were removed or not.

The failure of the clean perspex to hold off the voltage induced us to try surface coatings. First we tried RS anti-corona spray. When a streamer forms the coating liberates halons which are strongly electrophil ic and prevent the avalanche proceeding. This did not work so we coated the surface with vacuum pump oil. This also includes halons but also excludes dissolved gases from the surface. This was also unsuccessful. It is interesting to note that although streamers across the oil left highly carbonised regions these did not break down preferentially on later shots.

The one surface treatment which was partially effective was white petroleum jelly (Boots the Chemist). To exclude air from between the electrode and the interface the region was packed with jelly. All breakdowns started from the rim of the electrode not the smaller higher field region where it passed though the sheet. One photograph showed the electrode covered in jelly and a streamer going across it to the bare metal.

2.4.2 Electrodes and shielding

From Maxwell's equations it can be shown that the radial field inside a cylindrical coaxial transmission line goes as :

$$E = V/(a \ln(b/a)) \tag{2.1}$$

where a is the radius of the inner conductor and b is the radius of the outer. This has a minimum for $a = b/e$. For this reason the electrode at the interface with the sheet was enlarged to 56 cm. This reduced the field at the surface from 28 kV/cm to 20 kV/cm only 5% above the $1/e$ value. The interface was packed with petroleum jelly to exclude air. The new electrode did reduce the number and severity of the streamers but did not allow an increase in the operating voltage.

The heads of the bolts which attach the sheet to the line were covered by 40 mm diameter copper pipes. These formed an effective shield and streamers no longer terminated on the bolt heads. This reduced the severity of local damage.

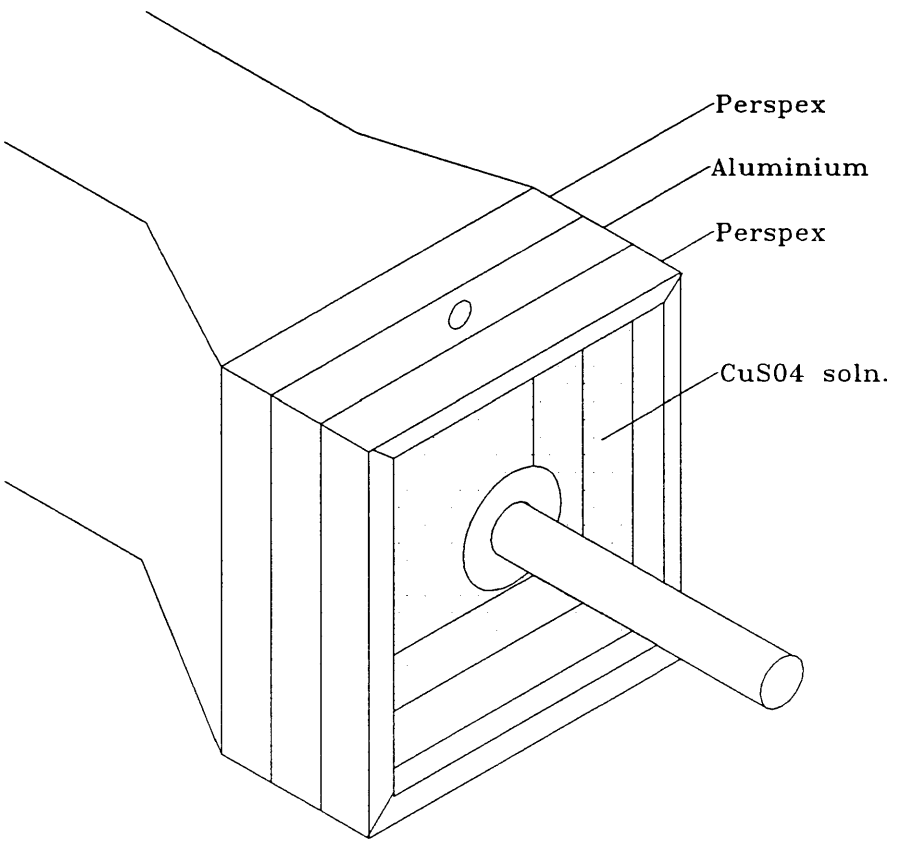


Figure 2.5: The distributed resistor at the line-marx interface

2.4.3 Moving the marx

To install the dump gap it was necessary to move the marx back in the cage. This was to prevent breakdown from the marx to the dump. By use of a block and tackle the entire marx was lifted by the top three capacitors and moved back 1 m. This made no difference to the rise time of the signal as the system is dominated by the inductance of the capacitors not the feed.

2.4.4 Distributed resistor

Unfortunately it was found that although this resistor effectively damped the line, it did not prevent breakdown. The copper sulphate solution was replaced with deionised water to prevent current loss.

2.4.5 Dump gap

To remove the energy from the line after the experiment a dump gap was installed. This consisted of an electrode pair in a large vessel of water. A series resistor connected the electrodes to ground as was shown in figure 2.4. This resistor was entirely under water to prevent tracking across its surface. The three values of resistance tried were 30, 15 and 10Ω. The current flowing in the dump was monitored by a single turn coil, the output of which was integrated by an RC circuit. The current which flowed in the gap was found to be proportional to $1/R$ showing it was working in the correct way. However the value of the resistance did not strongly affect the damping of the line. Modelling the line with BERTHA showed that the inductance between the dump gap and the interface reduces the damping of the line by the dump. This prompted us to minimise the inductance by placing the dump gap as close to the interface as possible.

The electrode separation was adjusted until the dump gap closed at the correct time. Figure 2.6 shows a current trace and photograph of the interface without the dump gap and figure 2.7 is the corresponding photographs with the dump gap. It can be seen that the dump gap damps the current and is effective in stopping breakdown across the interface. Using the dump allows an improvement in safe operating voltage of 140 kV from 310 to 450 kV.

2.5 Discussion of transmission line modifications

Many modifications have been made. These have shown that neither the field grading resistor nor surface treatments were effective but the addition of the dump gap allowed the breakdown-free region of operation to be extended from under 100 kA to 120 kA. This is an increase of 20% in current but because the plasma temperature is proportional to I^2 this is a 44% increase in temperature. However perhaps the most important modification is the addition of a second perspex sheet. The line is now fail safe, even if the interface should crack only a

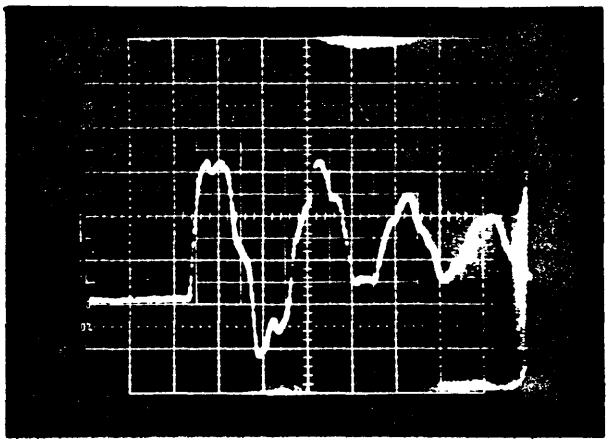




Figure 2.6: The current trace (100 ns, 30 kV/div) and the interface without the dump gap.

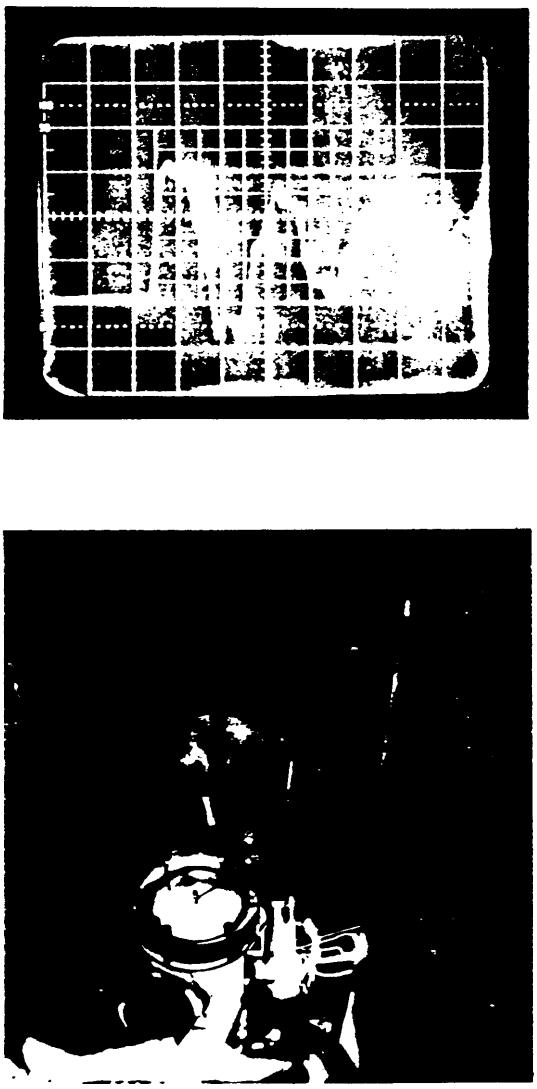


Figure 2.7: The current trace (100 ns, 30 kV/div) and the interface with the dump gap.

small amount of water can leak out of the line and it can be easily repaired. It was found that the line was very prone to breakdown across the perspex interface. With hindsight this is not surprising, as C. Martin states that the breakdown field in air, of a uniform field gap is,

$$E/(kV/cm) = 24.6p/(bar) + 6.7(p/bar)/(d/cm) \tag{2.2}$$

The separation of the inner electrode and the line outer is 56 cm and at a pressure of 1 bar this has a breakdown field of 25 kV/cm. The interface is not a uniform field gap, the presence of a tracking path massively degrades the stand off voltage. However it is interesting to compare the fields we can obtain with this figure. The marx has a maximum safe charging voltage of 70 kV per capacitor resulting in a line voltage of 450 kV producing 143 kA. Even with the new larger inner electrode this produces a surface field of 20 kV/cm.

This calculation shows that it is unlikely that the interface would ever have held off the maximum marx voltage in its original form and for reliability should be redesigned. Several modifications could be made which would interfere with the tracking mechanism. Perhaps the simplest would be to replace interface materials with a better one. Perspex has a very porous surface and is not ideal for high voltage work. When working at similar voltages the power companies use a reinforced resin such as TUFFNAL which has better properties. The surface could be grooved in such a way as to impede electron avalanche. If the interface were to be totally redesigned it would be made much larger and a low inductance dump gap would be incorporated. The high voltage feed need not be contained in air but could be in SF_6 or transformer oil either of which would eliminate the breakdown problem.

2.6 The new compressional pinch

Here we outline the design considerations which shaped the pinch and describe the final design. The pinch tube must be easy to fit and the system must make a good seal because a vacuum of 10^{-4} $torr$ must be attainable. To simplify the engineering it was decided to clamp the quartz tube between two O rings at the ends. This simple system had not been tried before because of the risk of mechanical shock waves breaking the tube.

It was originally planned to do a Thompson scattering experiment on the pinch. For this it is essential to have a beam dump. The optical path from the pinch to the beam dump must be as long as possible to improve the signal to noise ratio of the Thompson scattering by transit time isolation. The quartz tube requires the laser beam to be injected axially so the electrodes must be hollow and

it must be possible to put a dump behind the live electrode. In this experiment this position is within the transmission line. Figure 2.8 shows the engineering solution chosen: the vacuum system is extended within the line. The vacuum system and the pinch gas inlet valve are coupled to the pinch chamber by a X piece so that there is an unobstructed line of sight axially. The front of the hot electrode is removable and this allows the dump to replaced if it is damaged by the plasma.

The figure shows the return electrode is fixed to the front of a piston which slides in the load chamber, this enables pinch tubes of various lengths to be used. The return electrode contains a Regowskii coil, which gives a voltage that is proportional to the current derivative. The size of the coil was chosen to give a peak signal of about 500 V. The signal must be large to reduce the effect of noise but less than the voltage limit of the cable (1 kV). The $\dot{I}$ signal is integrated by an RC circuit, the whole system was calibrated and has a sensitivity of $31 \pm 5\%$ mV/kA. The calibration was made by discharging an high voltage capacitor thorough the electrode in series with a 1Ω resistor. The measured value is within 5% of that calculated.

The fronts of the electrodes which are in contact with the pinch tube are made of non- magnetic stainless steel and are detachable. This allows pinch tubes of different diameters to be used and the replacement of damaged surfaces. The inductance of the electrodes was measured to be 82 nH by using a copper bar in place of a plasma load. This is to be compared to a calculated pinch inductance of 43 nH. To ensure a good coupling of current into the pinch the chamber around the tube was filled with SF_6 which prevented a breakdown across the perspex interface.

2.7 Results - the new pinch assembly

The pinch performs well, the assembly is mechanically sound and there is not excessive electrical damage at joints. It was possible to take over 100 shots with out having to break the vacuum. The vacuum system is good, base pressures of 5×10^{-5} $torr$ have been obtained after a few hours pumping and some cleaning discharges. The leak- up rate which determines the amount of contamination of the filling gas is under 1 $mtorr/min$ which is an acceptable value. The simple design enables the pinch tube to be replaced in a few minutes.

It is normal to preionize the filling gas of a compressional pinch. This is thought to aid the creation of a good sheath when the main pulse is applied. In this experiment the transfer section was charged up by resistors across the gas switch. Measurements showed than when 10 kV was reached the pinch broke down and an LC oscillation of a few kA ensued. Figure 2.9 shows the preionisation and the main current pulse. This preionisation which is only 200 ns before current rise seemed to be as effective as the UV flash 1 μs before current rise which had been

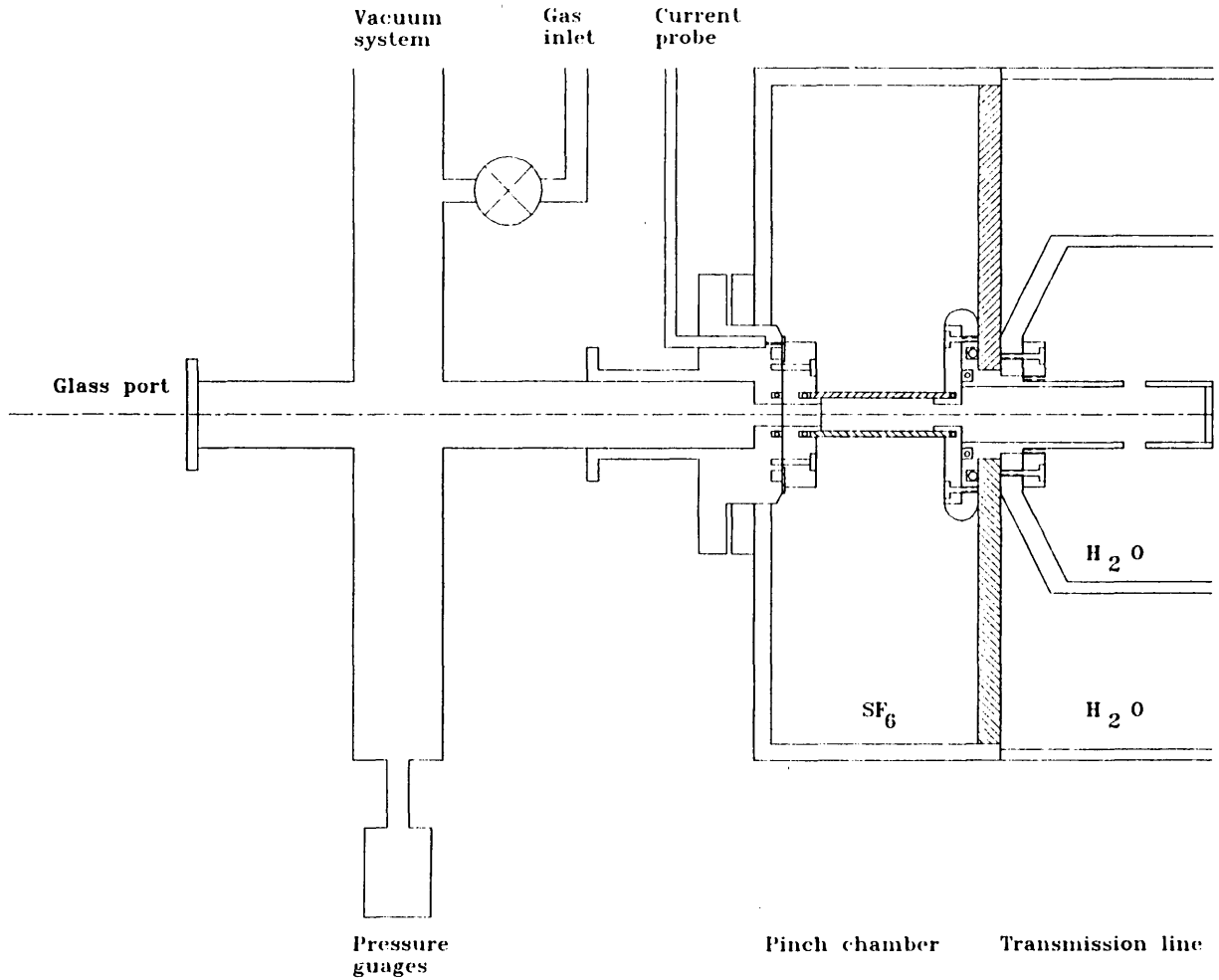


Figure 2.8: The pinch chamber

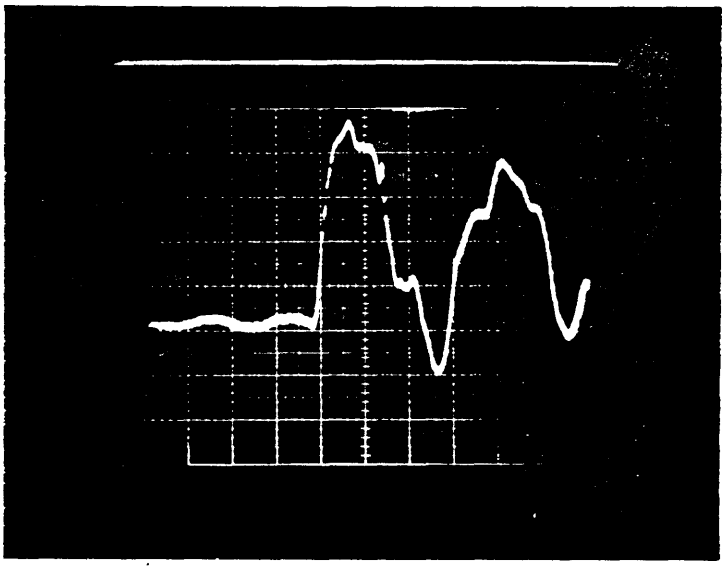


Figure 2.9 : The preionisation current
100 ns, 30 kA/div.

used in previous experiments. The new system of preionisation is very reliable which is an improvement on the earlier design.

2.8 Summary

A new compressional pinch has been designed and successfully installed on an existing transmission line. The line has been extensively modified at the marx interface and important factors in the performance established. It has been found that the addition of a dump gap increases the breakdown free operation of the line from under 100 to 120 kA. The most important modification has been the addition of a second perspex sheet at the Marx-line interface. The line is now fail safe and even if the interface breaks little water will be lost. The line can be worked at maximum voltage even with breakdowns because if these cause damage the sheet is easily replaced. Even though the dump does not prevent breakdown at the highest voltages it will reduce the energy in the streamers limiting the damage. The compressional pinch load assembly works well. A good base pressure is quickly obtained and a large number of shots can be taken without breaking the vacuum. The new system of preionisation is very reliable.

CHAPTER 3 : DIAGNOSTICS OF THE COMPRESSIONAL PINCH

3.0 An overview

The pinch was observed with an optical streak camera, a framing camera and holographic interferograms. These diagnostics were all time correlated with the current trace and are described in the next section.

To aid interpretation of the results computer programs were used. The collapse of the sheath which forms the pinch was compared to the predictions of numerical models. Details of the codes are given in section '3.2 Analysis' which also includes a discussion of the problems of interpreting interferograms and presents a computer program which assists in this task.

To make the holograms, a Q switched ruby laser was used and this determined the triggering requirements of the system. The trigger sequence is shown in figure 3.1 and described below. The laser flashlamps had to be fired 1 ms before the laser pulse could be produced. However once the rods are pumped they maintain a high gain for many microseconds so the exact time the laser is Q-switched is not critical. To synchronise the laser and the current pulse the flashlamps were fired first and after a delay the marx was erected. When the capacitive divider near the gas switch in the PFL detected a rising voltage a delay generator was triggered. This then triggered the cameras and opened the laser Pockels cell to Q switch the laser. The system was reliable because the gas PFL switch was overvolted and so opened reproducibly. The jitter in the arrival of the laser pulse compared with the current pulse was approximately 10 ns.

The streak photographs were the basic diagnostic which showed if a good pinch had formed. To correlate these with the other diagnostics the ruby laser pulse was used to provide fiducials. Fibre optic cables were placed in the laser housing so that they were in the wings of the laser pulse. Two fibres went to the streak camera and framing camera directly and one produced a photodiode signal which was added to the current trace. The fibre lengths were chosen so that the fiducial indicates the time on the current trace and photographs when the laser pulse hits the plasma ($\pm 2ns$).

3.1 Diagnostics

3.1.1 The gated image intensifier

A gated image intensifier is an electro-optical camera which can record a single image with a very fast shutter in relatively low light levels. A Kentech gated image intensifier driven by a Kentech MPS pulse generator was used.

The gated image intensifier consists of a photocathode in front of which is

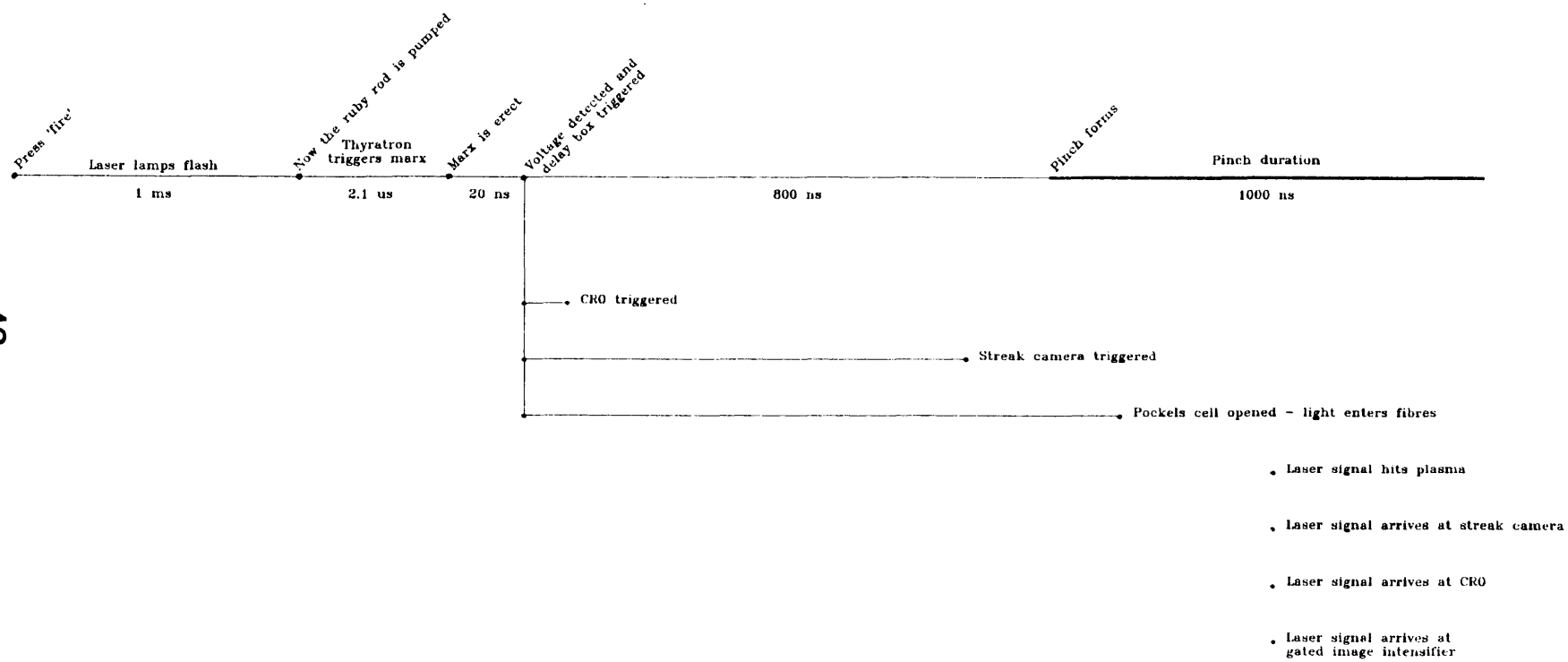


Figure 3.1: The timing sequence.

an extraction grid, a gate mesh and a microchannel plate. Plane mirrors and a lens was used to demagnify a side-on image of the pinch tube onto the $15mm$ diameter input. The gate mesh is negative with respect to the grid until a high voltage gate pulse is applied. Then the electrons which are being liberated from the input photocathode by the light falling on it enter the microchannel plate which has a large gain (≈ 500). The amplified electron image strikes a P20 output phosphor where it is recorded on conventional black and white film (Ilford HP5).The pulse generator produced a 10 ns long pulse 1.5 kV pulse. This was to long for our use and we reduced it to 1 ns by using a 25 Ω stub. As was stated above a fibre optic carrying the laser pulse was butted against the input. The detection of light in the fibre was used to confirm correct triggering.

3.1.2 The optical streak camera

The streak camera is another electro-optical device. It allows one to make time resolved measurements of the plasmas behaviour in one spatial dimension, for example radius. A example of a streak photograph was given in the Introduction (figure 1.3). The slit in front of the photocathode defines the direction of spatial resolution and the electron image is swept across the output phosphor normal to this. This is achieved by a pair of high voltage deflection plates in the streak tube. The camera (manufactured in-house to a Kentech design) used had a built in microchannel plate image intensifier (maximum gain 10^3). The available sweep speeds ranged between 100 ns and 1 ms over a 40 mm screen. The majority of results were recorded with windows of 1 μs and 300 ns. The pinch was viewed end on through a glass window. This was possible because hollow electrodes were used. Two relay lenses were used to take an image of the centre of the pinch to the streak slit. The magnification was 0.67. The anode obscured half a mm next to the wall so this region is not visible on the streak photographs. The photographs were recorded on Polaroid and Ilford HP5 which was developed with microphen.

3.1.3 Holographic interferometry

The optical diagnostics are limited because they cannot give quantitive measurements of electron density and after the wall plasma has formed the pinch is not visible. To measure the electron density of the pinch and observe it at late times we used holographic interferometry. A pulsed laser is used to record a hologram of the empty pinch tube and then a second hologram is recorded on the same plate when the plasma is present. When the plate is replayed both holograms are reconstructed simultaneously and they interfere. The fringe pattern indicates the change in optical path due to the presence of the plasma.

This form of interferometry has been used by many experimenters to measure

the electron density of the plasmas they produce and to detect instabilities. Jahoda (1972) reports the observation of an $m = 1$ instability in a large theta pinch and Favre Dominguez (1985) gives an example of an $m = 1$ in a gas embedded pinch. The former used an end-on configuration and the latter viewed from the side. End-on holography of small diameter pinches is not useful for detecting instabilities because of the many wavelengths that are typically present. However holographic diagnostics of high power compressional pinches have been limited to end-on configurations (Haines 1986). This is because it is very difficult to make holograms when the laser beam must pass through a small glass tube at the centre of a large vacuum chamber. Here we present a new method which solves the problems of making side-on holograms of the compressional pinch.

A Quantel Q-switched ruby laser (694.3 nm) was used. The pulse had a maximum energy of 300 mJ and a fwhm of 12 ns. The beam diameter when it left the laser was 10 mm and the first mirror it encountered was for high power laser use. The beam was then split into two and expanded to 40 mm diameter. The film was normal ($\pm 1°$) to the bisector of the scene and reference beams which were combined at an angle of $30 \pm 2°$. This is shown in figure 3.2.

When we first attempted to make side on holograms of an empty pinch the small diameter tube (ϕ_{tube} 20 mm cf $\phi_{chamber}$ 500 mm) had a very strong lensing effect and little laser light was incident on the collecting optics. Only rays which had passed through the central region of the tube were collected. Thus no information about the plasma near the wall was recorded and the fringes could not be traced.

This problem was solved by sandblasting one side of the tube to make it diffusing and making image plane diffusion holograms (Collier 1971 reviews holographic arrangements). This did not reduce the longevity of the tube and improved the quality of the holograms because more of the light was coupled into the vessel.

The successful arrangement is shown in figure 3.2 and important data is given in table 3.1. The energy in the scene beam was 0.14 $mJ\ cm^{-2}$ and that in the reference beam about 1.5 times this. The holograms were recorded on AGFA 8E75 HD holographic plates and developed with CPA (Aliaga 1990) developer and fixer. This is an exceptionally efficient developer which gives a large dynamic range. This is important because the lensing effect of the pinch tube results in an intensity variation of 10^3 on the plate.

The holograms were played back with an helium-neon laser and photographed with a SLR 35mm camera using Ilford HP4 black and white film. Measurements were made from black and white prints. The outer diameter of the tube is known and this enables one to calculate the scale.

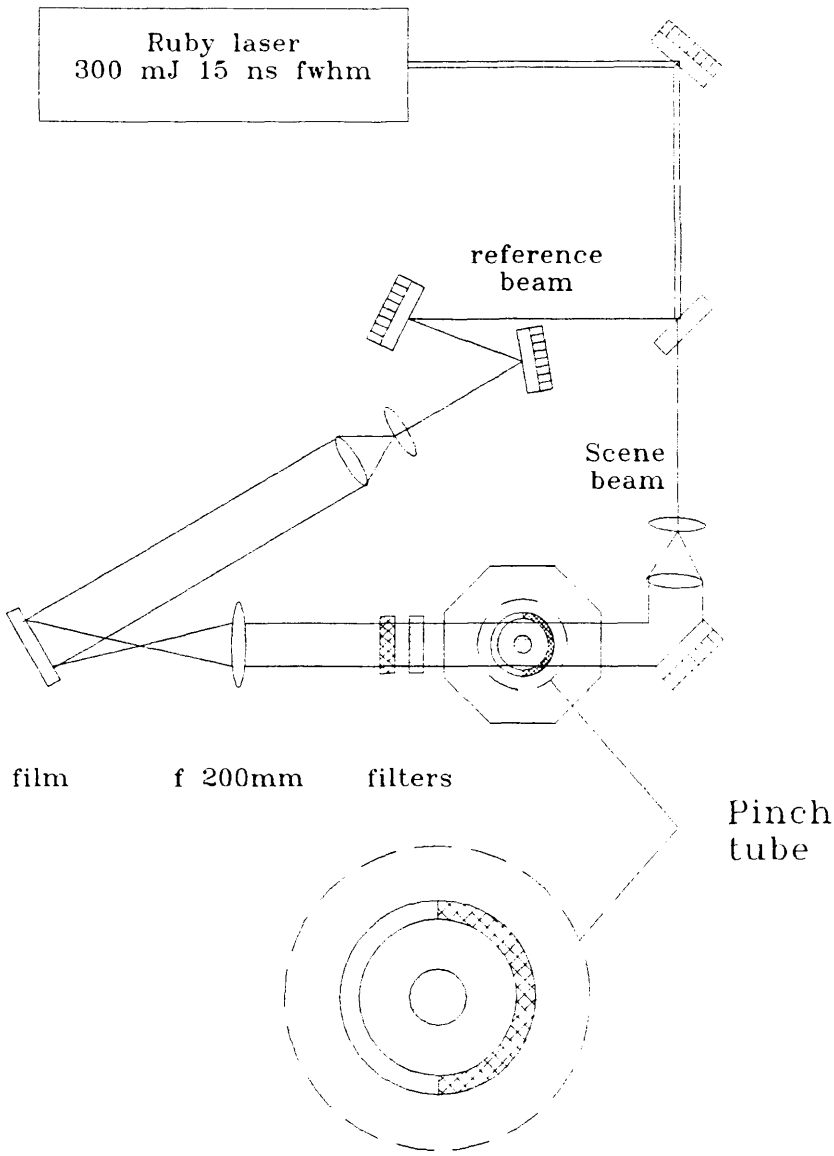


Figure 3.2: The arrangement for holographic interferometry with a diffuse scene beam. Inset: The quartz tube containing the pinch has one side diffusing.

Laser	649.3 nm 'Q' switched ruby with a double pass amplifier
Pulse length	12 ns
Maximum energy	900 mJ
Energy in reference beam	1.2 mJ 0.2 mJ cm^{-2}
Energy in scene beam	1.0 mJ 0.14 mJ cm^{-2}
Angle between beams	30° ± 1°
Plasma light filter	RG 665 (Shott red)
Lens	200 mm F3.5 Camera lens
Plasma - film distance	900 mm
Magnification plasma - film	≈ 1
Film	Agfa 8E75 HD
Developer	CPA (Aliaga 1990)

Table 3.1: Details of the holographic set up

3.2 Analysis

3.2.1 Models of the collapse

The collapse time can be predicted by using either the Snowplough model or the Slug model which were described in section 1.2. The snowplough model considers only the mass of the shell and the magnetic force upon it as it collapses. No other physics is included and for a linearly rising current an analytic solution is possible (eqn 1.2). The slug model (Potter 1978) includes more physics. It assumes a skin current and that a strong shock satisfying the Rankine-Hugoniot conditions propagates radially inwards. The paper referred to gave solutions to the equations for a constant current. Their adaptation for numerical solution and the inclusion of a realistic current profile are the author's own work.

3.2.2 The analysis of interferograms

Interferograms indicate the optical path through the plasma at various positions and from this we derive the electron density profile of the plasma. The interpretation of fringe patterns is not trivial. If the pinch plasma satisfies certain conditions of uniformity then the density profile can be measured analytically by the numerical inversion of the Abel integral. However in some of our experiments these conditions are not met and a computer simulation is required. This section derives the Abel integral and shows the need for a computer model to assist in analysis.

Interferograms are made because the plasma refractive index and hence the optical path of a ray passing through it depends on the electron density. The dispersion relation for a cold field free plasma is.

$$k^2 = \frac{\omega^2}{c^2}(1 - \omega_p^2/\omega^2) \tag{3.1}$$

Where k is the wave number in the plasma which has a plasma frequency ω_p of incident radiation which has a angular frequency ω. Thus refractive index is;

$$\mu = \frac{ck}{\omega} = (1 - \omega_p^2/\omega^2)^{1/2} \tag{3.2}$$

For small variations

$$\mu \approx (1 - \omega_p^2/2\omega^2) \tag{3.3}$$

The phase shift due to the presence of the plasma instead of vacuum ($\mu_{vac} = 1$) is:

$$\phi = \frac{2\pi}{\lambda}\int_{l_Y}(\mu - 1)\, dl = \frac{(2\pi)\lambda e^2}{m_e \epsilon_0 c^2}\int_{l_Y} n_e(\vec{r})dl \tag{3.4}$$

Figure 3.3 shows an interferogram being made and introduces the axes which will be referred to in this section. The pinch density is described in cylindrical

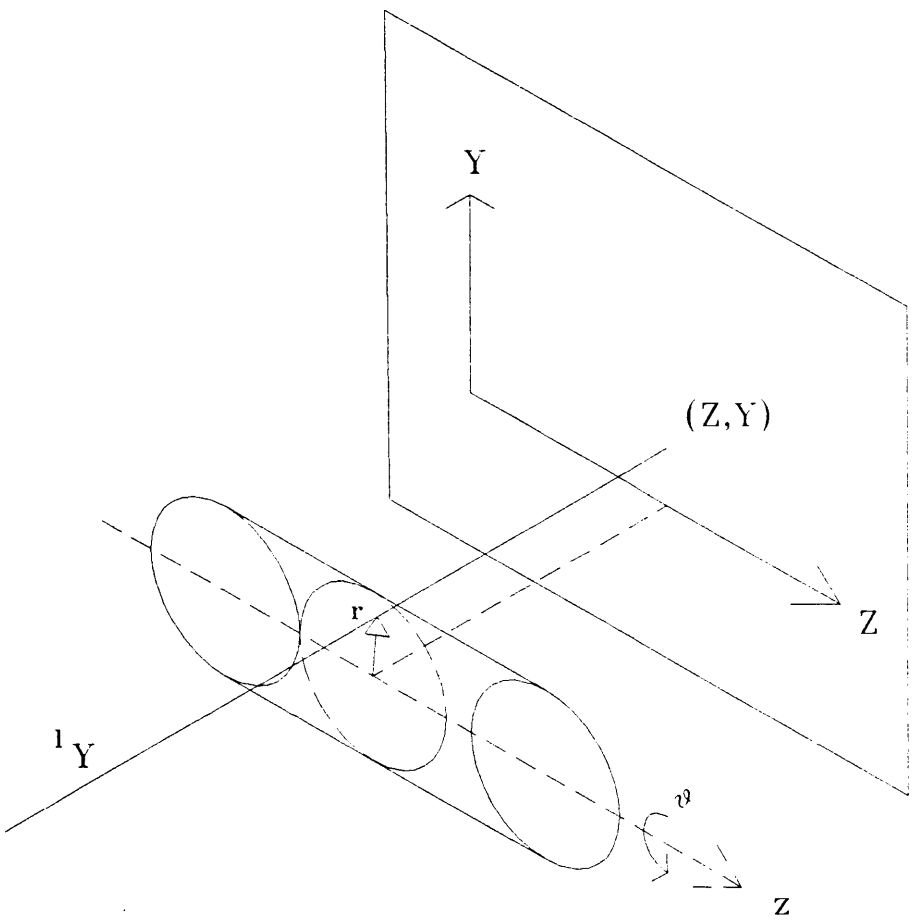


Figure 3.3: The coordinate system for analysing interferograms

coordinates r, θ, z. A ray of light passes through the plasma at an height Y along a path l_Y and hits the film at a point (Y,Z).

From a fringe pattern recorded in an interferogram it may be possible to deduce the electron number density profile of the object. However this often requires assumptions that the plasma is symmetric and is constant in time. If the plasma is moves to rapidly during the laser pulse the fringes may become blurred or cross and this can make interpretation difficult. However if the plasma is stationary the phase shift at a point on the film (Y,Z) is given by (for $\lambda = 694.3\ nm$):

$$\phi(Y,Z) = \frac{\pi}{3.2 \times 10^{21}} \int_{l_Y} n_e(\vec{r}) dl \tag{3.5}$$

If the phase shift is π then there will be destructive interference. In this discussion this will be represented by a black point (Y, Z). However this may be caused by any one of an infinite number of functions $n_e(\vec{r})$.

If a stationary plasma possesses some symmetry this facilitates interpretation. Assume the pinch is axially and azimuthally uniform and the radial density is given by:

$$n_e(r, \theta, z) = n_0\ g(r)\ for\ all\ z \tag{3.6}$$

The phase shift is now no longer a function of z because of axial uniformity, thus:

$$\phi(Y,Z) = \phi(Y) = \frac{\pi\ n_0}{3.2 \times 10^{21}} \int_{l_Y} g(r)\ dl \tag{3.7}$$

Using cylindrical symmetry and the fact that the plasma density falls to zero at the boundary we can put the integral into the following form.

$$\phi(Y) = \frac{2\pi}{3.2 \times 10^{21}} \int_{r=0}^{r=\infty} \frac{r\ g(r)}{(r^2 - Y^2)^{1/2}} dr \tag{3.8}$$

We have reduced the problem of finding n_e to solving a much simpler integral equation. This expression on the right hand side is known as the Abel integral. If we can measure $\phi(Y)$ we may be able to compute $g(r)$. $\phi(Y)$ can be read from the interferogram: if a point is black $\phi = \pi$, if it is white $\phi = 0$. However accurate interpolation between the points is difficult. To solve this problem we introduce a background pattern of vertical lines. This phase shift is added to the signal and produces a much more readable interferogram. We will now show that the phase change at a point Y, Z is proportional to the fringe shift at this point.

The background pattern is added by displacing the scene beam slightly between exposures. This is done by tilting a mirror, the more the mirror is tilted the

finer the fringes. The separation of the fringes is $1/\alpha$. Such a pattern is shown in figure 3.4. $Z = 0$ is a black fringe. In the absence of a plasma;

$$\phi(Y, Z) = \pi - \alpha Z \tag{3.9}$$

Consider two points one at $Z = 0$ and one at Z_1 , in the absence of plasma

$$\phi(Y, 0) = \pi \ (the\ point\ is\ black)$$

$$\phi(Y, Z_1) = \pi - \alpha Z_1 \tag{3.10}$$

In the presence of an axially uniform plasma which produces a phase shift of $\phi_p(Y)$ we have:

$$\phi(Y, 0) = \pi + \phi_p(Y) \tag{3.11}$$

$$\phi(Y, Z_1) = \pi + \phi_p(Y) - \alpha Z_1$$

At a height Y, Z_1 is black in the presence of plasma. Thus

$$\phi(Y, Z_1) = \pi \tag{3.12))}$$

and from (4.7)

$$\phi_p(Y) = \alpha Z_1 \tag{3.13))}$$

So if we measure the distance each black spot moves $Z_1(Y)$ we have obtained $\phi_p(Y)$. Normally Z is expressed as a fraction of a fringe separation. This is known as the fringe shift "f" at Y and is numerically equal to ϕ_p/π . Thus from 3.8 the fringe shift at Y is given by:

$$f(Y) = \frac{2}{3.2 \times 10^{21}} \int_{r=0}^{r=\infty} \frac{r\ g(r)}{(r^2 - Y^2)^{1/2}} dr \tag{3.14}$$

The numerical solution of this equation (inversion of the Abel integral) is described extensively by Figura (1989) and is not given here. To derive this equation we assumed that the plasma was stationary during the laser pulse (12 ns), it was axially uniform and that the density was only a function of radius.

These assumptions do not hold for plasmas of interest such as the sausage and helical kink instabilities. However if the wavelength of the variation of the plasma along z is large compared to the fringe separation and fringe shift, the approximation that the plasma is locally uniform can be made. Unfortunately it is known that z pinches favour instabilities with a wavelength approximately equal to the radius. In our experiments the plasma was 3 mm radius and the fringe separation 1.3 mm. If an instability was present the plasma would have very

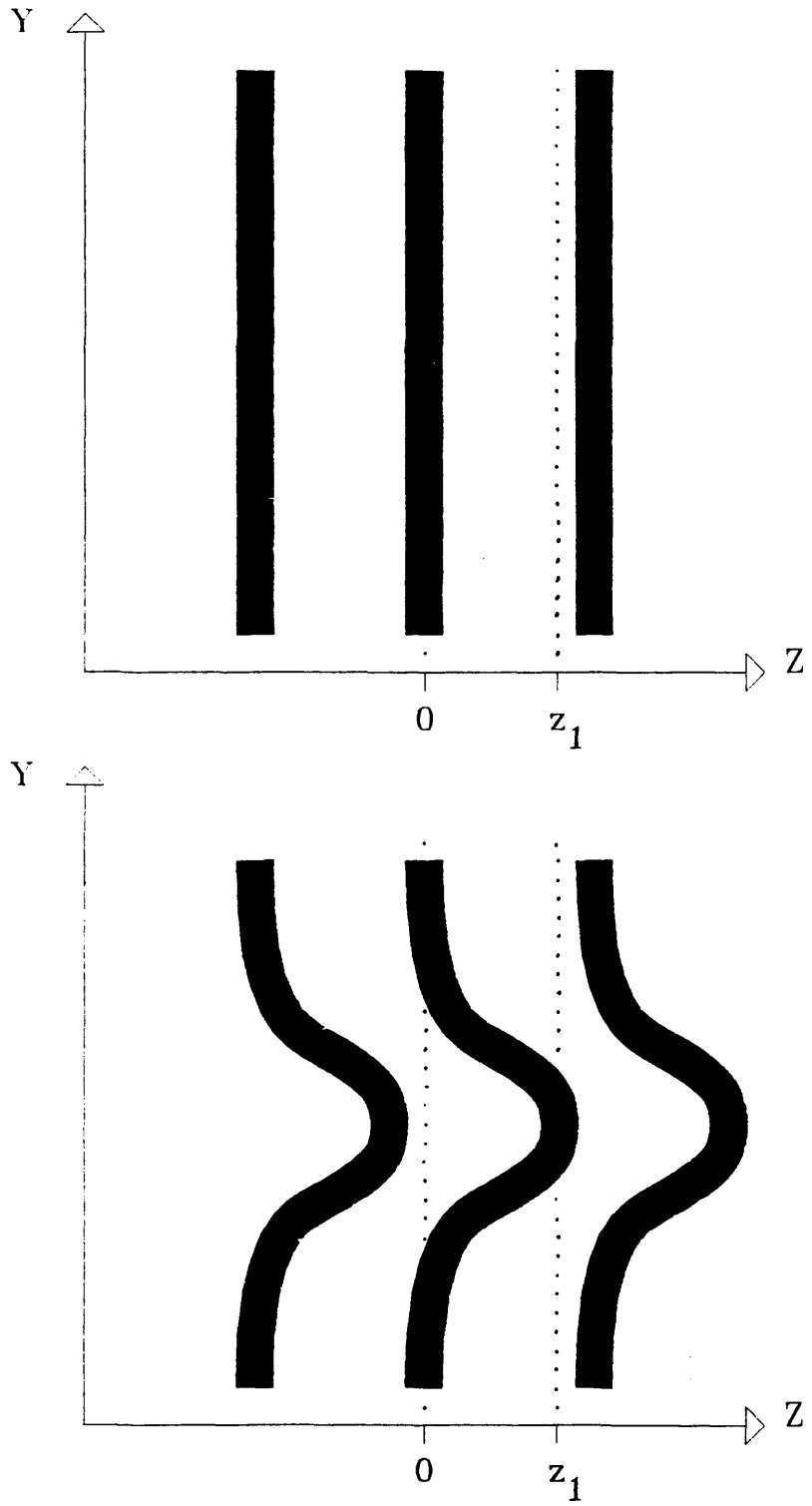


Figure 3.4 : A background fringe pattern and the fringe shift caused by a axially uniform cylindrical plasma.

strong density variations on the fringe scalelength and analytic inversion would not be possible. A further complication is the presence of a wall plasma, the effect of which on the information content of the interferogram is not understood.

To overcome the problems of analysis a computer program was developed which is described in the next section.

3.2.3 The computer program FRINGE

It was decided that because analytic inversion of some interferograms was not possible a computer program should be written. The user specifies $n_e(r,z)$ for the pinch and wall plasmas and the angle and fringe separation of the background pattern. The program finds the resulting fringe pattern by tracing the path of every ray through the plasma and calculating the integral of $n_e dl$ and hence the phase change. This is explicitly applying the equation 3.14 for all Y. The phase shift due to the background is added in and if the resultant shift is $\pi \pm \pi/4$ then a black point is plotted. There are no grey levels. By comparing the interferograms produced by the program with those experimentally obtained, estimates of the electron density profile in both r and z can be made.

FRINGE is especially useful because we can make fringe patterns of the wall plasma in the absence of the pinch, something which is not experimentally possible! The wall plasma was modelled as a gaussian function, thickness d_w and peaked on the wall at r_w. The convenient variable is the line density N_w. The electron density in the wall plasma is given by:

$$n_w(r) = n_0 e^{\left[\frac{(r_w - r)}{d_w}\right]^2} \tag{3.15}$$

Where n_0 has been normalised to get the correct line density.

Examples of the output of this program and how it can be used to produce both qualitative and quantitative results are given in the following sections.

CHAPTER 4: COMPRESSIONAL PINCH RESULTS

4.0 An overview

The observations of the pinch are reported in three sections, the initial collapse of the sheath, the wall plasma, and the pinch its instability and subsequent expansion.

Figure 4.1 shows a streak photograph of a 2 torr hydrogen pinch at 150 kA and current trace. The three regions, collapse, pinch and wall plasma are clearly visible. The plasma sheath is not visible until 40 ns and the shock hits the axis at 70 ns. The pinch forms and bounces slightly. The wall plasma is bright by 150 ns and the contrast between the pinch and the background decreases near 300 ns. The fiducial on the streak matches that on the current trace. The presence of an instability at 160 ns is not detectable on the streak photograph because it does not cause a gross expansion and the camera is viewing the end of the pinch. This was one reason for using side-on holographic interferometry.

Figure 4.2 shows a streak photograph of an argon pinch together with a sequence of framing photographs (taken on different shots).

4.1 The collapse

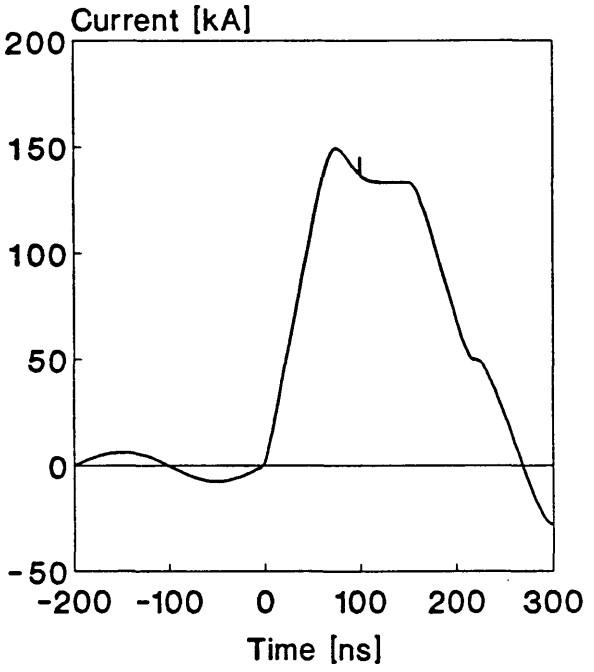
Streak photographs of the collapse were made with filling pressures in the range 50 $mtorr$ to 2 $torr$ hydrogen and 50 $mtorr$ to 1 $torr$ Argon. The time at which the shock hits the axis and the radius of the pinch are compared with the predictions of the slug model in table 4.1.

Figure 4.3 shows an interferogram and figure 4.4 a side on framing photograph when the pinch has just formed. The sheaths are uniform and do not show any instability. From the interferogram we measure the sheath to be 0.67 ± 0.15 mm thick and have a density of $4 \times 10^{23} \pm 20\%$ m^{-3}.

4.2 The wall plasma

As was seen in the streak photograph shown in figure 4.1 the wall plasma is present by 150 ns when the external circuit current begins to fall. The wall plasma is not visible on the holograms until about 180 ns when it is approximately half a fringe shift and peaks 1 mm from the wall. The shift at the wall increases to a 1 $shift$ at 200 ns and 2 $shifts$ at 300ns. The effect is less at lower fill pressures.

Careful comparison of the observed patterns with those computed by the model FRINGE show that when we observe a fringe shift of 1.0 with a peak 1.0 mm from the wall the plasma parameters are those in table 4.2. We see that the wall plasma line density 4.0×10^{19} m^{-1} is approximately the same as the pinch line density which is 3×10^{19} m^{-1}.



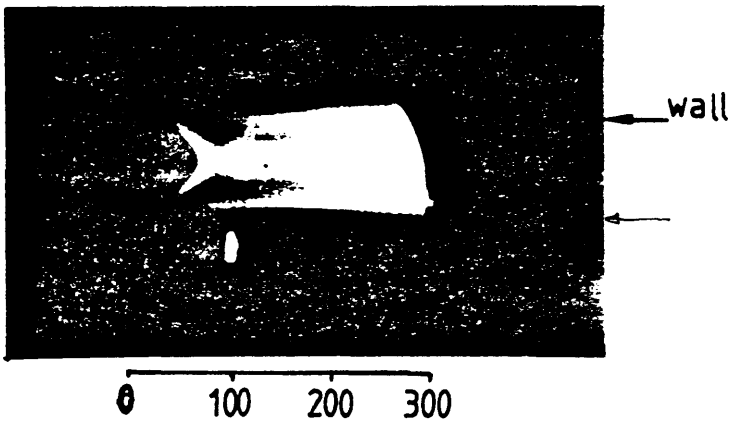


Figure 4.1: The current trace and a streak photograph

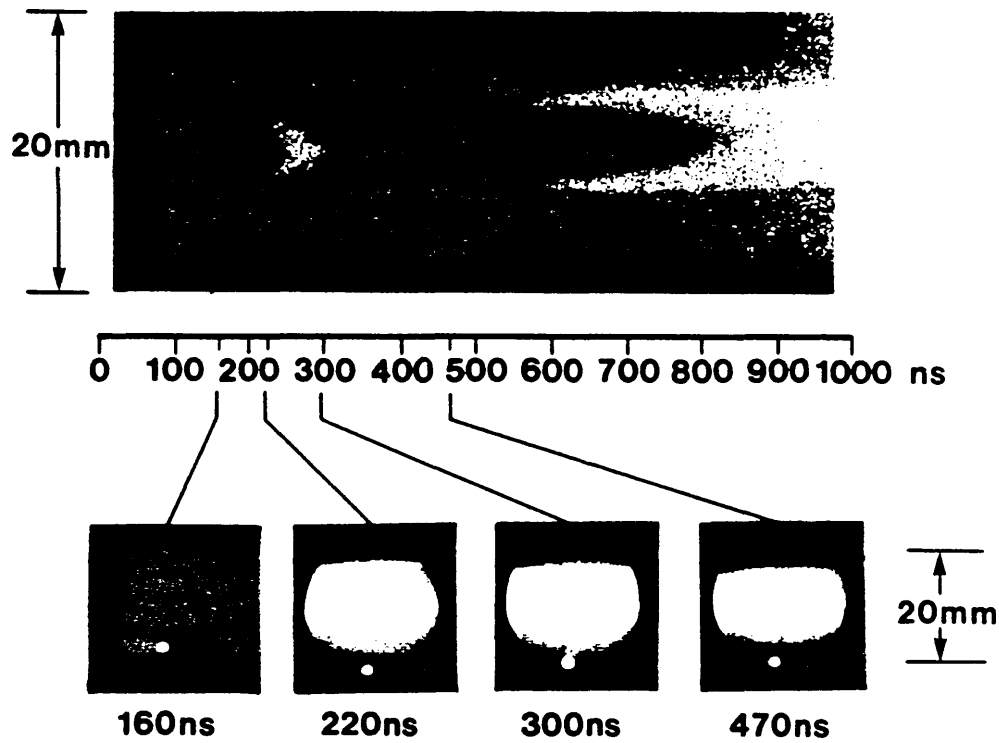


Figure 4.2: A streak photograph and side on frames. 4 times, 1 torr argon, 100 kA.

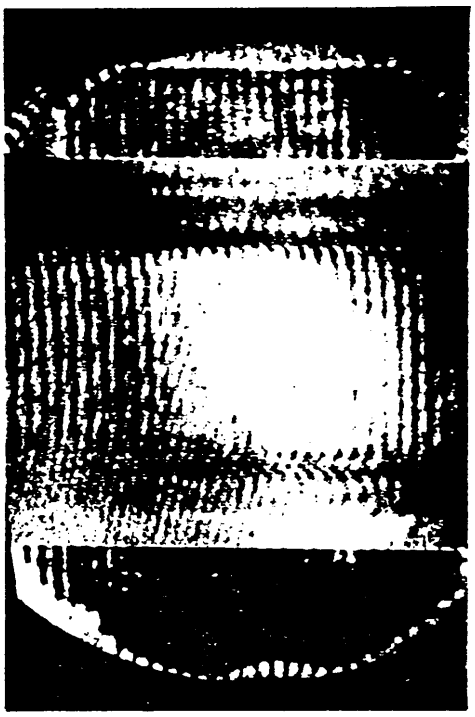


Figure 4.3 : An interferogram of a collapsing H_2 pinch.

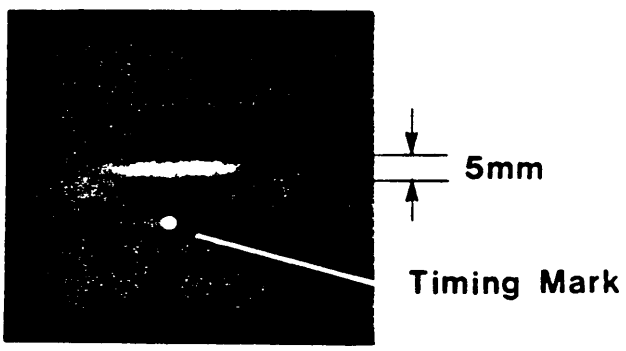


Figure 4.4: A side-on framing photograph taken at peak current, 1 torr H2, 100 kA, t = 80 ns.

I [kA]	p [torr]	t_p*[ns]	r_p*[mm]	t_s [ns]	r_s[mm]	t_p/t_s	r_p/r_s
Hydrogen							
150	2.0	69	3.2	75	2.3	0.92	1.4
	1.0	58	3.2	64	2.2	0.90	1.6
100	1.0	93	3.0	78	2.4	1.2	1.25
	0.5	70	2.5	64	2.1	1.1	1.2
	0.2	52	2.8	52	2.1	1.0	1.3
Argon							
100	1.0	215	2.7	245	2.6	0.88	1.0
	0.80	190	2.9	217	2.6	0.87	1.1
	0.40	140	2.5	157	2.0	0.89	1.3
	0.20	110	1.6	122	1.9	0.90	0.84
	0.10	67	1.2	92	1.8	0.72	0.67
	0.05	52	1.7	80	1.6	0.65	1.1

* ± 10%

I = maximum pinch current
p = filling pressure
t_p = time the shock hits axis
r_p = pinch radius when the shock hits the axis
t_s = slug model prediction of time to axis
r_s = slug model prediction of pinch radius

Table 4.1: Comparison of pinch parameters to the slug model

fringe shift 1.0

distance of peak from wall 1.0 mm

d_w= (1.5 ± 0.5) x 10^{-3} m

N_w= (4.0 ± 1.0) x 10^{19} m^{-1}

n_0= (9.3 ± 0.1) x 10^{23} m^{-3}

Table 4.2: Wall plasma parameters

4.3 The pinch

Holograms were made of 1 and 2 *torr* pinches at 20 *ns* intervals during their life. A specimen set of holograms is shown in figures 4.5. From the holograms we can measure the radius of the pinch and for axially uniform plasmas the electron density profile by Abel inversion and then by integration we can find the line density. When Abel inversion was not possible the line density was approximated as a $constant \times fringeshift \times observed\ radius$. A method which is accurate to about 10%.

The pinch radius against time is shown in figure 4.6 and figure 4.7 shows the density profiles obtained by Abel inversion at various times. Figure 4.8 shows the pinch line density with time. Table 4.3 gives various pinch parameters at the time the pinch disappears.

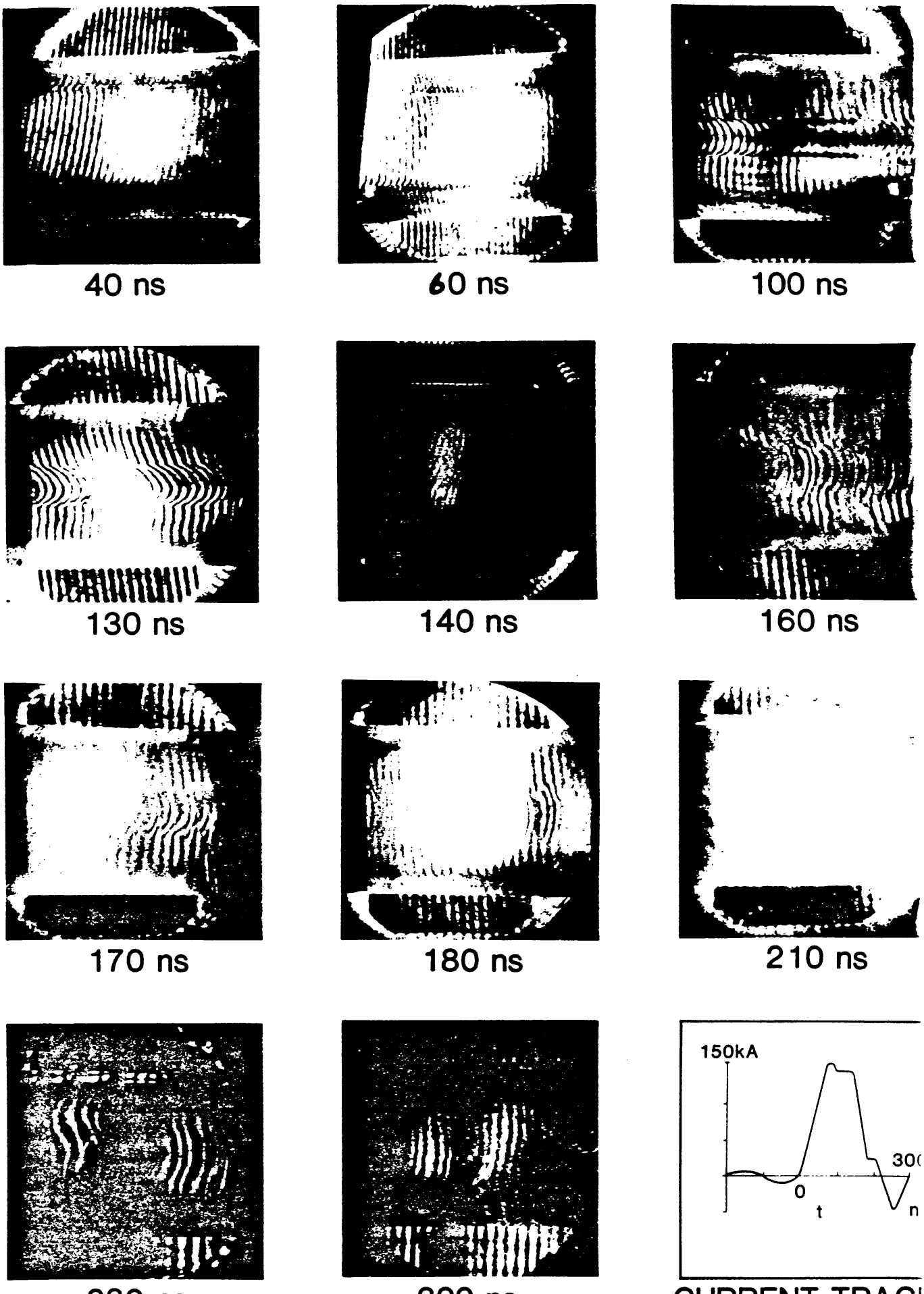
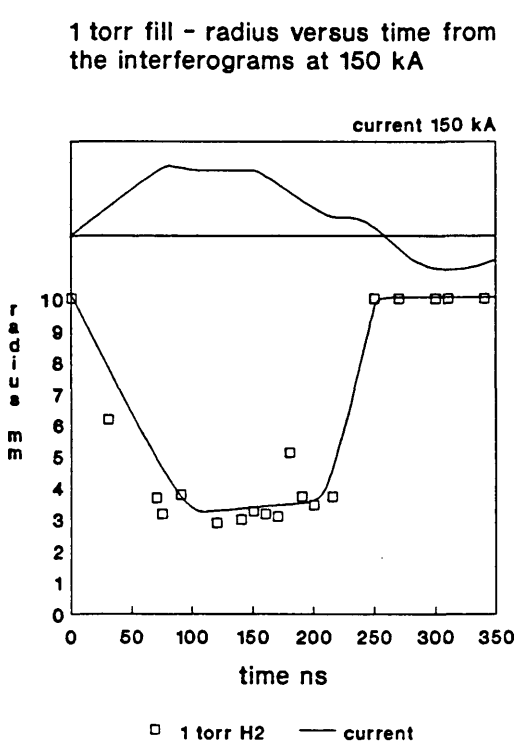


Figure 4.5 : A sequence of interferograms of the 2 torr, 150 kA compressional pinch.



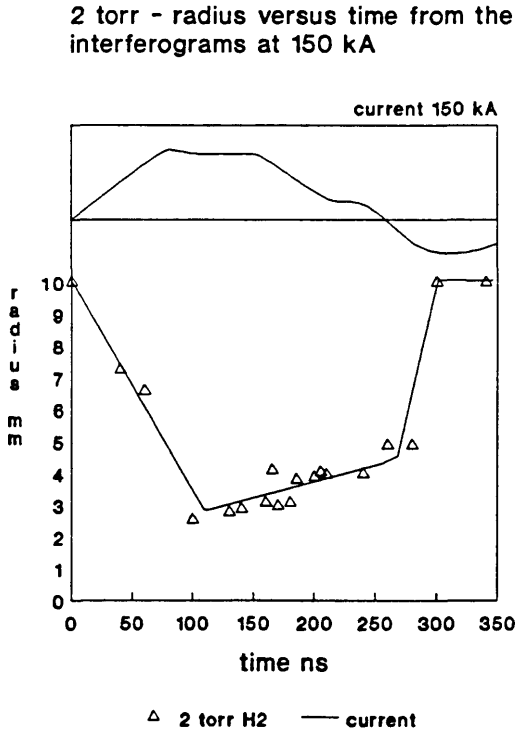
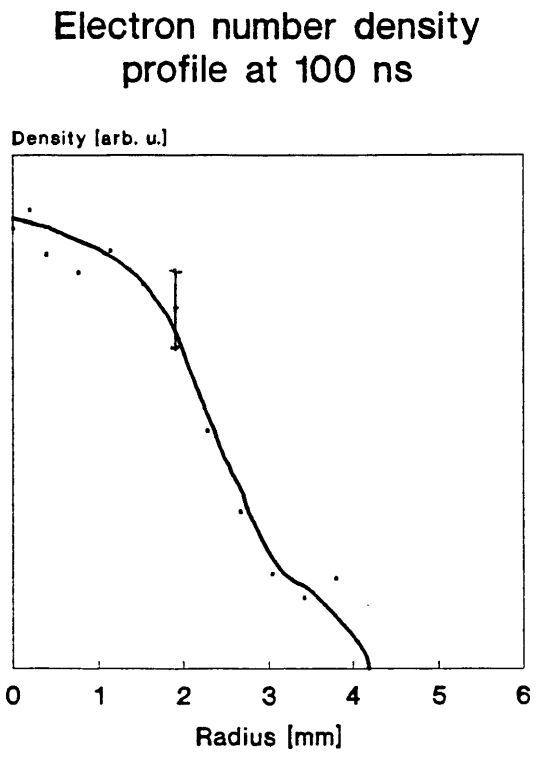


Figure 4.6: Radius v time for the 1 and 2 torr H2 pinches



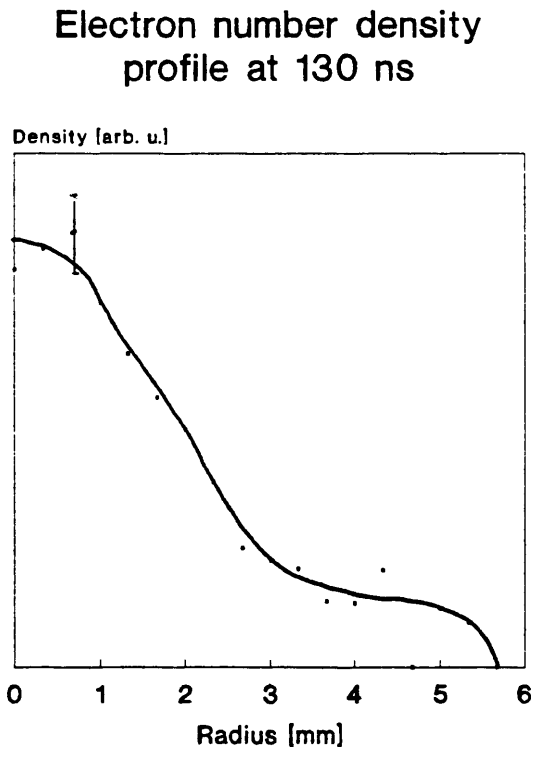
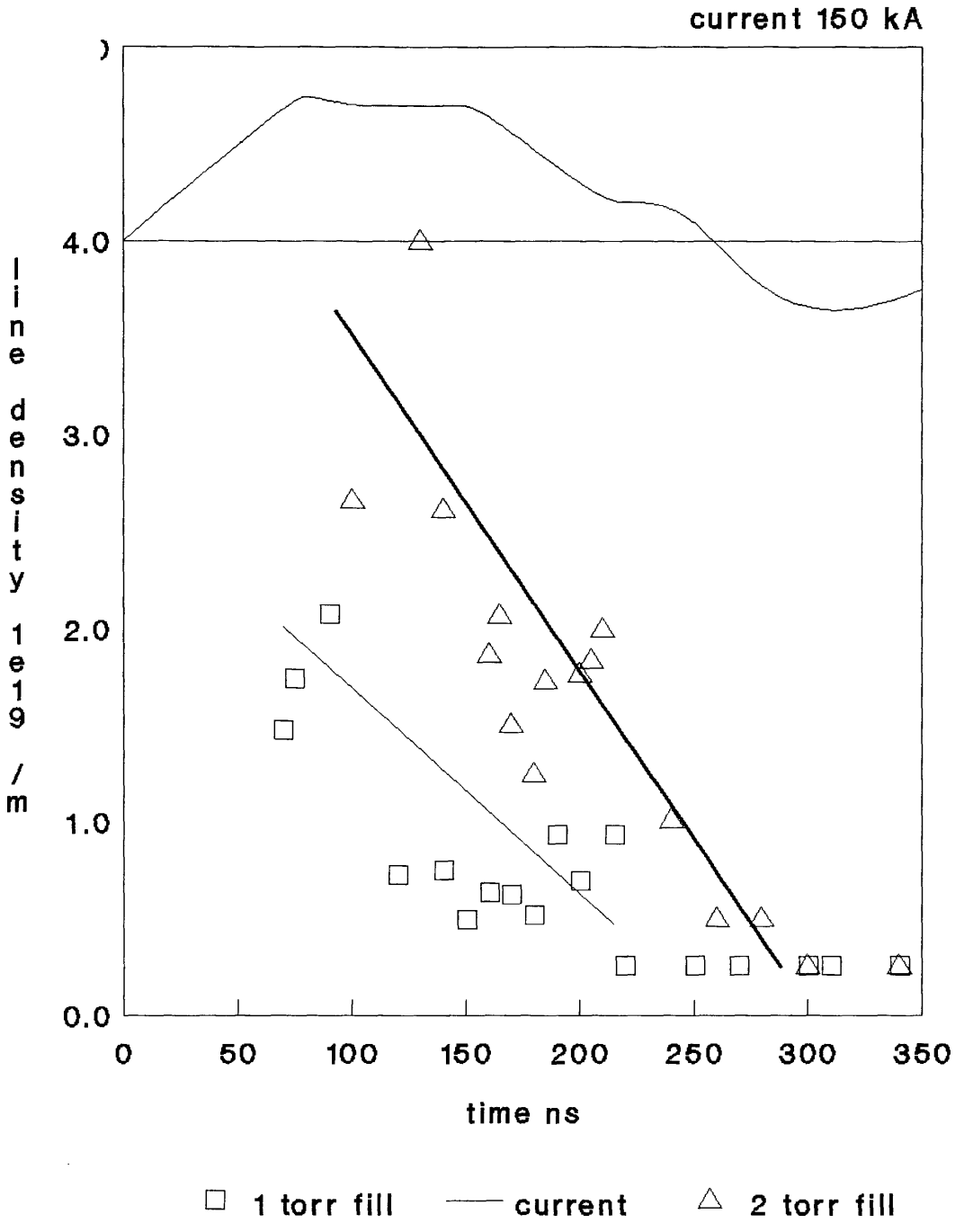


Figure 4.7: Electron density profiles of the 2 torr, 150 kA hydrogen pinch obtained by Abel inversion.

Figure 4.8: Line density versus time
from the interferograms at 150 kA



	2 torr fill	1 torr fill		
t	= 290 ± 10	230 ± 10		ns
N_i	= 2.0 ± 15%	0.9 ± 15%	x 10^{19}	m^{-1}
T_B	= 175 ± 15%	390 ± 15%		ev
v_{th}	= 2.2 ± 10%	3.3 ± 10%	x 10^5	ms^{-1}
v_{ex}	= 1.2 ± 30%	1.8 ± 30%	x 10^5	ms^{-1}
$T_{1/2}$	= 100	75		ns
$\tau_{1/2}$	= 170	113		ns
τ_{mhd}	= 13 ± 20%	9 ± 20%		ns

Table 4.3: Pinch data interferograms at the time the pinches disappear.

CHAPTER 5: INTERPRETATION OF COMPRESSIONAL PINCH RESULTS

5.1 The collapse

The collapse was observed with side on holograms and framing photographs (section 4.1) and these showed that it was very uniform along the length of the pinch. This is an indication that the preionisation was adequate.

The collapse was modelled using the slug model. Figures 5.1a and 5.1b show two runs: 100 kA, 1 $torr$ hydrogen and 100 kA, 50 $mtorr$ hydrogen. The upper and lower curve on the figures represent the magnetic piston and the shock front respectively. Between them lies hot plasma. These graphs can be compared directly to the streak photographs. Notice that at early times the sheath is very thin and remains very close to the wall and that in the low pressure shot the sheath accelerates very rapidly.

Argon pinches were also modelled. Figure 5.1c shows the dynamics of a 1 $torr$ shot with the experimental current profile. The code predicts that the pinch will not form if the current falls at the rate measured in the external circuit. To get the pinch to form it is necessary to assume the current falls slowly. The fastest the current may fall to zero is 350 ns. The collapse for a slowly falling pinch current is shown in 5.1d.

For hydrogen pinches the time to pinch predicted by the snowplough equation (1.2) and the slug model differ by only 1%. This shows that the time to pinch is a very robust parameter, it is only strongly dependent on the mass of filling gas and the size of the current. The detailed physics of the implosion have little effect on the pinch time.

Table 4.1 presented all the data we obtained and compares it to the predictions of the slug model. The argon data shows that for all 100 kA pinches the pinch is formed in less than the time predicted by the slug model. Above 200 $mtorr$ the collapse time is $0.89 \pm 5\%\ t_{slug}$. At 100 kA the hydrogen data is a good fit to the slug model the pinch forming in $1.1 \pm 10\%\ t_{slug}$ but at 150 kA the collapse is slightly faster than predicted. From comparing the measured collapse time with that predicted by the snowplough and slug models we conclude that at higher currents and lower fill pressures the pinch does not contain all the filling gas. This will result in a hotter pinch with a lower line density. This is confirmed by the holographic measurement of the line density of the 2 $torr$ hydrogen pinch. This showed that the line density immediately after formation corresponded to 75% of the initial fill. This is sufficient to account for the increased collapse rate.

The radii of the pinches as measured from the streak photographs are generally larger than predicted. This could be because the optical emission from the pinch

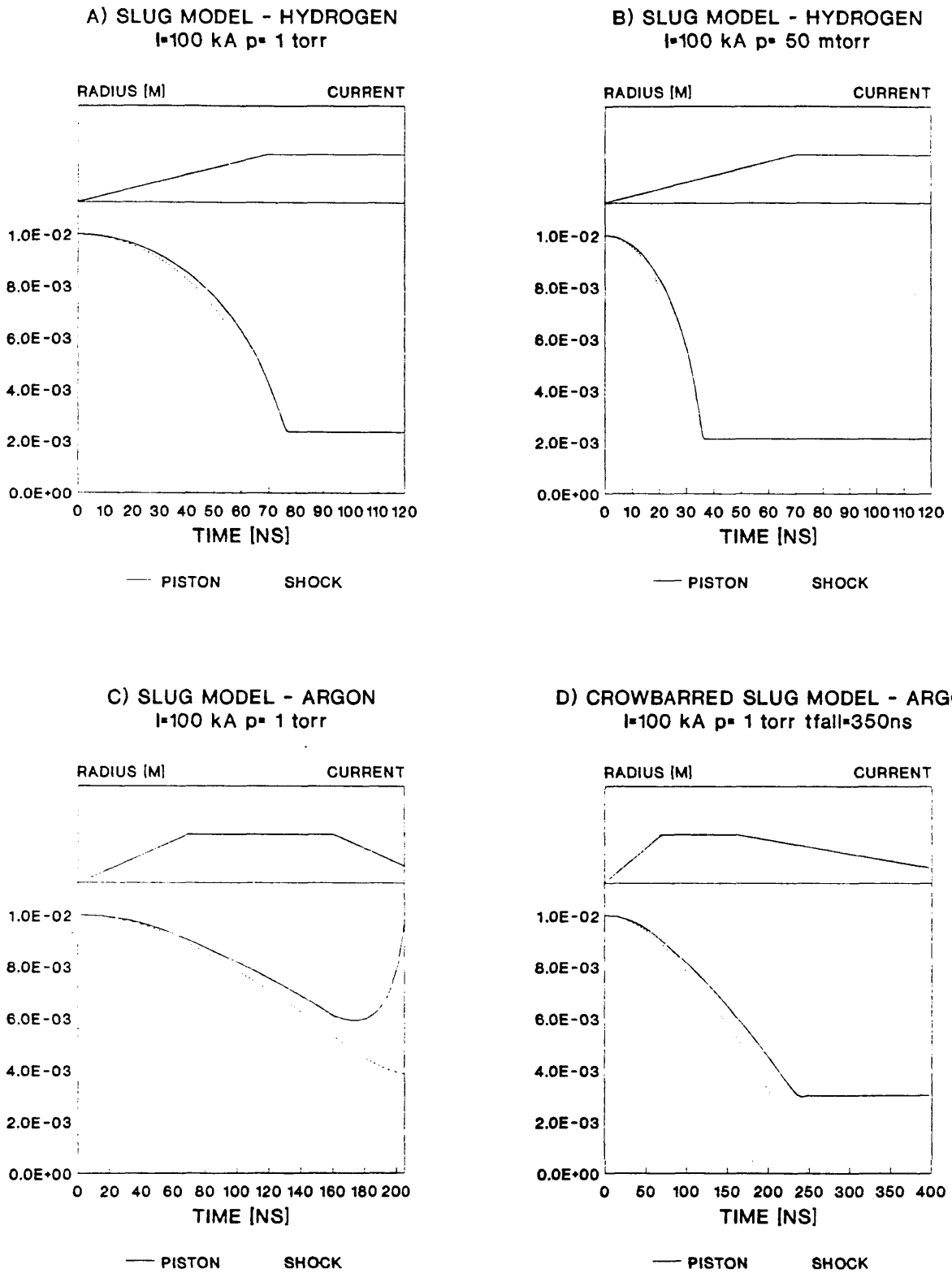


Figure 5.1: The slug model

is not a very good measure of the density profile and hence the radius.

Choi and more recently Baldock observed that the formation of the collapsing sheath began after the rise of current. The computer generated figures which show the positions of the shock and the piston predicted by the slug model, show that the sheath is very thin and has a low velocity during the early stages of its formation. At later times it is thicker and has a much higher velocity. If one extrapolated back the collapse using this higher velocity one would see a hang-up. We believe that the streak photographs are consistent with an initially slowly moving pinch and no wall hang up.

The hydrogen pinch is observed to bounce and appears to be contained by the beginning of a wall plasma.

5.2 The wall plasma

There are two factors affecting the visibility of the pinch in the photographic diagnostics. The absolute brightness of the pinch plasma and its brightness against the wall plasma. The brightness of the wall plasma may render the pinch invisible due to saturation of the detector. On the streak photographs we see that the wall plasma lights up as the current falls between 150 and 300 ns. It then expands inward and hits the pinch at 600 ns. The values of density given in the results section were found by use of the program FRINGE.

Figure 5.2 is a computer generated model of an interferogram of a wall plasma. Note how at the centre of the tube the fringe is only displaced by a small amount but close to the wall the displacement is large. Although the fringes do connect with the background pattern at the wall it is difficult to trace their path. This is seen on the interferograms (eg. figure 5.3) where the region near the wall is often blurred.

The important point for our interpretation of the pinch interferograms is that the wall plasma is not present at the times we are most interested in $0 - 200$ ns. At later times a strong wall plasma is present but the middle of a fringe is only displaced by a small amount. Since the pinch is at the centre of the tube the effect on our measurements is small.

5.3 The pinch

It is known that the current in the pinch is decoupled from the external circuit and falls slowly due to a current crowbar (section 1.2) and in the previous section the maximum rate of fall of current was calculated by considering the slug model. In the following discussion it is assumed that the current does not follow the external circuit value but rather falls slowly.

The holograms provide us with several measurements. A very important

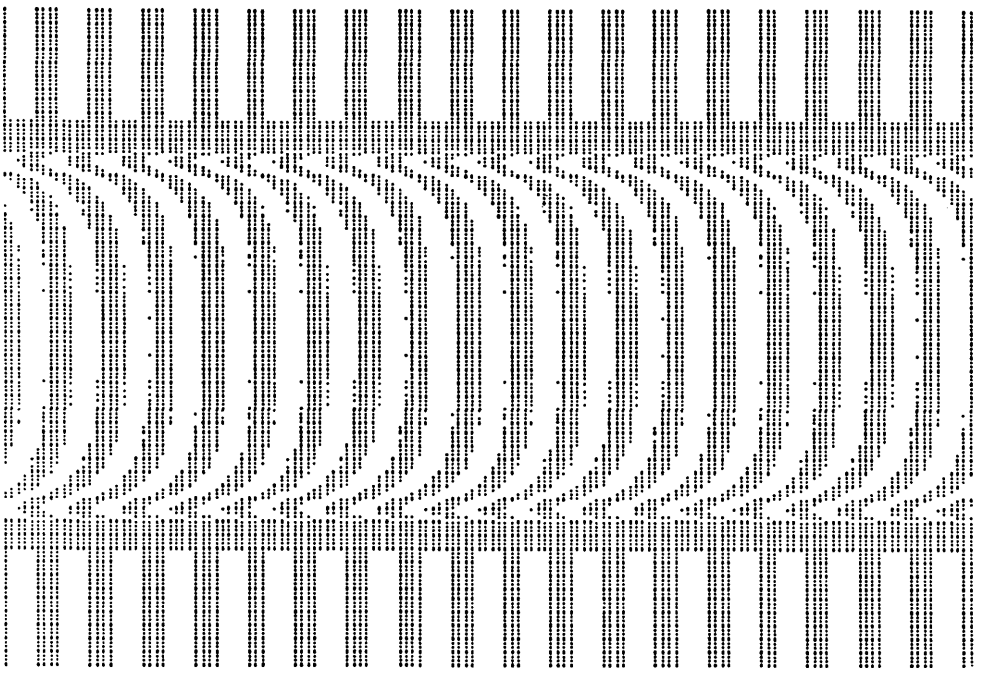


Figure 5.2 : A computer generated model of an interferogram of the wall plasma.

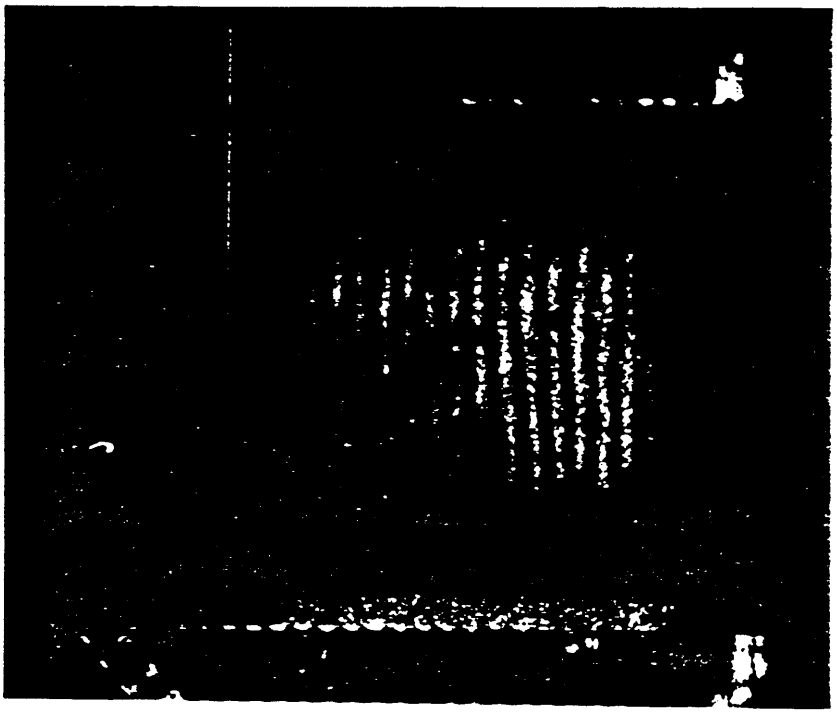


Figure 5.3: An interferogram showing the wall plasma, 1 torr H2 pinch, 150 kA, t = 300 ns.

parameter for interpreting the results is the ion thermal velocity. This is calculated from the Bennett temperature of the pinch, which in turn is governed by the line density. Figure 4.8 shows that the line density of the pinch drops throughout the current pulse and thus the temperature is larger than we may have expected (eqn. 5.2). The simplest explanation for the loss of particles is that plasma is flowing out through the hollow electrodes at both ends of the pinch. The characteristic time scale for this would be $\tau = L/2v_{th}$. The increasing temperature also effects the growth time τ_{mhd} of an mhd instability which is a/v_{th} .

$$T_B = \frac{\mu_0 I^2}{16\pi N_i e} \; [eV] \tag{5.1}$$

$$v_{th} = \left[\frac{3T_B e}{m_i}\right]^{1/2} \tag{5.2}$$

Figure 4.6 showed the radius versus time for the two pinches. There are several comparisons which can be made. The pinches differ in their behaviour: the 1 *torr* pinch remains at a radius of $3.3 \pm 10\%$ *mm* until it disappears at 230 ± 10 *ns*, the 2 *torr* pinch expands from a minimum radius of 2.6 *mm* to 4.9 *mm* before it disappears at 290 ± 10 *ns*. The sudden disappearance of the pinch must be due to expansion and so a velocity v_{ex} can be estimated.

Table 4.3 gives values for parameters when the pinch expands which are calculated from the data in the figures. From the table we see that the expansion velocity is about half the thermal velocity of the pinch. This rapid expansion happens at least 70 *ns* after the external circuit current begins to fall at 160 *ns*. This additional confinement shows the current must have crowbarred through the wall plasma and the pinch current is greater than the external circuit current. The loss of particles from the pinch is about 1.5 times that predicted by the crude $L/2v_{th}$ approximation. To model plasma diffusion across magnetic field lines is very difficult and will not be attempted here.

5.4 Pinch stability

The comparison of the holograms with the computer models is most useful for the 2 *torr* initial fill because the fringe shift is sufficient for the pinch structure to be investigated. The behaviour of the 1 *torr* pinch is qualitatively similar to that of the 2 *torr* pinch but the fringe shift is too small for quantitative analysis.

Just after the 2 torr pinch has formed at 100 ns the Abel inversion (figure 4.7a) of the interferogram shows that the electron density is centrally peaked. By 130 *ns* (figures 4.7b, 5.4a) the density profile is still centrally peaked but has wings. This may be due to the saturation of short wavelength instabilities which have high growth rates and are localised near the surface of the pinch (Coppins



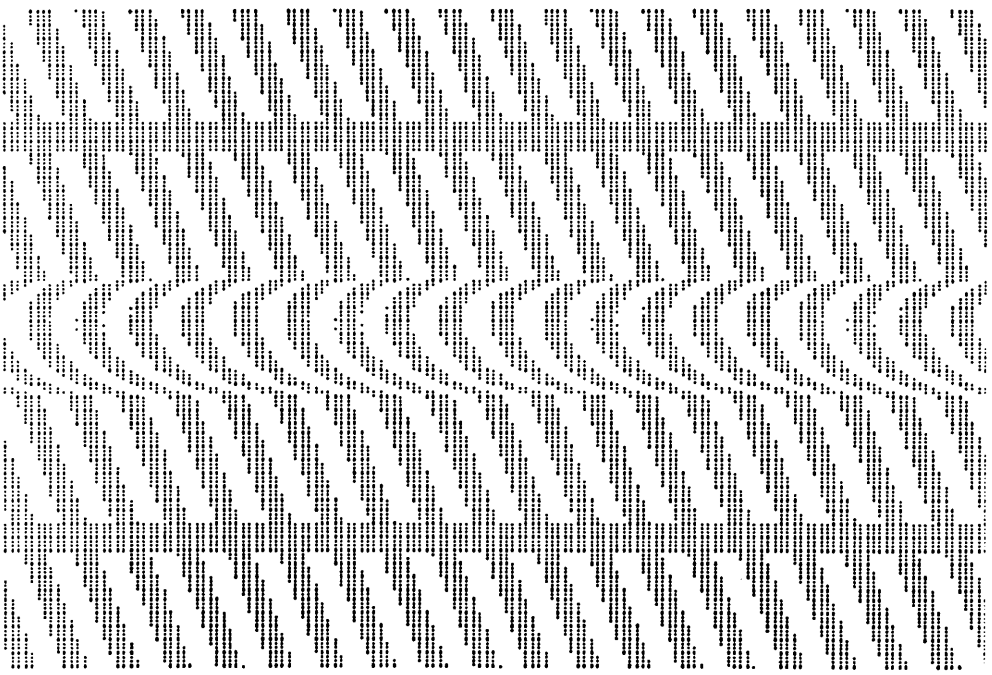


Figure 5.4a: 2 torr H2, 150 kA, t = 130 ns.
An interferogram and its computer model.

1988). Later at 180 ns (figure 5.4) the fringe structure is different and there is a periodic perturbation to the boundary. The computer pattern in the figure was generated using the simplest possible model of an $m = 0$ instability; the line density in each element dz is unchanged and the pinch simply expands or contracts with no axial mass flow. Thus the density increases in the necks and decreases in the bulges.

The boundary of the pinch is perturbed by 0.1 mm at 100 ns (figure 4.5). Assuming the plasma is at the Bennett temperature of the observed line density we calculate that 100 to 140 ns is 6.3 ideal mhd growth times ($ka = 6, \tau_{mhd} = 7\ ns$ growth rates taken from Coppins 1988). This would result in a perturbation of 5 mm and the total destruction of the pinch. However at 140 ns the perturbation is about 10% thus the growth rate is about 0.3 the ideal mhd value.

At 160 ns the perturbation saturates at about 30% and the holograms taken up to 210 ns clearly show that the instability remains at this amplitude without disrupting the pinch. After this time we cannot resolve the instability but a pinch is observed until 280 ns. The subsequent disappearance of the pinch may be due to particle loss or the effect of a falling current.

If we assume the pinch is in Bennett equilibrium the ratio of ion Larmor radius to pinch radius, the collisionality and the resistivity (parameterised by the Lunquist number S) are only functions of line density , current and radius (Haines 1989).

$$a_i/a = 8.0 \times 10^8 N^{-1/2} = 0.18 \tag{5.4}$$

$$\omega_i \tau_{ii} = 7.3 \times 10^{30} \frac{I^4 a}{N^{5/2}} = 7 \tag{5.5}$$

$$S = 5.45 \times 10^{23} \frac{I^4 a}{N^2} = 1.6 \times 10^3 \tag{5.6}$$

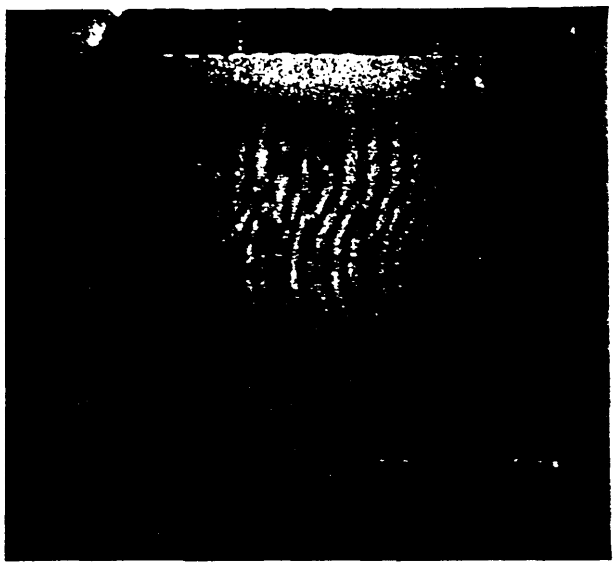
Thus the plasma is collisionless and non-resistive and is possible that finite Larmor radius effects rather than resistive effect are responsible for the enhanced stability of the pinch.

5.5 Summary

A new holographic technique has been developed and this has enabled new results to be obtained.

It was found that particle loss through the hollow electrodes was an important effect and the number of particles in the pinch halved in approximately $(1.5)L/2v_{th}$.

The pinch does not expand immediately the external current begins to fall. We know from the numerical modelling discussed in chapter 3 that this implies that the current has crowbarred and the current in the pinch is greater than that in the external circuit.



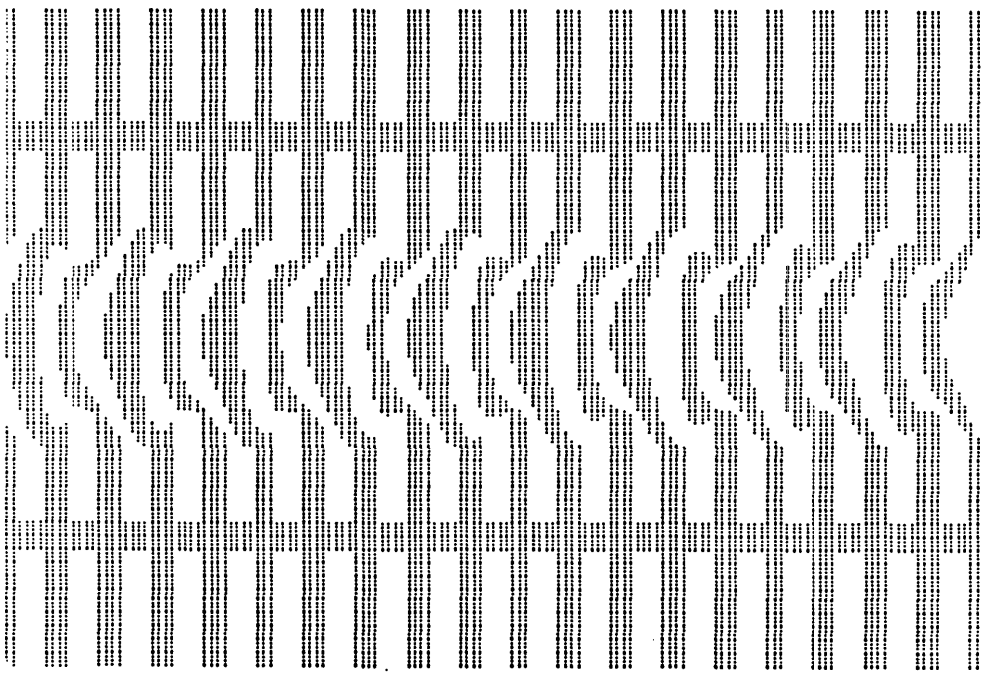


Figure 5.4b: 2 torr H2, 150 kA, t = 180 ns.
An interferogram and its computer model
showing an m = 0 instability.

$m = 0$ instabilities are observed and are seen to increase in amplitude. However their growth rate is reduced from the ideal mhd value and they saturate at about 30% and do not cause the immediate destruction of the pinch. Although the instability is seen before the current begins to fall its development may be affected by the decreasing current. Whether the final loss of the pinch is caused by the falling current or the instability is not known.

CHAPTER 6: THE DÜSSELDORF SPEED2 PLASMA FOCUS

6.0 Introduction

The geometry and operation of the plasma focus Z-pinch was described in section 1.3 of the introduction.

The work presented here results from the author being invited to assist the plasma physics group at the University of Düsseldorf to install a gas injection system for their plasma focus and to diagnose the pinches produced. The aim was to study the effect of collapsing the plasma sheath onto a stream of a heavy gas such as argon. We were particularly interested in the production of hotspots. A successful system was developed and many diagnostics utilised. The space, time and wavelength resolving diagnostics included filtered pinhole photographs, x-ray streak photography, x-ray diodes and a crystal spectrometer. In addition neutron counts and electrical signals were recorded. The next section deals with the design philosophy of the SPEED 2 plasma focus and details the diagnostics used. Then data is presented to show the effect of increasing the amount of argon added to the pinch. Finally the hotspots and argon spectra are discussed.

6.1 SPEED 2 - a new design philosophy for the plasma focus

A comparison of different experiments of the late seventies showed that the neutron yield of foci goes as I_{max}^4 (Decker 1980). This prompted the building of SPEED 2 which is a plasma focus with a high impedance (60 $m\Omega$) and a high current efficiency ($27A/J$). The design is described in detail by Decker et al. (1986). It was believed and subsequently demonstrated that it is desirable to have a fast current rise. This results in a thin hot sheath which stops magnetic field diffusion into the pinch which would reduce the final pinch pressure. Table 6.1 is a table of parameters of SPEED 2.

6.2 The argon valve

As was stated in the introduction (1.3) attempts to add argon to the pinch by adding it to the deuterium gas at filling were unsuccessful because of sheath break up. It was decided to stream in argon though a hole in the anode. This arrangement is shown in figure 6.1. The solenoid driven valve is connected to the high voltage anode by a length of plastic hose. The valve is triggered a few milliseconds before the capacitor bank is discharged. The length of this delay (1 – 10 ms) and the length of the insulating hose (0.1 – 0.3 m) determine the quantity of argon in the pinch. The performance of the valve which was obtained from the focus group at the University of Stuttgart has not been measured so we do not know the precise amount of argon added. Initially the insulation between the

Energy	W_0	=	187	kJ
Voltage	V_0	=	300	kV
Capacitance	C	=	4.16	μF
Short circuit current	I_0	=	5	MA
Initial current rise	I_0	=	$> 2 \times 10^{13}$	As^{-1}
Inductance	L_0	=	15	nH
Current rise time	$\tau_0/4$	=	400	ns
Impedance	Z_0	=	60	mΩ
Pinch current	I_p	=	> 2	MA

Table 6.1: SPEED2 parameters

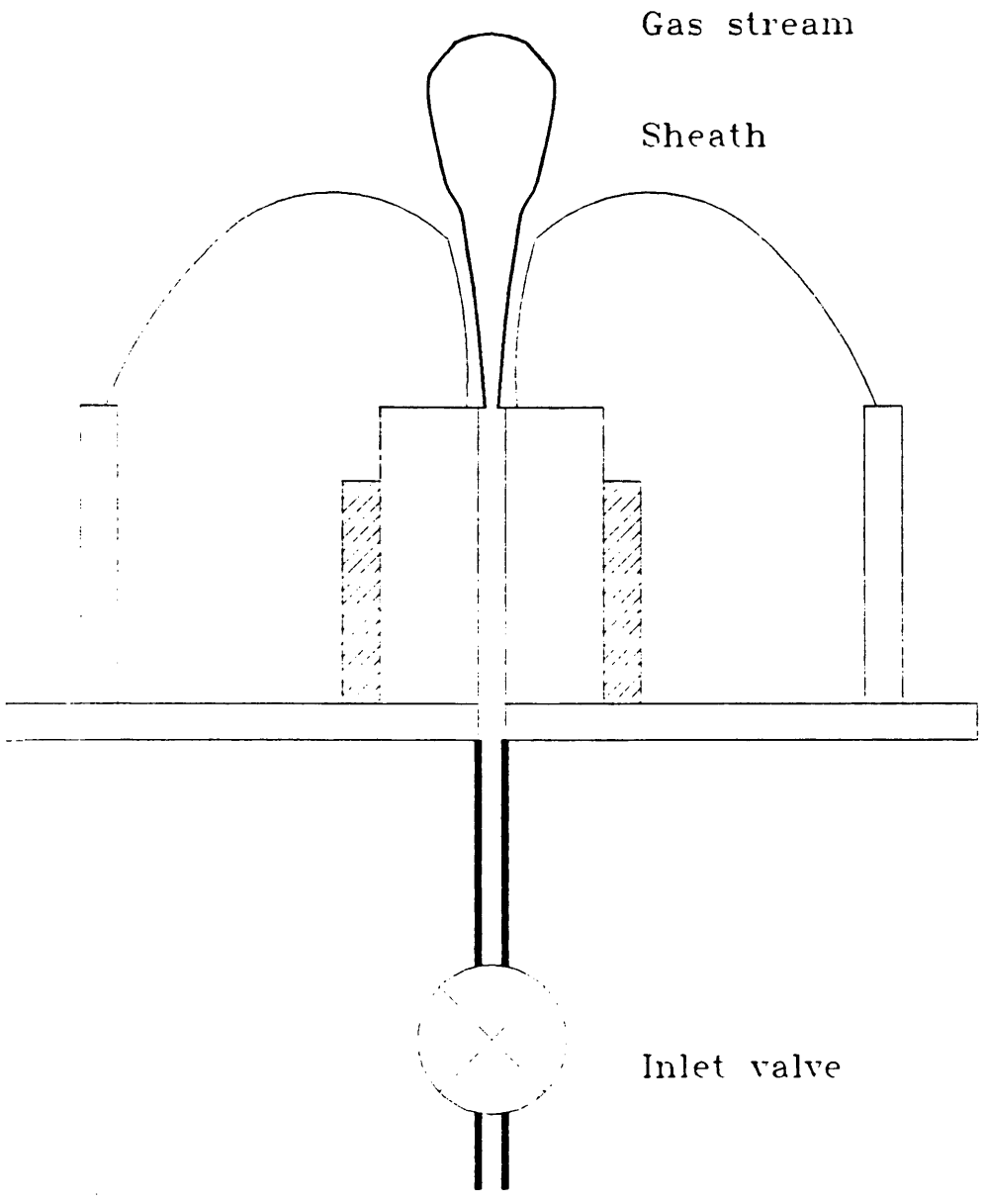


Figure 6.1: Plasma focus with gas inlet valve

anode and the valve firing electronics was found to be deficient and after each shot the electronics had to be repaired. This problem was caused by tracking through the argon gas in the tube between the valve and the anode. A further break down through the silicon rubber between the valve body and the solenoid then destroyed the solenoid driver. This problem was finally solved by enclosing the valve and solenoid in a bath of transformer oil.

6.3 Diagnostics

Here we discuss the time and space resolving diagnostics which were used. A selection of which are shown in figure 6.2.

6.3.1 Kentech X-ray streak camera

To observe the pinch and to look for hot spots we used a Kentech X-ray streak camera with a gold photocathode (10 nm on 0.1 μm mylar). The pinch was imaged 1:1 onto the photocathode by a 0.3 mm pinhole 0.5 m from the pinch. The pinhole was covered by a vacuum-tight 10 μm beryllium filter to isolate the camera from the focus and block out UV radiation. The camera was used without a slit, the time resolution being given by the small size of the pinch and hotspots.

The camera was used with a 50/40 image intensifier but when we tried to streak the argon spectra (see below) it was found that the camera was not sufficiently sensitive. So the gold photocathode was replaced by a low density CsI photocathode (Exitech, Abingdon, U.K.) which according to Day et al (1981) is 30 times more sensitive at 0.4 nm. The geometry used to streak the lines is shown in figure 6.3. A 0.5 mm slit was used at a variety of sweep speeds. The slowest useful speed was 2.5 ns/mm and the fastest possible 250 ps/mm.

6.3.2 The X-ray crystal spectrometer

To look at helium-like and lithium-like argon lines an X-ray crystal spectrometer was employed. The dispersive element was a curved quartz crystal $(10\bar{1}0)$ mounted in a Johann configuration. This produces sharp lines but does not form an image of the source because we do not use an entrance slit. The spectra were recorded by both film and the X-ray streak camera.

6.3.3 Neutron Counters

Three systems were employed to count the neutrons produced by the pinch. Two in-house silver activation counters and a fast photomultiplier (5 ns) with a plastic scintillator in front. The photomultiplier was shielded with 14 cm of lead to reduce its sensitivity to hard x-rays.

6.3.4 Pinhole camera

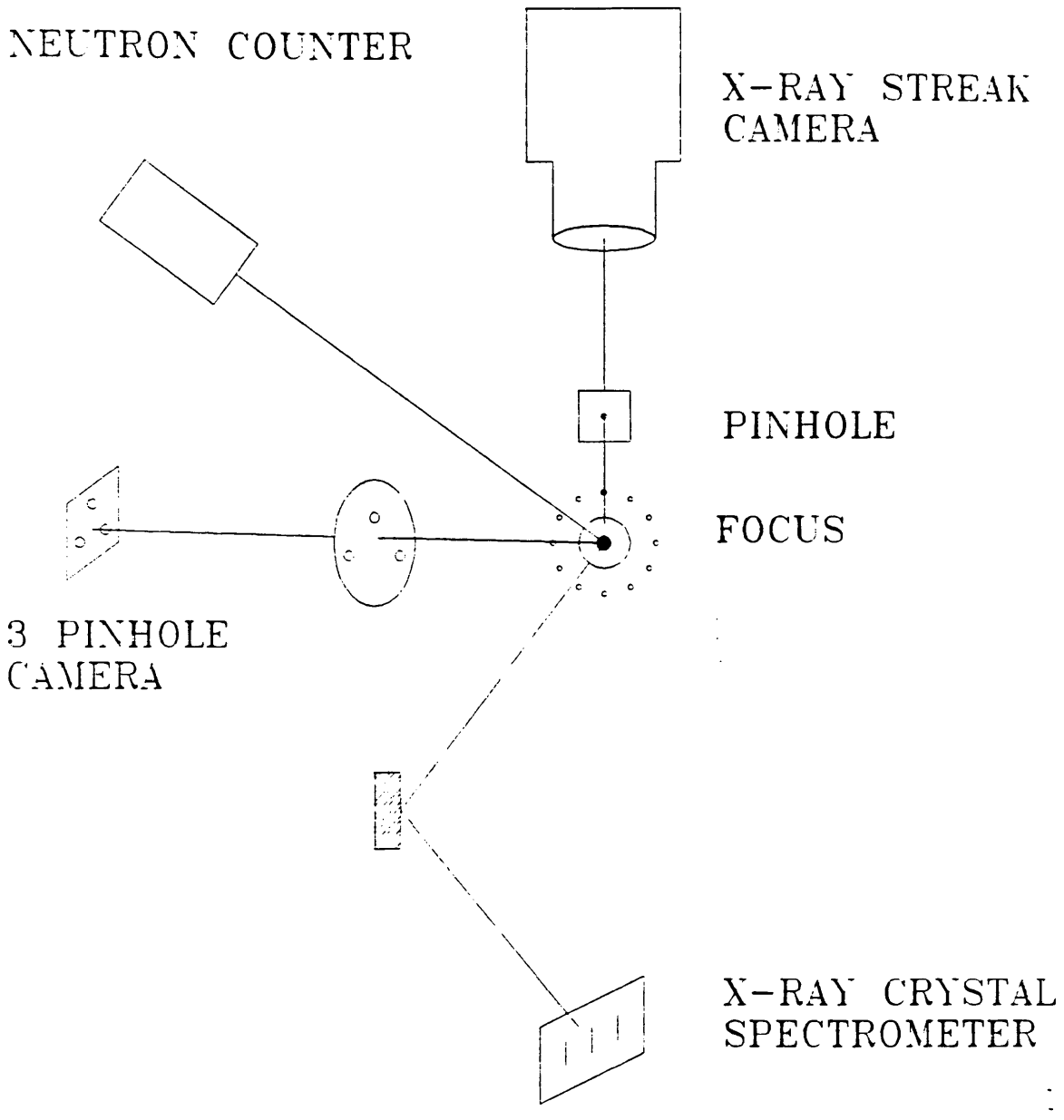


Figure 6.2: Focus and diagnostics

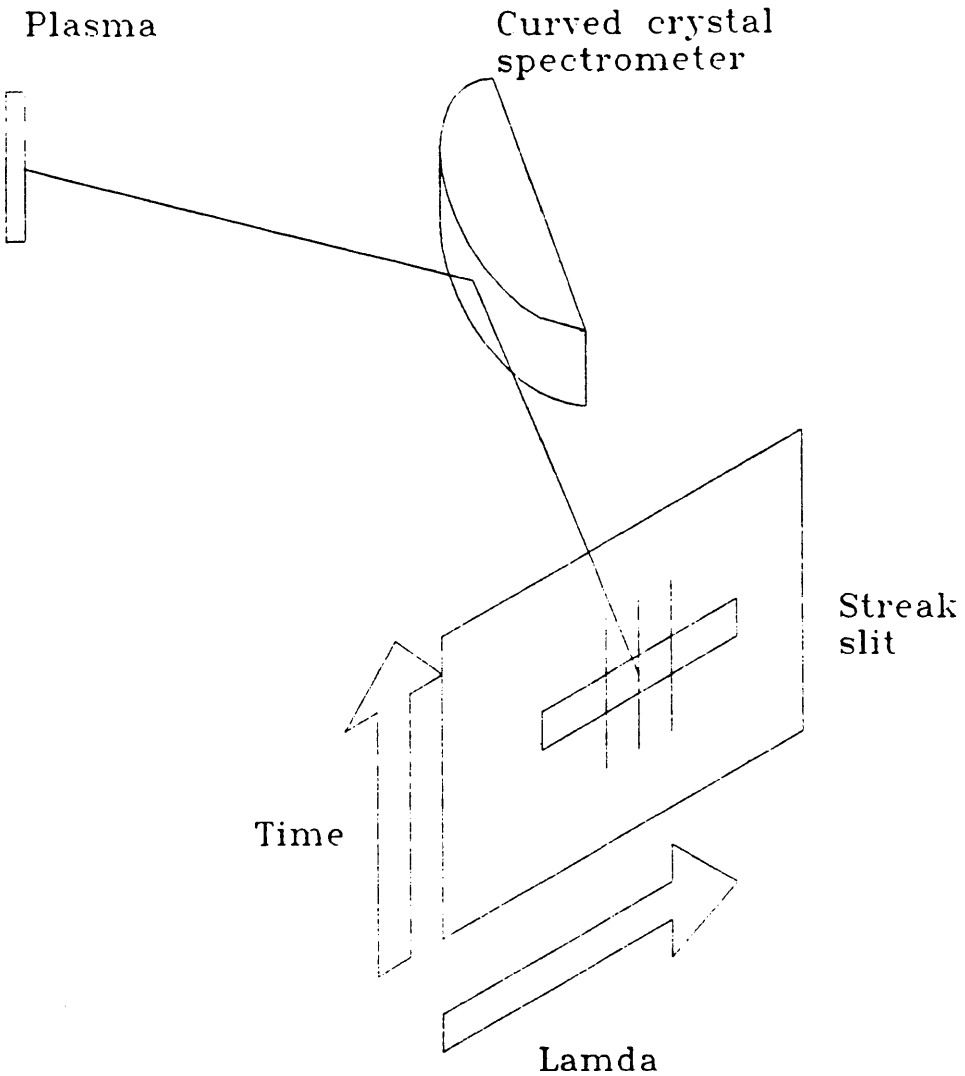


Figure 6.3: The geometry used to streak the x-ray spectra.

Several pinhole cameras were used. These included a single 30 μm pinhole filtered with 10 μm Beryllium (passes $\lambda \leq 2.0\ nm$) and a three pinhole camera with 300 μm apertures. A different filter could be fitted to each pinhole. Various filters were used including 10 $\mu m\ Be + 200\ \mu m$ polyester (passes $\lambda \leq 0.5\ nm$).

6.3.5 X-ray diodes

An XRD is shown in figure 6.4 and its sensitivity is shown in figure 6.5 (Day et al 1981). Photons strike the cathode surface and photoelectrons are emitted. The time resolution is extremely high and one is usually limited by the bandwidth of the oscilloscope used. A crude spectral sensitivity can be obtained by using different filters on two identical diodes. These diodes are most sensitive in the UV because at shorter wavelengths the photons are absorbed to deeply in the surface for photoelectrons to be released. Therefore at the wavelengths we are interested in , $0.1 - 2.0\ nm$ very large fluxes are required. To remove the UV the diodes were filtered with a light blocking material such as 100 nm of aluminium on 6 μm plastic.

6.3.6 Electrical signals

The electrical signals were not changed at all from their normal (deuterium) characteristics. A uniform pinch with a large neutron yield was often indicated by a large negative excursion of $\dot{I}$.

6.3.7 P.I.N. diodes

P.I.N. diodes (commonly referred to as pin diodes) are silicon diodes with a positively doped-intrinsic and intrinsic-negatively doped junction. They are identical in operation to a normal photodiode but have a larger area and a thicker junction and can work at higher voltage. These make them more sensitive to hard x-rays. They are widely used for detecting radiation in the $0.1 - 1.0\ nm$ region. These diodes are sensitive to visible light and must be filtered with a light blocking material. The diode used was a Quantrad 100-pin-200 (Alrad Components) with various filters. The sensitivity is shown in figure 6.5.

6.4 Results and discussion

6.4.1 Effect of argon on neutron output

The measured neutron output of the deuterium pinch is typically between 10,000 and 30,000 counts which corresponds to total yield of about 10^{11} neutrons. The addition of argon reduced this count to between 1,000 and 8,000. Possibly because of the high shot to shot variations no trend was discernible as the amount of argon was increased to the point of no pinch.

6.4.2 Electron beam activity - XRD and PIN diode signals

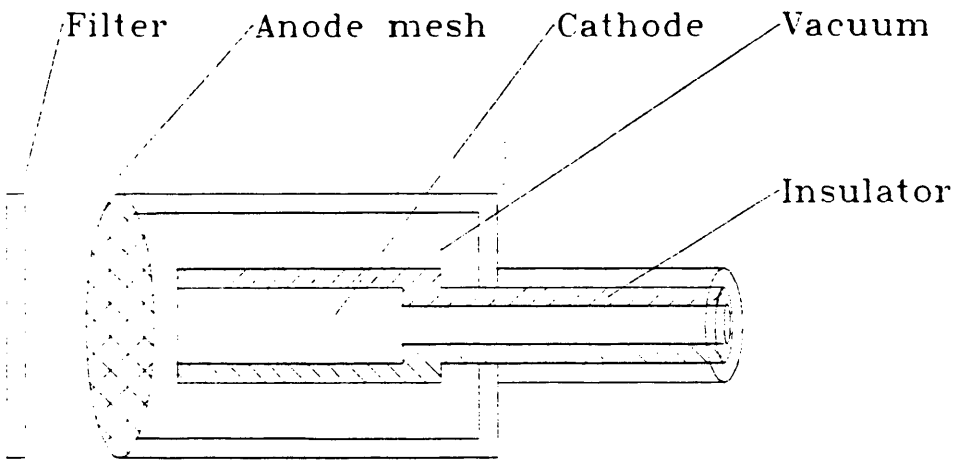
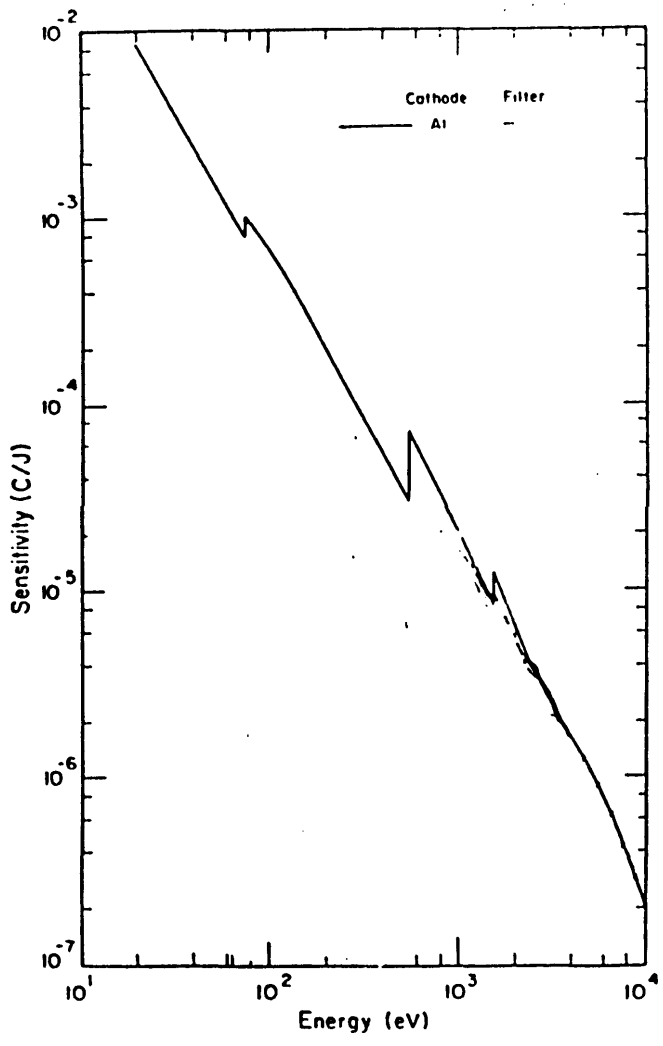


Figure 6.4: An X-Ray Diode



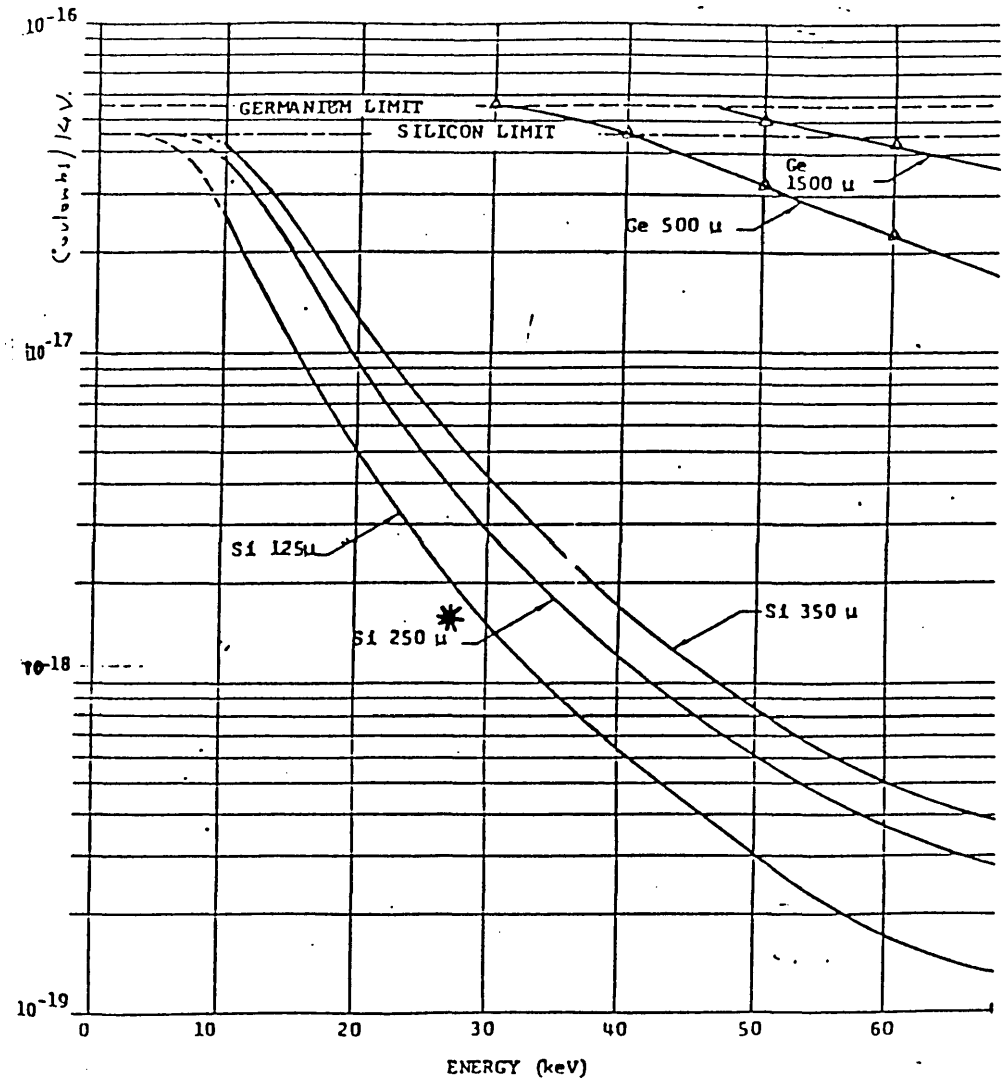


Figure 6.5: X-ray diode and pin diode sensitivities.

It was known that hard x-rays $\leq 0.1\ nm$ would be present in the experiment. These are produced by electron beams striking the copper anode. To measure this effect and subtract it from our soft x-ray signal the pin diode and were filtered with 4 mm of perspex and placed in drift tubes where they could not see the anode. The XRD was totally insensitive to this radiation but the pin diode detected it during the run down of the sheath and at pinch time. The pin diode signal at pinch time was very erratic and frequently so large that it saturated, so because of this it was not possible to make correlations between plasma dynamics and electron beam activity.

Figure 6.5 showed the sensitivity of the two diodes; the response of XRDs falls very strongly with increasing photon energy but that of the pin diode remains high. For this reason the aluminium cathode should be the preferred diagnostic for soft x-ray emission. Figure 6.6 shows a typical signal.

6.4.3 The pinch

The amount of argon in the pinch was optimised for maximum x-ray yield by increasing the delay between opening the argon inlet valve and forming the pinch. Estimates of the amount of emission from the pinch were made using the x-ray film density (Henke 1986) and the signal from the aluminium cathode (Day 1981). Both these methods indicate that the total emission in the region of $0.1 - 2.0\ nm$ is of order 1 J.

Comparison of time integrated spectra recorded on Polaroid 665 pos-neg instant film and pinhole photographs recorded on KODAK Xchron film showed that if there were no hotspots there was no helium-like argon radiation from the pinch. The bulk plasma emits softer radiation and only the hotspots are emitting K shell and recombination radiation. This is shown by figure 6.7 which shows two pinhole images of the same shot. The image in 6.7a is filtered with $10\mu m$ of Beryllium which passes radiation up to approximately 2.0 nm and that in figure 6.7b is filtered with an additional 200 μm of polyester which only passes radiation below about 0.5 nm. We can see that the hotspots (which in these images are projections of the pinholes) are very well aligned. To spatially resolve the hotspots a $30\mu m$ pinhole was used. The resulting image is shown in figure 6.8. When viewed end-on the pinch is a small source of only $700\mu m$ diameter. The maximum permissible delay between putting the argon in and forming the pinch was determined from the intensity of the radiation, the fusion neutron signal and the change in the current derivative at pinch time. All these indicated when the amount of argon was preventing the formation of a good pinch. This may have been due to contamination of the insulator or sheath during the rundown phase of the plasma.

The soft x-ray emission from the pinch was imaged with a $300\mu m$ pinhole

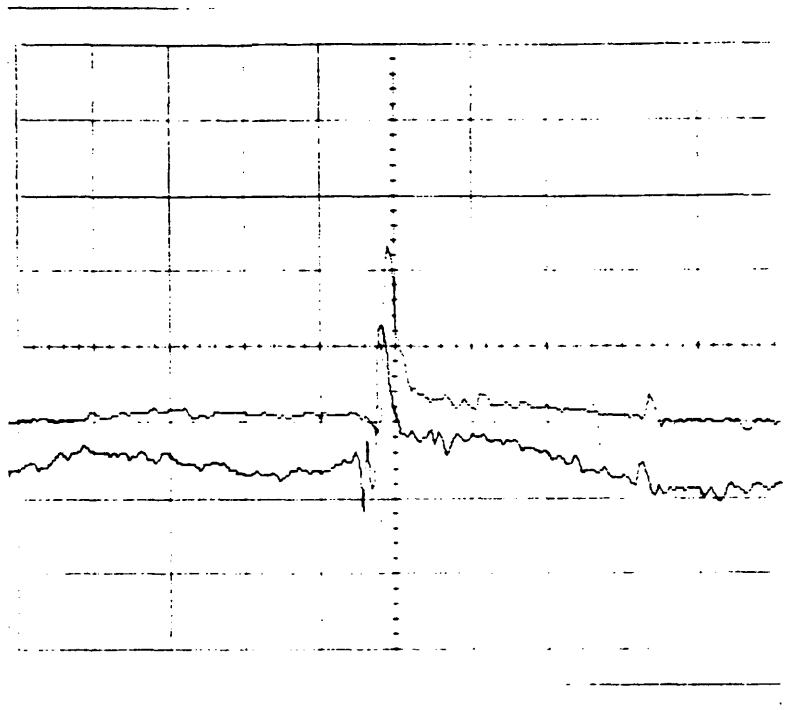
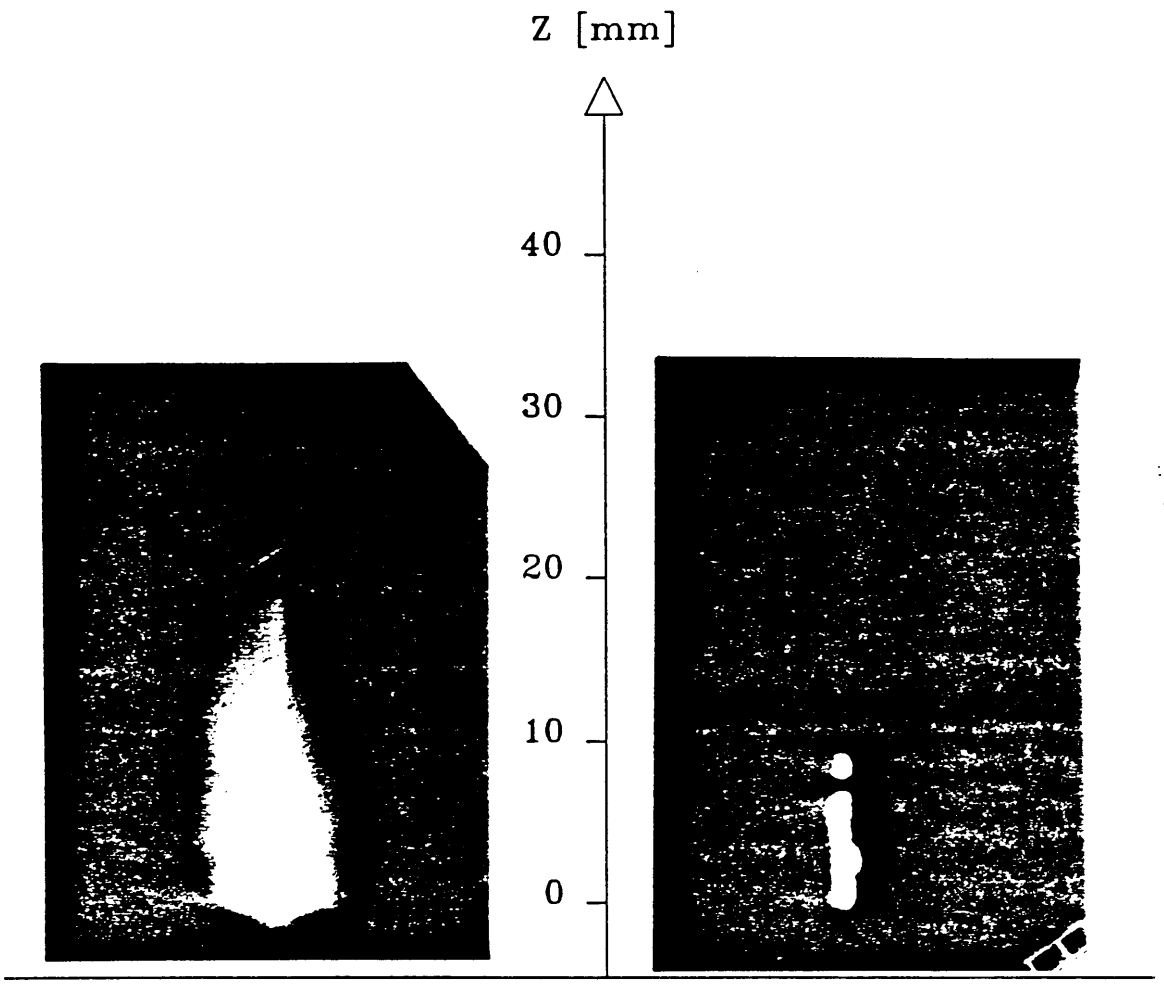


Figure 6.6: Typical signals from a pair of filtered X-ray diodes.
Upper trace (green): 0.16 um Al on 12 um mylar
50 mV, 50 ns/div
Lower trace (black): 10 um Cu, 20 mV, 50ns/div



a) 10 um Be

b) 10 um Be + 200 um polyester.

Figure 6.7: Pinhole camera images of shot 4028 taken through different filters.

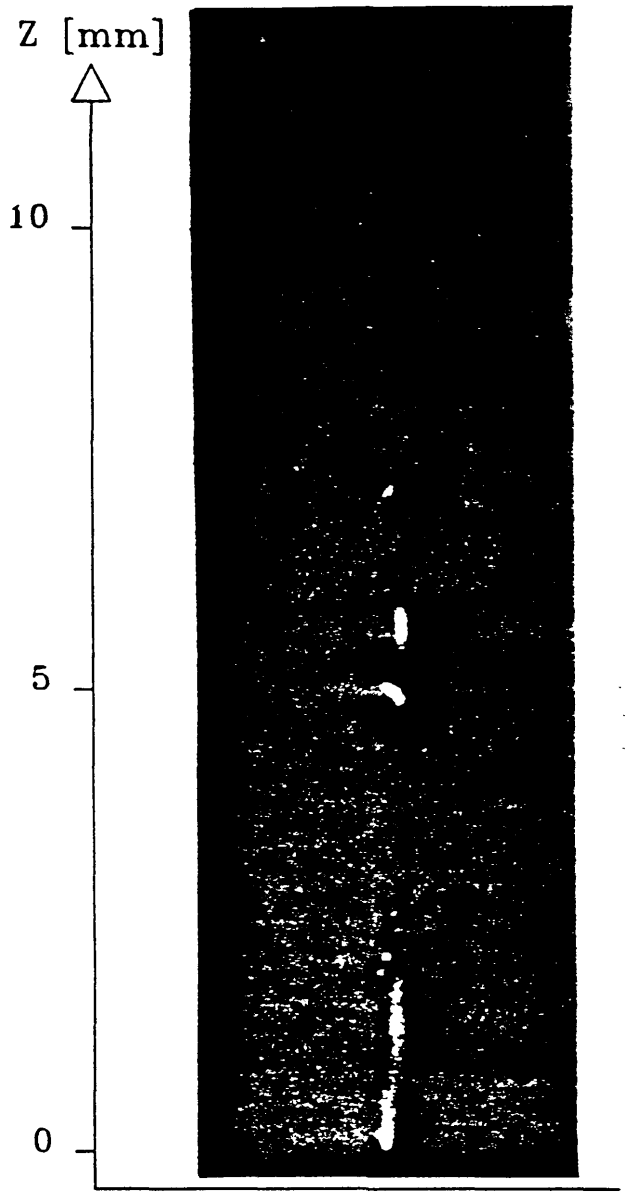


Figure 6.8: Pinhole camera picture
30 um pinhole, 10 um Be filter.

filtered with $10\mu m$ of Beryllium and time resolved by streaking with an X-ray streak camera. The right hand side of figure 6.9 shows a streak photograph and the left hand side shows the corresponding time integrated pinhole photograph. The streak photograph shows that the pinch forms and emits a lot of soft X-rays from the high density bulk plasma. This radiation is bremsstrahlung and L shell line radiation because it is not present in streak photographs taken with a filter which only passes $\lambda \leq 0.5\ nm$ ($10\ \mu m$ Be + $200\mu m$ polyester). We can see that the pinch forms on the anode first and then at higher Z positions which is the behaviour we would predict from the normal characteristics of a deuterium focus. At each axial point there is only soft x-ray emission for 2 ns then the intensity drops which may indicate the pinch is expanding. It is during the pinch's expansion that hotspots appear. The streak photographs show that the hotspots emit soft x-rays for only about 1 ns and the pinhole photographs show their size $\approx 200\ \mu m$ ($\lambda \leq 2.0\ nm$) or $30\ \mu m$ ($\lambda \leq 0.5\ nm$).

One way of measuring the temperature and density of hotspots is analysis of the He-like emission. Figure 6.10 shows a microdensitometer scan of a time integrated spectrum recorded on KODAK Xchron film.

The correct analysis of spectral lines should include the time history of the population levels, different ion and electron temperatures, opacity and departures from maxwellian velocity and energy distributions. In the analysis of real spectra compromises have to be made. It has been common practise in the literature (eg Spielman 1989) to assume a static coronal radiative equilibrium (CRE) and model the plasma with computer programs of varying sophistication. We use this method to obtain a preliminary estimate of the density and temperature.

RATION the CRE code at the Rutherford laboratory (Lee et al 1984) was developed for laser plasmas and works well in the temperature and density regime of interest. The model assumes that the plasma is in a steady state and then the populations are calculated from the rate equations including all the relevant collision and radiative processes. The populations of the hydrogen, helium and lithium-like stages are calculated explicitly and all others are lumped into one level. A spectrum is then derived which includes the effects of the microfield on the line shapes and allows for the instrument resolution and the effect of opacity which is important at these densities. Using the expression of McWhirter (1965) (which is not strictly valid at this density) we may estimate the time to establish a CRE equilibrium.

$$\tau = \frac{10^{18}}{n_e} \tag{6.1}$$

Which for a density of $10^{28}\ m^{-3}$ is 100 ps. This is similar to the time scale of the

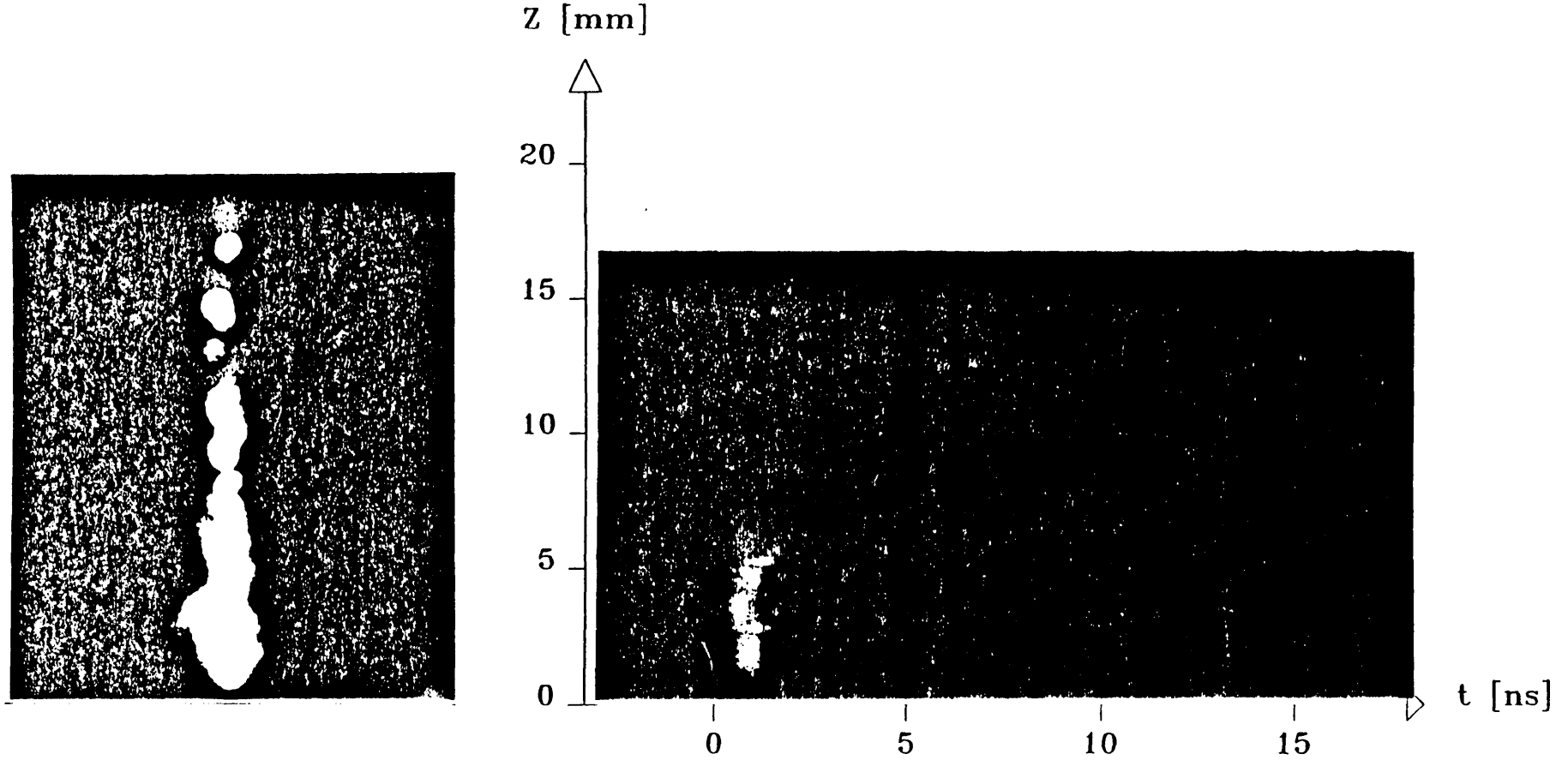


Figure 6.9: (shot 4192) The image on the left is a time integrated pinhole camera picture (300 um pinhole, 510 um Be filter). The image on the right is an X-ray streak photograph of the same pinch (300 um pinhole, 10 um Be)

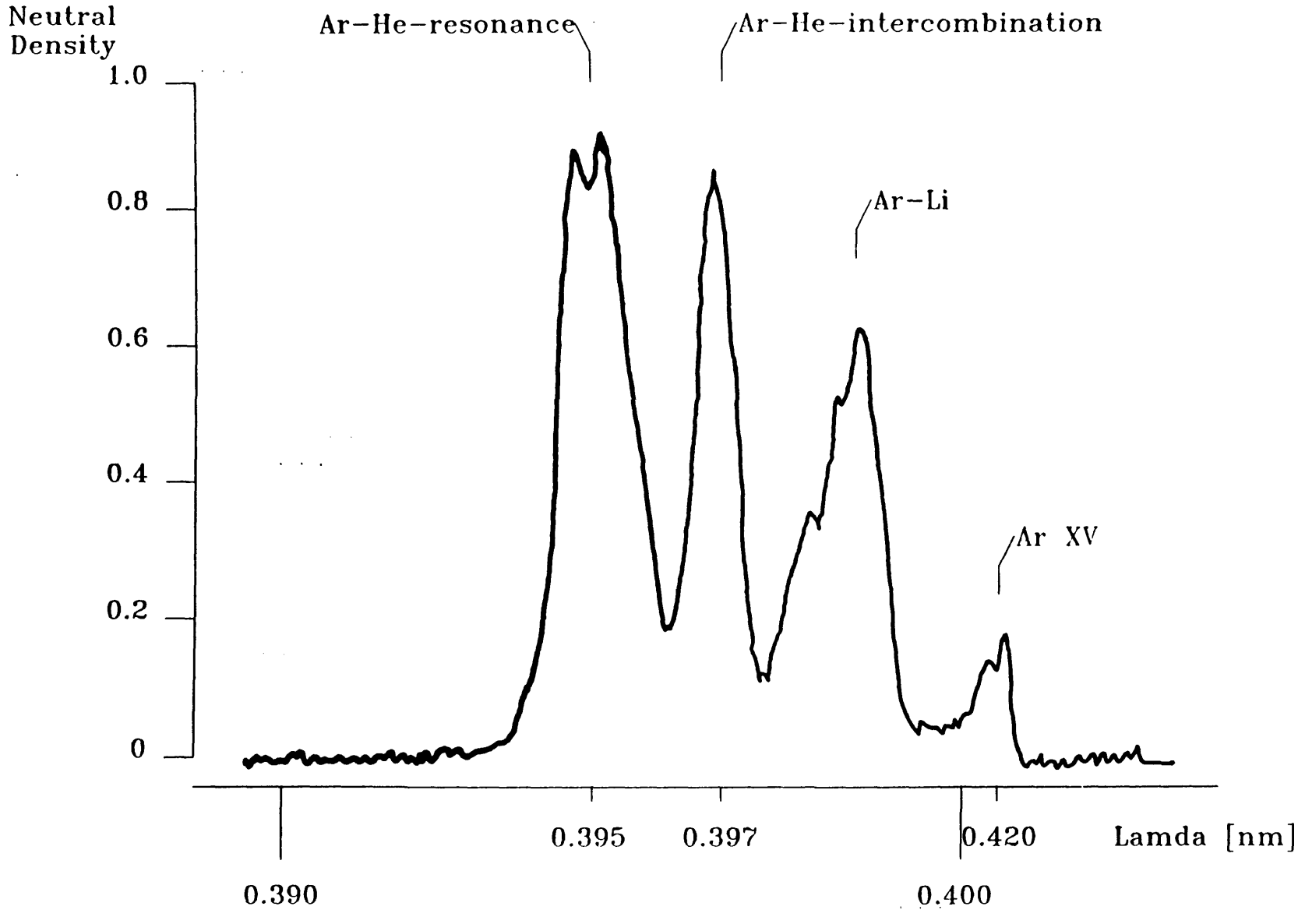


Figure 6.10: A microdensitometer trace of the argon spectrum near the helium-like lines.

hotspots.

By comparison of the predictions of the code with the observed spectrum (figure 6.11) we estimate that the mean temperature of the hotspots is 1.5 keV and a density is of order $10^{28} m^{-3}$. It has been suggested to me by the spectroscopists Koshelev (Institute for Spectroscopy, Troitsk, USSR) and Schmidt (University of Bochum) that the high implosion velocity is responsible for the asymmetry visible in the lines and that the effect on line shape is such that the true mean density of the hotspot is probably 10 times greater than has been estimated here.

A time resolved spectrum is shown in figure 6.12. The temporal resolution is 125 ps. This streak photograph shows 10 ns of the pinch emission which usually lasts for about 30 ns. There is a constant background in most of the lines from hotspots which are not in the plane of the crystal and camera or low level emission from the bulk plasma. On this photograph we can see 4 hotspots which are marked. The K shell emission from each hotspot has a duration of only 250 ps and all the lines turn on simultaneously. This shows that the increase in density is a very fast event.

6.5. Summary

We have developed a new soft x-ray source which can produce about 1 J per shot of soft x-rays from a very straight line of hotspots. When viewed end-on the pinch is a small source of 700 μm diameter.

The X-ray streak photographs show that the bulk of the pinch emits soft X-rays from a $1-2$ mm diameter cylinder for about 15 ns. This short period of emission is probably terminated by the expansion of the pinch. This reduces n_e and hence the radiation. It is during this expansion we see hotspots. These have been well characterised and have a temperature of 1.5 keV, a density of 10^{28} m^{-3} , a lifetime of less than 1 ns and are about 30 μm diameter ($\lambda \leq 0.5$ nm). We have found that the important K shell emission may be present for only 250 ps.

The neutron production of the pinch is reduced as the amount of argon is increased and there are a lot of electron beams during a discharge. It has been found that where the x- ray flux is sufficiently large to permit their use XRDs are to be preferred to PIN diodes because they are insensitive to the hard X-rays produced by the electron beams and so can be used to measure plasma emission.

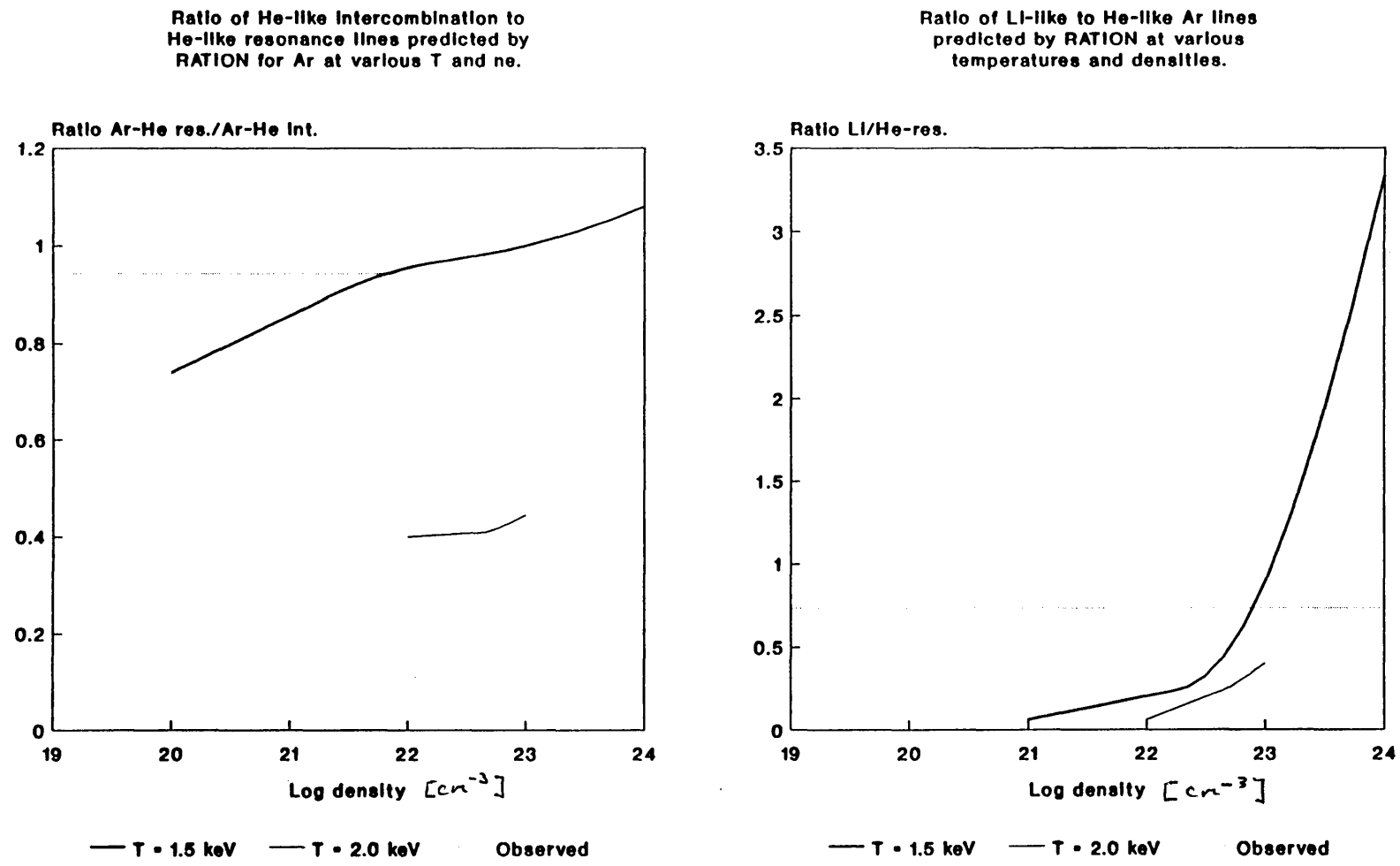


Figure 6.11: Line ratios predicted by RATION and SPECTRA

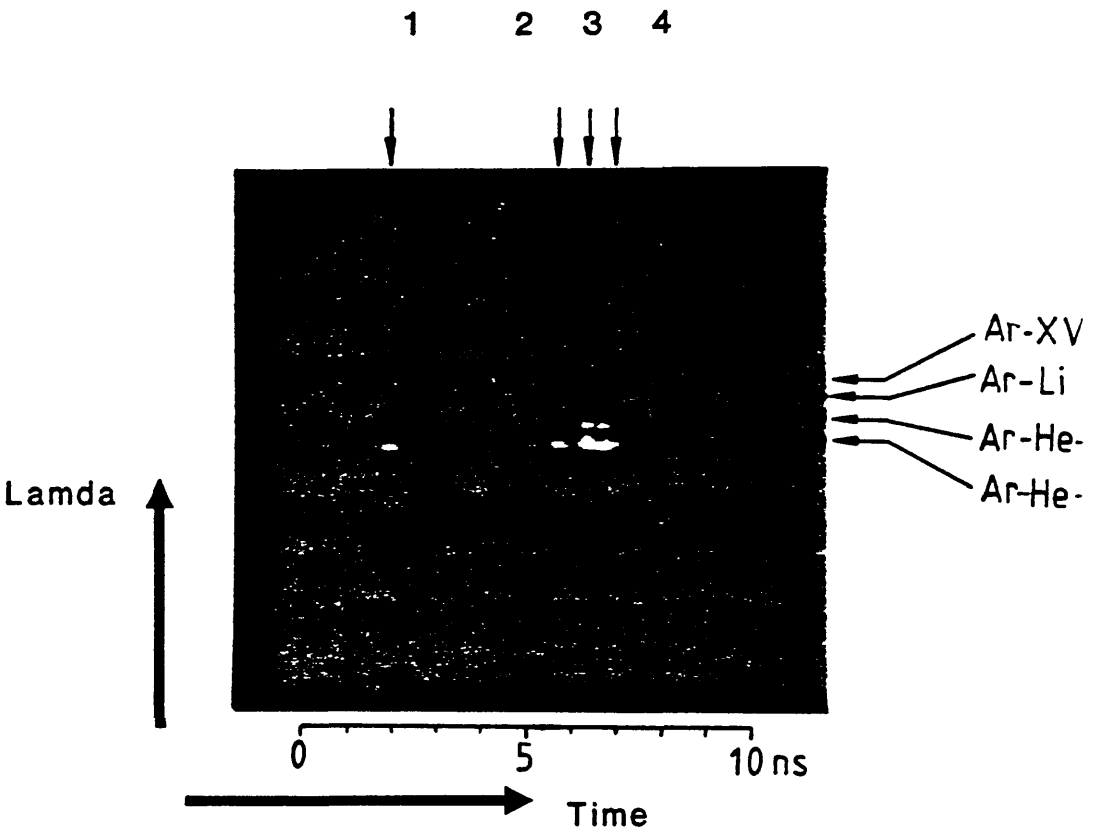


Figure 6.12: A streak photograph of the argon lines. (10 ns full screen)

CHAPTER 7: CONCLUSION

7.0 Introduction

This chapter will summarise the results and then discuss them and draw conclusions. First the compressional pinch results and then those of the plasma focus are described. Finally the author makes some suggestions for further investigations.

7.1 Summary of compressional pinch results

In this section the results of chapters 2, 3, 4 and 5 are summarised.

This thesis has presented the design, construction and investigation of a new Z-pinch experiment. The pinch chamber design and the modifications to the transmission line which were described in chapter 2 have been successful. The line can now safely supply 150 kA into a compressional pinch load and over 100 shots without a vacuum break has been achieved.

In Chapter 3 we described a new diagnostic – side-on image plane double exposure holographic interferometry with a diffuse scene beam, which for the first time allowed direct observations of the stability of a high power compressional pinch.

The optical streak photographs presented in Chapter 4 were used to investigate the radial dynamics of the collapse and pinch phase. The streaks were consistent with the sheath forming the moment the current began to rise (to the limit of experimental resolution – 10 ns). The side-on holographic interferograms of the hydrogen pinch agreed with the optical framing photographs which showed the sheath was very uniform along its length during the collapse. This indicated that our new method of preionisation was adequate. The slug model was used to model the collapse and showed that the 1 $torr$ argon pinch could not have formed unless the current had crowbarred. Further evidence of the current crowbar was that side-on framing photographs of the argon pinches and side-on interferograms of the hydrogen pinches show they remained confined even after the external circuit current began to fall. It was observed that as the sheath velocity was increased by either reducing the line density or increasing the current the collapse became faster than predicted. Comparison of the time to pinch predicted by the slug and snowplough models showed that the pinch time was a very robust parameter which depended little on the physical model and strongly on the filling density. The faster collapse indicated that not all the filling gas was accreted by the incoming sheath. This was confirmed by the holographic interferograms which measured a pinch line density which was initially only 75% of the filling density. This difference in line density is sufficient to account for the observed collapse time.

It was found that optical streak photographs and framing pictures could not detect the hydrogen pinch at the time we were most interested in for stability studies. This was because the pinch fades at about 160 ns when the current begins to fall. The wall plasma however, increases in intensity so the pinch cannot be seen simply by increasing the detector sensitivity. The interferograms showed that this reduction in optical emission from the pinch could be due to a falling density as well as a falling current. It was to detect the expansion of the pinch and the presence of instabilities that the interferograms referred to above were employed. The pinch studied was in a particularly interesting regime as is shown on the Haines Coppins stability diagram figure 7.1. The line density of the pinch is about $2.0 \times 10^{19} m^{-1}$ which means the plasma is collisionless ($\omega_i \tau_{ii} = 7$), has negligible resistivity ($S = 1.6 \times 10^3$) and the radius of a Larmor orbit is a finite fraction of the pinch radius ($a_i/a = 0.18$). These figures and many others of experimental and theoretical interest are given in table 7.1 (formulae supplied by Coppins (1986)).

An extensive set of interferograms were made. It was shown in chapter 4 that for the majority of plasmas which have an axial density variation it is not possible to analytically invert the fringe shift to get the electron density profile. A new computer model was made; the user specified the electron density profile $n_e(r, z)$ which may be inhomogeneous or discontinuous and the computer calculated the resulting fringe pattern. By using the model and Abel inversion of the fringe profiles we were able to make definite statements about the pinch density profile in r and z. Just after the pinch formed (100 ns) it had a centrally peaked density and was axially uniform with only small perturbations at the boundary. At 130 ns wings have developed on the radial density profile which may be due the saturation of short wave-length instabilities. By 140 ns an $\approx$ 10% $m = 0$ instability was visible. It was shown in chapter 5 that such a small amplitude after such a time means that the total growth of the instability is much less than would be predicted from linear ideal mhd. If we model the increased stability with a new linear growth rate we have $\gamma_{FLR} = 0.3\gamma_{mhd}$. (This result should be treated with caution because we are applying linear theory to a non-linear situation however it does provide a useful frame of reference). The instability is observed to saturate and remain at $\approx$ 30% for 50 ns and although the instability was not resolved after this time the pinch remains for an additional 50 ns.

7.2 Compressional Z-pinch Conclusion

It has been demonstrated that Potter's slug model is sufficiently accurate to assist in the design and interpretation of high power compressional Z-pinch experiments.

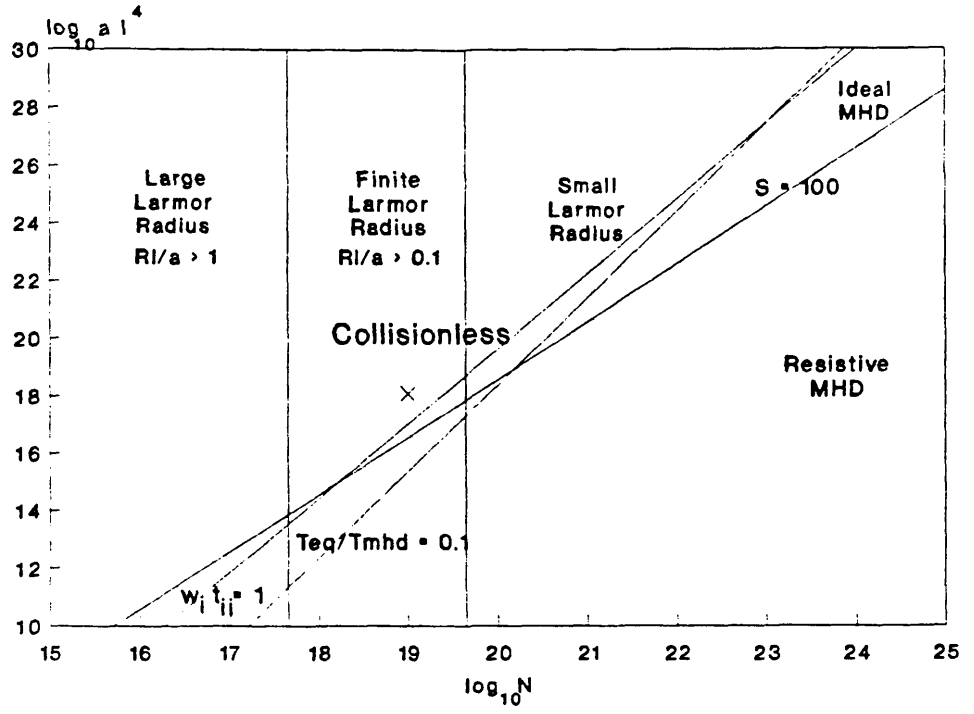


Figure 7.1: The Haines Coppins diagram of stability regimes of the hydrogen Z-pinch.

Filling gas	hydrogen			
Atomic number	Z	1		
Atomic mass	A	1		
elect. line den	N_e	2.0×10^{19}	m^{-1}	observed
Ion line den.	N_i	2.0×10^{19}	m^{-1}	assuming $N_i = N_e$
Radius	a	3.3×10^{-3}	m	observed
Length	l	7.5×10^{-2}	m	
Inductance	L	4.2×10^{-8}	H	$L = \mu_0.l.\ln(r_{chamber}/a)/2\pi$
Ion density	n_i	5.8×10^{23}	m^{-3}	N_i/a^2
Current	I	1.5×10^{5}	A	observed
Ion temperature	T_i*	$T_i = T_e = T_{ev}$	eV	$T_i/T_e = (2+\gamma)/\gamma$, $\gamma = \mu_0 e^2 N_i/\pi m_i$
Temperature	T_{ev}	175	eV	$T_{ev} = \mu_0 I^2/(16.\pi.e.l^2)$
Resistivity	η*	2.4×10^{-7}	Ωm	$\eta = 5.52 \times 10^{-4}/ T_{ev}^{3/2}$
Resistance	R	5.1×10^{-4}	Ω	$R = \eta l/\pi a^2$
Mag. field	B	4.5	T	$B = B(a)/2 = \mu_0 I/4\pi a$
Mag. pressure	$p_{mag.}$	80	bar	$p_{mag} = B^2/2\mu_0$
Ion cycl. fq.	$\bar{\omega}_i$	7.8×10^{8}	Hz	$\bar{\omega}_i = eB/m_i$
Ion coll. time	τ_{ii}	5.6×10^{-9}	s	$\tau_{ii} = 1.4 \times 10^{12} T_{ev}^{3/2}/n_i$
Ion thermal vel.	v_i	2.2×10^{5}	ms^{-1}	$v_i = (3.T_{ev}.e/m_i)^{1/2}$
Mhd growth time	τ_{mhd}	1.5×10^{-8}	s	$\tau_{mhd} = a/v_i$
Collisionality	$1/\tau_{ii}\omega_i$*	0.15		$\tau_{ii}\omega_i = 7.3x10^{30} I^4 a/AN^{5/2}$
F.L.R.	a_i/a*	0.18		$a_i/a = 8.0 \times 10^{8} N^{-1/2}$
Mag. Lnqst. no	S*	1.6×10^{3}		$S = 5.45 \times 10^{23} I^4 a/N^2 A^{1/2}$
Mhd equipartion	τ_{eq}/τ_{mhd}*	4.3		$\tau_{eq}/\tau_{mhd} = 2.1x10^{40} I^4 aA/N_i^3$

* Equations for these quantities taken from;
M.G. Haines et al 'Proceedings of the 2nd International conference on Dense Z-pinches, Laguna Beach CA 1989', AIP Conf. Proc. 195

Table 7.1: Values of important parameters of the Imperial College compressional pinch

From optical and interferographic diagnostics of the collapse and the pinch phase we conclude that the pinch current crowbars. The physical picture is shown in figure 7.2.

The use of a new side-on holographic interferometric experiment and computer aided interpretation has shown that the stability of a hydrogen compressional pinch in the collisionless finite Larmor radius regime is enhanced over the predictions of linear ideal mhd. An $m = 0$ instability develops but it saturates at about 30% and does not result in the immediate destruction of the pinch. It is not known whether the final disappearance of the pinch is caused solely by instability, or the falling current, or by both factors.

The saturation and the non-destructive nature of the $m = 0$ instability and its reduced growth rate offers encouragement to those planning fusion experiments in the FLR regime.

7.3 Summary of plasma focus pinch results

A new method of using a plasma focus as a soft X-ray source has been demonstrated. Pinhole camera photographs show that 1 J of Argon K shell and recombination radiation ($\lambda \leq 0.5\ nm$) comes from many hotspots which are located on the pinch axis. Time resolved diagnostics of the x-ray emission from the pinch and hotspots show that they form during the expansion of the pinch. The hotspots form first near the anode and then further up the pinch. This is because the pinch forms near the anode first and then progresses upwards. We have time resolved the helium-like line radiation both from the pinch and from individual hotspots and shown that hotspots are the major source of K shell emission in this pinch. It has been shown that many of these hotspots have a lifetime of less than 1 ns. From the analysis of time integrated spectra in a CRE model we estimate the mean density and temperature of these hotspots to be 1.5 keV and $10^{28}\ m^{-3}$. From pinhole photographs we measure a diameter of 250 μm ($\lambda \leq 2\ nm$) or 30 μm ($\lambda \leq 0.5\ nm$).

7.4 Plasma focus - discussion

The plasma focus with a gas stream which generates Joules of soft X-rays at powers of 100 MW in a single shot has been developed and diagnosed. We have made no attempt to optimise the total yield from this machine configuration. Previous work (Pereira and Davis 1988) has shown that the K-shell yield of Z-pinch plasmas in this current regime goes as $I^4 Z^{-8}$ so the emission $\leq 2.0\ nm$ could be greatly increased either by using neon or by working at a higher current. Conversely the total radiation yield could be increased by using a higher Z gas such as Xenon (Spielman et al. 1989). When viewed end-on the pinch is a source of only 700 μm

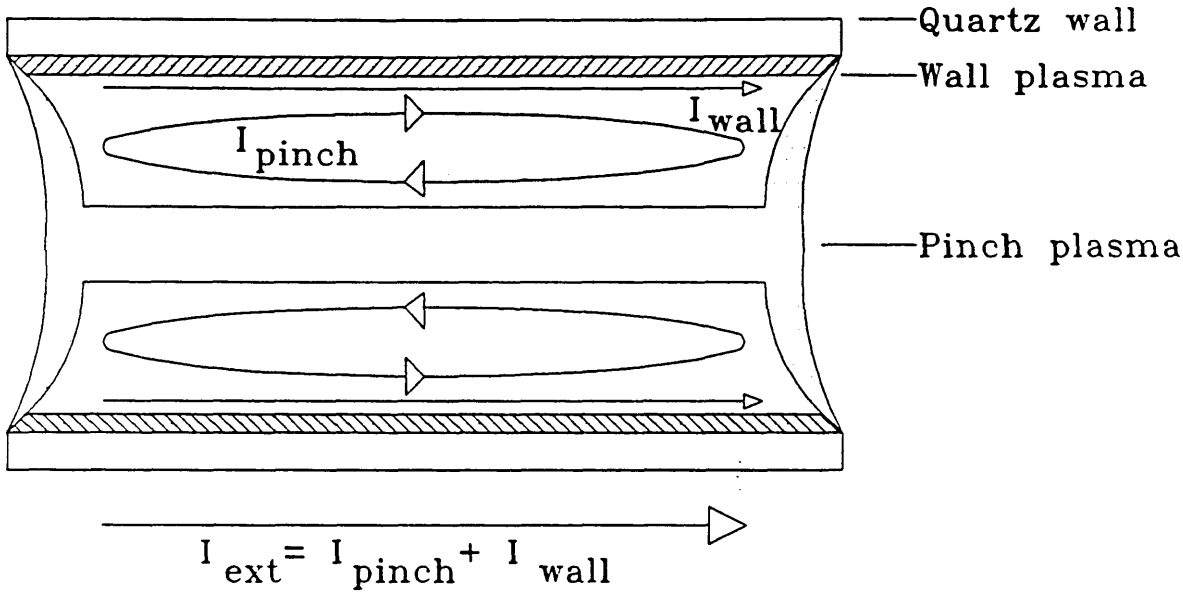


Figure 7.2: The crowbared pinch.

diameter. Such precise emission together with a large energy per shot that we have demonstrated could be very useful in a variety of soft x-ray applications such as microscopy and lithography.

Three possible mechanisms for the formation of hotspots were suggested in the introduction; $m = 0$ instabilities, radiative collapse (isothermal or under pressure balance) and electron beam-plasma interactions. The hotspots are 1 ns duration and form sequentially over a 30 ns time as the zippering pinch stagnates and bounces. However this does not immediately help us distinguish between these mechanisms. The mhd growth time of a 1 MA pinch is of order 1 ns and the hotspot formation is consistent with the expansion of the pinch triggering an $m = 0$ instability. This expansion will cause a large inductive voltage in the pinch which may drive an electron beam in the plasma and considerable electron beam activity was observed. The radiative loss of energy is clearly important in both these mechanisms because it reduces the pressure and aids the collapse. It would have been fortunate if the measurements of the K shell line emission had resulted in the temperature and density history of the pinch. What they did show was that the collapse to high density happens within 250 ps which is much faster than had been previously reported.

The results which have been presented are the first to investigate hotspots with a time resolution of 125 ps. They show that to get a detailed understanding of hotspot formation and extinction, which may take only 1 ns, we will require more diagnostics with a resolution on this time scale.

7.5 Suggestions for further work

It has been demonstrated that side-on holographic interferometry of the compressional pinch is a valuable tool in investigating Z-pinch stability. To extend this work we should look at a larger area of the I^4a, N plane. The primary requirement is for a visible laser giving a 300 mJ, 1 ns pulse. The short pulse length will enable us to resolve the plasma on a timescale much less than the mhd growth times of a very wide variety of plasmas. The shorter pulse length will also enable multiframe holography to be undertaken to explicitly measure the growth rate of an instability on a single shot.

The plasma focus has been shown to be capable of producing very large fluxes of soft x- ray radiation from hotspots. This has important commercial and scientific applications which can be investigated. The large plasma focus may be a very cost effective source for the exposure of resists used in the manufacture of silicon chips (for the technical background see Richer et al. 1989). The use of nitrogen instead of argon in the gas stream may enable flash x-ray microscopy of living cells (Lebert 1989). The x-ray yield and the pinch behaviour should be investigated

with a variety of different gases.

To investigate the formation of hotspots we are currently developing a multi-frame schlieren system and a holographic system using a mode-locked laser which produces 100 *ps* pulses. This would enable us to observe mass flow during the life of the hotspot.

It is hoped to continue the collaboration between Imperial College and Düsseldorf University. Düsseldorf have close links with the spectroscopy group at Bochum University (Kunze et al) and it is possible that they will assist us in the sophisticated analysis of the spectra we have obtained.

REFERENCES

Allen, J. E.,(1957), Proc. Phys. Soc., **70**, p24

Aliaga, R., Chuaqui, H., and Pedraza, P.,(1990), Appl. Opt. **29**, p2861

Anderson, O. A., Baker, W.R., Colgate, S.A., Furth, H.P., Ise, J., Pyle, R.V., and Wright, R.E., (1958), Phys Rev. **109**, p612

Atkinson, R. E. and Houtermans, F. G., (1929) Z. Physik **54,9**, p656

Baldock, P. and Dangor, A.E.,(1988), Proc Z pinch and Plasma Focus workshop, Nice

Bateman, G.,(1978), " MHD Instabilities", MIT Press, Cambridge, Mass.

Bennett, W. H.,(1934), Phys. Rev. **45**, p890

Bodin, H.A.B., Newton, A.A. and Peacock, N.J., (1960), Nuc. Fus. **1**, p54

Braginskii, S. I., (1958), Sov. Phys. JETP, **6**, p494

Carruthers, R. and Davenport, P. A., (1957),Proc. Phys. Soc. **B70**, p49

Chew, G. F., Goldberger M. L., and Low, F. E.,(1956) Proc. R. Soc. London **A236**, p112

Chittenden, J.P., and Haines, M.G.,(1989), Phys. Fluids **B2**, p1889

Choi, P., Dangor,A.E., Folkierski, A.,Kahan, E., Potter, D.E., Slade, P.D., Webb, S.J. (1979), Plasma physics and controlled nuclear fusion research, IAEA, Vienna **2**, p69

Choi, P. and Baldock, P. (1988), private communication

Choi, P., (1989), private communication

Choi, P.,(1988), Nuc. Fus. **28**, p1771

Christie, M., (1981), J.Phys. D.: Appl. Phys., **14**, L73

Collier, R.J., "Optical Holography", Academic Press 1971

Coppins, M., (1986), private communication

Coppins, M., (1988), private communication

Cousins, S.W., and Ware, A.A., (1951), Proc. Phys. Soc. **B64**, p159

Culverwell, I.D., Coppins, M., Haines, M.G., Bell, A.R., and Rickard, G.J.,(1989), Plas. Phys. and Cont. Fus. **31**, p387

Culverwell, I.D., Coppins, M., and Haines, M.G.,(1989a) Proc. 2nd Int. Conf. on Dense Z-pinch, Laguna Beach, AIP **195**

Curzon, F.L., Folkierski, A., Lathem, R., and Nathion, J.A., (1960), Proc. Roy. Soc. Lond. **A257**, p386

Dangor, A. E., (1986), Plas. Phys. and Cont. Fus., **28**, p1931

Day, R.H.,Lee, P., Saloman, E.B., and Nagel, D.J.,(1981),J. Appl. Phys. **52**,p6965

Decker, G., and Herold, H., (1980) Phys. Blatter **11**, p36

Decker, G., Kies, W., Mälzig, M., van Calker, C. and Ziethen, G., (1986), Nuc. Inst. and Meth. **A249**, p477

Deeney, C. (1988), "Measurements of hotspots and electron beams in Z pinch devices" Thesis: Imperial College, University of London

Favre-Dominguez, M. B., (1985) "Experimental Investigations of a gas- embedded Z-pinch" Thesis: Imperial College, University of London

Figura, E,"Observations of z-pinches driven by a high voltage pulsed power source". Thesis: Imperial College, University of London

Filippov, N. V., Filipopova, T.I., and Vinogradov, V.P.,(1962), Nucl. Fusion Suppl., **2**, p577

Gamow, G. and Critchfield, C.L., (1949), "Theory of Atomic Nucleus and Nuclear Energy Sources", Clarendon Press, Oxford.

Haines, M. G.,(1959), Proc. Phys. Soc. Lond. **74**, p576

Haines, M. G.,(1978), J. Phys. D. **11**, p1709

Haines, M. G.,(1982), Physica Scr. **T2/2**, p380

Haines, M. G., (1986) Dangor, A.E.,Folkierski, A.,Baldock, P., Challis, C.D., Choi, P., Coppins, M., Deeney, C., Favre-Dominguez, M.B., Figura, E., Sethian, J.D., , Proc. 11th I.A.E.A. conference on plasma physics and controlled nuclear fusion research, Kyoto, Japan

Haines, M. G.,(1989), Proc. 2nd Int. Conf. on high density Z-pinches, Laguna Beach, Calif.

Hecht and Zajac, 'Optics', Addison-Wesley Publishing, Reading

Henke, B.L., Uejio, J.Y., Stone, G.F., Dittmore, C.H., Fujiwara,F.G.,(1986), J. Opt. Soc. Am. B3 Herold, H. and Jager, Nucl. Fus. **27,2**

Jahoda, F.C. and Siemon, R.E. (1972), "Holographic Interferometry cookbook", Los Alamos informal report,, LA-5058-MS UC-37

Kies, W., (1987), 'Z- pinch plasmas for nuclear fusion?', Habilitationsschrift, University of Düsseldorf

Kies, W., (1989), Private communication

Krall, N.A. and Trivelpiece, A.W.,(1973)." Principles of plasma physics", McGraw Hill, New York

Kruskal, M. and Schwartzchild, M., (1954) Proc. Roy. Soc. **A223**, p348

Lee, T. N.,(1975), Annals New York Acad. Sci., **251**, p112

Lee, R.W., Kilkenny, J.D., Kaufman, R.L., and Mathews D.L.,(1984), J. Quant. Spectrosc. Radiat. Transfer vol **31**, p83

Lebert, R., Neff, W., Holz,R.,and Richer, F., Proc 2nd Int. Conf. on High Density Z pinches, Laguna Beach, Calif.

Mather, J. W., (1965), Phys. Fluids, **8**, p366

Martin, C., 'Nanosecond pulse techniques'. Aldermaston Unclassified report, SSWA/JCM/704/49

McWhirter, R.W.P. in "Plasma diagnostic techniques", edited by R.H Huddlestone and S.L. Leonard, Academic Press (1965)

Negus, C.R. and Peacock, N.J.,(1979),J. Phys. D., **12**,p91

Pease, R.S.,(1957) Proc. Phys. Soc. London **B 70**, p11

Pereira, N.R., and Davis J.(1988), J. Ap. Phy. , **64(3)**

Potter, D., (1971), Phys. Fluids, **14**, p1911

Potter, D., (1978), Nucl. Fus. **18 (6)**

Richer, F., Eberle, J.,Holz, R.,Neff, W.,and Lebert, R., 'Proc. 2 nd Int. Conf. on High Density Z-pinches', Laguna Beach, Calif.

Rosenbluth, M., et al(1954), Los Alomos report- LA-1850

Sethian, J.D., Robson, A.E., Gerber, K.A. and deSilva, A.W., (1987), Phys. Rev. Lett., **59**, p892

Shearer, J.W.,(1976), Phys. Fluids, **19**, p1426

Spielman, R.B., Dukart, R.J., Hanson, D.L., Hammel, B.A.,Hsing, W.W.,Matzen, M.K., and Porter, J.L.,(1989), Proc 2nd Int. Conf. on Dense Z pinches, AIP Conference proceedings no 195

Thonemann, P.C., and Cowhig, W.T., (1951), Nature **166**,p903

Tonks,L.,(1939), Phys. Rev., **56**, p360

Vikherev, V.V.,(1977), Sov. J. Plasma Phys., **3**, p539

Vikhrev, V.V.,(1986), Sov. J. Plasma Phys., **12**,p262